The Life of Nanoparticles in Contact with Biological Media and Entities

Tran Thi Thanh Ngoc

Tesis doctoral

Estudis de Doctorat en Ciència de Materials

Director: Dr. Víctor F. Puntes

Tutor: Dr. Jordi Pascual i Gainza

Departament de Física

Facultat de Ciències

2014

The Life of Nanoparticles in Contact with Biological Media and Entities

Memòria presentada per aspirar al Grau de Doctor
per Tran Thi Thanh Ngoc

Dr. Victor F. Puntes Dr. Jordi Pascual i Gainza

Bellaterra, Setembre de 2014

Por la ciencia, como por el arte, se va al mismo sitio:

A la verdad.

Gregorio Marañón

Contents

Acknowledgements

The last 3 years have quickly passed providing me lots of valuable knowledge and experiences from which this thesis dissertation is formed. To achieve this, it is inevitable to acknowledge the contribution of a great deal of individuals including:

- First of all, Dr. Victor F. Puntes, my supervisor, who has been inspiring and guiding me in doing research with his diversified intellectuality.
- Dr. Jordi Pascual i Gainza as my thesis´s tutor.
- All members of Inorganics Nanoparticles Group (both past and present) led by Dr. Victor F. Puntes, especially Dr. Eudald Casals and Dr. Cecilia Lopez, for their enthusiastic helps, useful discussion, caring and enjoyable sharing moments.
- Pablo Garcia from Catalan Institute of Nanoscience and Nanotechnology for the XRD measurements and Dr. Belén Ballesteros from Catalan Institute of Nanoscience and Nanotechnology for the EDX measurements and discussions.
- All NanoTOES partners for their collaboration, especially Prof. Albert Duschl ´s group at PLUS, Dr. Diana Boraschi´s group at CNR, Dr. Voetz Matthias´s team at Bayer and Dr. Claus Svendsen´s group at CEH for their training and exchanging knowledge during my secondments.
- Marie-Curie Fellowship for the opportunity and the financial support. This study is supported by the EU 7th framework programme, Marie Curie Actions, Network for Initial Training NanoTOES (PITN-GA-2010-264506).
- Manuel Ramos and Antonia Macias together with their great family, whom I consider as my second family, for their unconditional love and caring.
- And last but not least, my beloved family and friends who are not only my biggest spiritual support, but also the motivation that leads me to success.

From the bottom of my heart, THANK YOU SO MUCH. XIN CHÂN THÀNH CÁM ?N.

Structure of the Thesis

This thesis has been presented in following order:

Objectives states the aims of the dissertation

Chapter one gives a brief introduction on behaviors of nanoparticles in biological media, the needs and challenges in characterization and the safe design of nanoparticles.

Chapter two reveals the changes (aggregation, protein adsorption and dissolution) the silver nanoparticles suffer in simulated body fluids at different portals of entry.

Chapter three shows the comprehensive study on dissolution of silver nanoparticles in complete cell culture media (cCCM) including its controlling. Ag partition and speciation in these media is also presented.

Chapter four focuses on controlling the chemical reactivity of silver nanoparticles in biological media using core-shell approach. In particular, the synthesis of core-shell NPs and their exposure to cCCM are reported.

Chapter five mentions several aspects (size, charge, pre-incubation with protein and presence of contamination effects) in examining the biological response of the nanoparticles.

Finally, **chapter six** resumes general conclusions of the thesis.

In addition, an appendix, list of abbreviations and list of publications are also included.

Objectives

Contributing to an increasing requirement of strict material characterization in the field of nanotoxicology, the study of toxicity and safety issues of nanomaterials, this thesis dissertation aims at describing the evolution of the identity of nanoparticles, focusing on silver, a highly commercialized material, when they are exposed to biological environments. This complete identity can be a result of individual processes including aggregation, agglomeration, protein (or biomolecule) adsorption, corrosion and dissolution or mixtures of them.

Chemical reactivity of nanoparticles, which make them useful for many products, may, at the same time, cause concern about adverse health effect. This concern can be solved by increasing the persistence of the nanoparticles. However, the possibility to lose the desired reactivity due to increased persistency should also be considered. Hence, it is important to control and balance these two properties. In such circumstances, this thesis also aims to investigate the chemical reactivity and persistency of silver nanoparticles (AgNPs) in biological media as well as how to control them. Particularly, dissolution of AgNPs with different surface properties has been studied in complete cell culture media and the generated species due to this process have been identified and quantified. Then, chemical reactivity of AgNPs has been tuned using different approaches including surface passivation, equilibrium driving and core-shell structures.

Additionally, correlating the behaviors of nanoparticles in biological environments with their corresponding biological response is crucial to better understand the response

mechanism. Thankful to short visits to different biology laboratory, various considerations in determining toxic effects (cytotoxicity, immunotoxicity and ecotoxicity) have been explored.

Chapter 1

INTRODUCTION

1.1. Behaviors of nanoparticles in biological media

Last decades, nanoparticles (NPs), due to their unique properties, have been incorporated in a wide range of bio-applications, especially medicine[1-4]. While quantum dots can be used for imaging and tracking by fluorescence, multifunctional iron oxide particles are utilized in imaging and tracking by MRI (magnetic resonance imaging)[1]. In addition, gold and silver are commonly found as good candidates for diagnostics and drug delivery[4]. As a consequence, the ability to integrate NPs into biological systems, which are complex aqueous mixtures of electrolytes, proteins, metabolites, etc., has increased greatly. But, what happens to the NPs when they are brought into these systems where their components are ready to interact with NPs? Will these events be responsible for biological responses of NPs? Understanding the physical and chemical interaction of NPs with biological media is essential to reveal these answers. In addition, depending on their application, NPs are preferred to be persistent or degradable, and the extent of persistency can also vary. For instance, those NPs used in implantation purpose are wished to be bio-persistent while NPs which function is to release ion (Ag in antibacterial product, iron oxide in ferumoxytol to treat anemia) should be degradable. Besides, administered NPs, as contrast agents for examples, are preferred to be cleared out instead of accumulating inside body. In this case, smaller NPs can be an option to increase the renal clearance. However,

reducing the particle size below 5 nm, especially noble metal NPs, will significantly influence their surface-plasmon based properties[3]. One potential solution is to develop NPs that can dissociate into smaller species during/after they complete their mission. Obviously, regardless of application, colloidal stability of NPs is crucial. Thus, understanding the behaviors of NPs in biological media not only helps to verify their biological effects, but also assists in designing proper NPs for desired purposes. This is also the main aim of this thesis and will be discussed throughout the chapters.

NPs, due to their high surface energy, readily undergo processes towards more stable states to minimize their reactivity (Figure 1.1). These processes usually aim at the decrease in exposed surface of NPs. Indeed, following Derjaguin and Landau, Verwey and Overbeek (DLVO) theory, NPs tend to aggregate due to Van der Waals attraction force, forming bigger objects. On the contrary, governed by the Gibbs-Thomson effect, NPs dissolve as their surface energy increases. Also, NPs can interact with biomolecules (e. g. proteins, lipids) and/or synthetic contaminants changing NP identity.

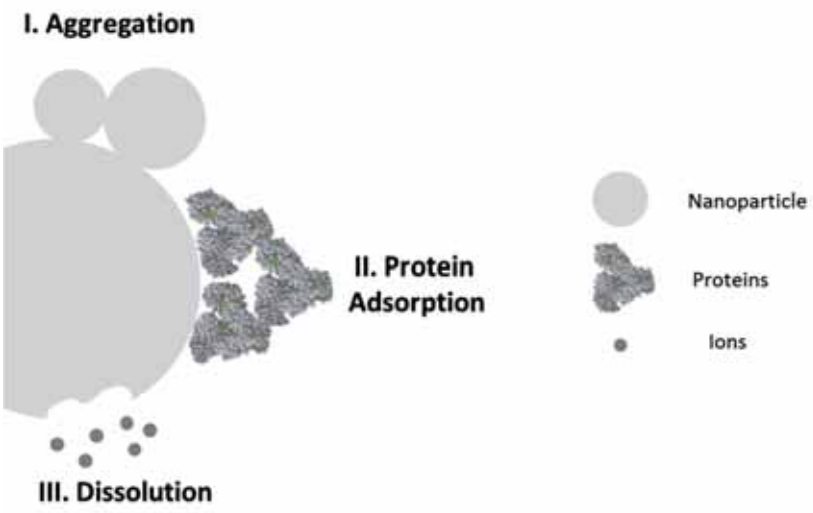

***Figure 1.1**. Main processes a NP will experience in biological media can be classified in: (I) aggregation, (II) protein adsorption and (II) dissolution.*

1.1.1. Aggregation

Aggregation is a process where aggregates are formed from the association of dispersed particles. To do this, the particles with Brownian movement must come into contact and interactions between colliding particles must be strong enough. In a solution, the stability of NPs can be maintained by repulsion forces, either electrostatic or steric[5]. It is well-known how the colloidal stability of NPs depends on their intrinsic properties (surface charge, coating) as well as on the medium (ionic strength, pH) in which they are dispersed. For instance, coating molecules providing steric stabilization are found to have higher resistivity to high salt concentrations than electrostatic one[6]. In biological media, which usually possess high ionic strength, aggregation of electrostatic stabilized NPs following by sedimentation can occur due to the screening of the surface charge by present electrolytes[7]. In this case, resulting from the shielding of electric field, the NPs come close to each other, and this eventually causes the agglomeration. NPs were also reported to show a dramatic change in their dispersibility when being transferred from a buffered aqueous solution to cell culture medium or physiological environment[8-10].

It should be noted that this behavior is different from the precipitation of NPs due to saturation where dispersed concentration of NPs is higher than a certain limit. Under this condition, the NPs are too crowded that they are brought into close contact. However, the ´real´ aggregation occurs depending on how strong the interaction between individual NPs is. Then, a good dispersity can be recovered when decreasing the NP concentration. Meanwhile, in the other case, NPs may end up with irreversible aggregation that cannot be re-suspended. The concentration at which the NPs still maintain a good dispersion is between 10^{12} to 10^{16} NP/ml varying on different materials. This equals to a mass concentration of up to few mg/ml[11]. At concentrations below 10^{10} NPs/ml, there would be no collisions and no aggregation occurs.

Regardless of how the NPs are repulsed out of their solution, whether destabilization or saturation, the morphology of the NPs and their unique properties (optical, catalytic, etc.) that arise at the nanoscale are modified or even lost. A study on near-

field interaction of two identical gold NPs showed that decreasing interparticle distance will cause a significant redshift of the surface plasmon extinction peak for the parallel polarization[12]. Li et al. reported the effect of aggregation of magnetic particles on their magnetization property[13] while Rosicka even pointed out how structure of iron NPs in aggregates affects their magnetic properties[14]. In addition, photocatalytic activity of semiconductors like TiO_2 and ZnO NPs in generating free hydroxyl radicals was reduced via aggregation of NPs varying on aggregate size and structure[15].

Aggregation, i.e. changing in effective size of NPs, leads to the variation in surface area and concentration of NPs which consequently affects the doses in terms of these parameters. Therefore, among all the physicochemical parameters of nanomaterials including size, shape, surface area, solubility, chemical composition etc. , their aggregation tendency is critical in investigating cellular responses in *in vitro* and *in vivo*[16]. In fact, aggregation of NPs in biological environments, as cell culture media, can impede the targeting efficiency of NPs to cells via influencing the degree of uptake and toxicity depending on the NP properties and the cell type. Recently, Tripathy et al. found that the ZnO NP aggregation in PBS can be modulated by changing NP concentration and that smaller aggregates caused higher damage to mitochondrial, generated elevated intracellular ROS and cell apoptosis in RAW 264.7 (Mouse leukaemic monocyte macrophage) cell than the larger aggregates[17]. In their study on effect of AuNP aggregation on cell uptake, Albanese et al. reported that in comparison to monodisperse NPs, aggregated NPs showed a 25% decrease in uptake by HeLa and A549 cells. However, largest aggregates were uptaken two times higher by MDA-MB-435 (melanoma) cell[18]. From these findings, the correlation between aggregation state of NPs and in vitro toxicity for a same mass concentration can be postulated as shown in Figure 1.2.

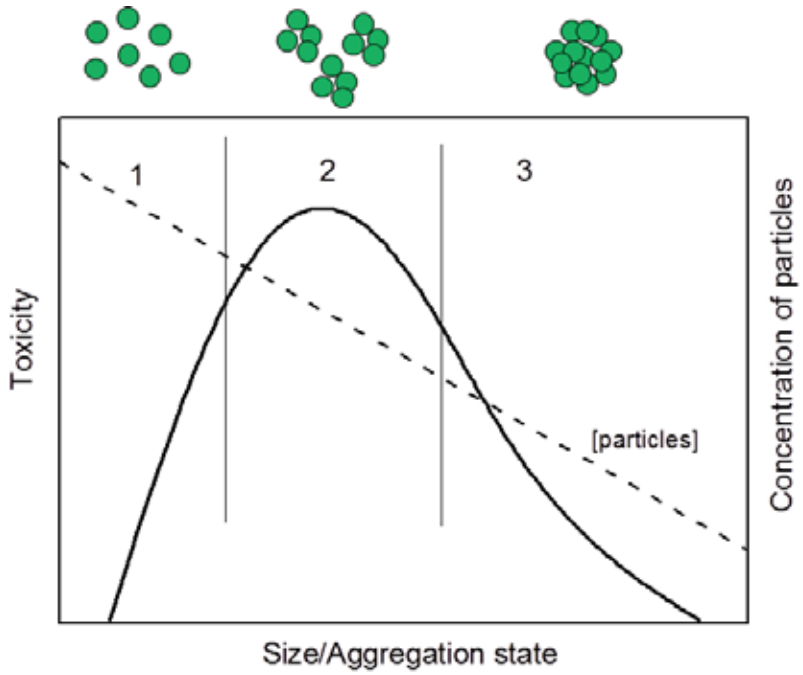

Figure 1.2. *The dependence of toxicity on different aggregation degree of NPs (generated from similar initial concentration of NPs): (1) stable dispersion, (2) small aggregates (a lot) and (3) big aggregate (few).*

Despite of either the change in properties or the trigger of undesirable biological effects of NPs due to aggregation, the ability to control this behavior can bring a light to a variety of applications including electronic and optical devices as well as biosensors. The color change that results from aggregation of metal NPs (gold, silver) has been exploited to develop colorimetric-based assays for detection of different species including DNA and bacterial toxins[19-21]. In comparison to little enhancement yielded by single particles, remarkable SERS enhancement was observed for silver aggregates with multiple NPs due to the enormous electromagnetic field at junction sites (hot spots)[22]. Gold NP aggregate was found to easily bind to and give a large SERS enhancement of 10^7-10^9 for R6G (Rhodamine 6G) which is generally difficult to be detected on gold substrates[23].

1.1.2. Adsorption of biomolecules

The adsorption of biomolecules, such as proteins, is of high interest and physiological relevance since both intravenous administration and environmental release of

nanomaterials increase. Most proteins are amphiphatic, i.e. they contain both polar and nonpolar residues giving them the possibility to interact with almost any surfaces that they are brought into contact. Therefore, when NPs are in biological media where biomolecules are often available, the interfacial interaction between them is unavoidable. Being named recently as protein corona (PC) formation, this process has indeed been aware of over decades or even centuries. Back to 1910´s, among the first to study protein adsorption at a solid-liquid interface, Biltz et al. reported the dependence of adsorbed amount to ferric oxide and kaolin on the protein concentration[24]. Later, in 1925, Hitchcock found a film of protein adhering to collodion membranes which altered the electrolytes diffusion properties of these bags and also observed that the adsorption of proteins follow Langmuir adsorption isotherm[25]. Nowadays, a vast number of researches and publications on different aspects of PC including its biological implication show the increasing awareness of the importance of this process.

The interfacial interaction between proteins and inorganic surfaces is a dynamic, competitive process (Vroman effect), first reported by Leo Vroman in 1962[26]. This effect postulated that proteins with higher mobility arrived first to the adsorbed surface and then they were replaced by less motile proteins that possess higher affinity. Particularly in serum, serum albumin, which is the most abundant protein and a natural carrier of small molecules, was found on the particles surface at the initial stage. However, over time, these albumins were replaced with proteins that are less abundant but have higher association rate constant, mainly factor V and fibrinogen[27]. Thus, PC is not a fix layer and its composition varies depending on the adsorption kinetic of each biological macromolecules. The biomolecules layer formed at the initial stage is called ´soft´ corona, and this layer will evolve with time up to hours to a more stable one so-called ´hard´ corona[9]. ´Soft´ corona is also used to indicate a loosely bound outer layer of biomolecules which interact weakly to NPs with hard corona[28]. In this case, ´soft´ corona proteins interact with the ´hard´ corona via weak protein-protein interactions of serum proteins and immobilized proteins.

From the NP aspect, various parameters including NP size, shape, surface charge, surface coating, hydrophobicity and composition can affect the formation of PC either in composition or conformation of proteins[29]. Among them, hydrophobicity and surface charge are more significant than others since these factors directly influence the interaction in protein adsorption. Using gold surfaces modified with self-assembled monolayers (SAMs) consisted of alkyl chains with different terminal groups, Prime and Whitesides pointed out that the higher the hydrophobicity of gold surface was, the more proteins adsorbed[30]. It has been reported that the protein adsorption also increased with the increasing of surface charge. Casals et al. observed the immediate formation of hard corona with positively charged AuNPs which was absent in the case of negatively charged NPs[9]. In the same study, the effect of NP size to PC formation was also investigated in which they found a size regime where a hard corona was formed. No complete PC was present if the NPs are too small (4nm) or big enough (40nm). Consistently, Dobrovolskaia et al. reported that 30nm AuNPs adsorbed more proteins than 50nm ones[31]. However, Cedervall et al. claimed that there was a distinct difference in the coverage extent of protein on copolymer NP surface between different sizes in which they found larger degree of protein coverage on larger NPs[32]. This conflict indicates the effect of NP composition to the PC formation. Moreover, NP material not only influences the adsorption extent but also the pattern of adsorption. Serum albumin was found to be the most abundant protein coated on single-walled carbon nanotubes (SWCNTs) but not on silica NP[33]. Meanwhile, different plasma proteins were identified on metal oxide NPs (TiO_2, SiO_2 and ZnO) of similar surface charge. For instance, transferrin was found on ZnO NP surface but not on the others[34]. It should be noted that, experimental challenges in this young field could be the reason for disparity.

In another aspect, the formation of PC is definitely affected by the media composition. Using Dulbecco´s Modified Eagle Medium (DMEM) and Roswell Park Memorial Institute (RPMI) medium, which contain varying amount of amino acid, glucose and salt, supplemented with Fetal Bovine Serum (FBS) to incubate the NPs, Maiorano et al. observed strongly different kinetics of protein adsorption between these two media[35].

Particularly, a more abundant and stable PC on AuNPs of different sizes was formed with DMEM in comparison with RPMI. Also, Dutta et al. reported the influence of protein source where they found albumin as the major fetal bovine or human serum/plasma protein adsorbed onto SWCNTs, while a distinct adsorbed protein profile was observed when using plasma from the Nagase analbuminemic rat[33]. While other physicochemical factors have been studied deeply, a parameter that is usually ignored but recently investigated is temperature at which the PC formation occurs. This ignored factor is very important for the *in vivo* applications of NPs where the body temperature can vary depending on body state. It has been shown that heat inactivation of proteins (preheating at 56^{o}C) can change the composition of PC[36]. Mahmoudi and his group probed the effect of incubation temperature on the PC of magnetic FePt NPs and found that the degree of protein coverage as well as the composition of the adsorbed proteins on the NPs' surface varied with temperature.

An issue which is worth to mention is that unavoidable biomolecules adsorption on NPs in biological media will give the NPs a new biological identity. This biological identity is what is really ´seen´ by cells and determines the physiological response of NPs including cellular uptake, biodistribution and toxicity. Particularly, adsorbing proteins (i) may improve the biocompatibility of NPs which could result in their detoxification; (ii) may either facilitate the uptake of coated materials by the presence of certain proteins (opsonins) which determine NP recognition by cells or inhibit it due to loss of adsorbed protein conformation; (iii) may direct and target the NP to a particular site. For example, it has been observed that toxicity of graphene oxide to human cells was mitigated by incubating it with FBS proteins[37]. Similarly, reactive oxygen species (ROS) production, an acute cellular response, by THP-1 (human monocytic) cells was found to be reduced in CoO NPs preincubated in complete cell culture media respect to the non-preincubated ones[38]. The adsorption of SP-A (Surfactant protein A), a lung protein, on magnetite NPs was found to enhance their uptake by macrophages[39] while the uptake of carboxyl-functionalized FePt NPs by HeLa cells was strongly suppressed with the adsorption of human transferrin[40]. In addition, it has been proposed that the binding of certain apolipoproteins to the

surface of the NP can assist them in crossing the blood brain barrier (BBB) to enter the brain via receptor-mediated mechanism[41]. Therefore, the effects of NPs in contact with biological systems have to be investigated in parallel with their PC formation.

1.1.3. Dissolution

Oxidative dissolution or corrosion is a common process that we usually observe in normal life as the formation of iron rust. Generally, this process is a gradual destruction of materials by chemical reaction with their surroundings. In solution, dissolution involves the migration of constituent components of the dissolving materials from their surface to the solution. Thus, concentration gradient is considered as the driving force for this dynamic process. NPs, which are thermodynamically unstable, can undergo chemical dissolution if kinetic restrictions (e. g., a non-solvent-soluble surface coating) are absent. Due to their reduced size, NPs possess large specific surface area, high radii of curvature what corresponds to low coordinated atoms at the surface which enhances their dissolution in comparison with the respective bulk material. While this process is usually negligible for Au, it shows high importance for less stable NPs including Ag and CdSe. In biological environments, NPs corrosion can effectively influence their persistence and also results in the release of ionic species that may be toxic themselves. As a result, from a nanotoxicological point of view, the answer to which the real culprit for the induced effect is has been still a challenge. Therefore, it is crucial to determine the extent of dissolution as well as the relative contribution of both NPs and dissolved species to comprehensively understand the potential biological effects of NPs.

Several factors that can affect the dissolution of NP in biological media include physicochemical properties of NP (size, shape, surface coating, crystallinity, etc.) and the nature of the media (protein content, ionic strength, pH). Among them, NP size is considered as the primary one in which it is generally assumed that reduction in particles size may increase their solubility. For CuO NPs, there have been sufficiently experimental data showing an increase in dissolution when decreasing the NP size[42-43]. Similar tendency of size effect was observed in the case of AgNPs[44]. Nevertheless, no

significant difference in dissolution between nano and bulk ZnO NPs were noted in either algal test medium[45] or Osterhout´s medium[42]. Surface-chemistry has been shown to considerably alter the NP solubility wherein the capping agents have been found to affect the dissolution of NPs. When being exposed to natural river water, the amount of ion released from bare or citrate-coated AgNPs after 15 days was equal to the amount released by Tween-stabilized NPs only after 6h[7]. McLeod and his group suggested in their study that stable surface coatings might decrease the probability for ZnO NPs to dissolve in biological media[46]. Apart from the intrinsic properties of the NPs, the characteristics of the exposure media also affect the dissolution of NPs in a more often way of changing their suspension stability which may lead to aggregation resulted in reduced surface area. ZnO NPs were found to dissolve in RPMI-1640 at the extent of 5mg/L, while this number exceeded 34mg/L when the NPs were exposed to DMEM[47]. In addition, the presence of organic matters can enhance the dissolution of NP with media through complexation with free ions. Indeed, ion release from CuO NPs in LB (Luria-Bertani) broth, a popular medium for bacteria growth, is strongly enhanced by the presence of organic tryptone and yeast extract[43]. Wang et al. reported the pH-dependent NP dissolution where CuO NP dissolved at lysosomal pH (4-5), but not at neutral pH of pure water. However, in near-neutral cell culture medium, the authors observed a significant dissolution of the NPs due to the ligand-assisted ion release contributed with the amino acid complexation[48]. Similarly, AgNPs dissolution was also increased by the presence of cysteine[49].

As mentioned previously, metal ions themselves may produce the observed biological effects. For instance, ingestion of copper salt can lead to hepatic necrosis, a characteristic of copper poisoning; Cu (II) and Fe (III) can cause DNA damage; lipid peroxidation is elevated with exposure to Cadmium (Cd^{2+}); ionic Ag and Zn are found to be toxic to bacteria, etc. Therefore, NPs as a reservoir of cations are potentially toxic to organisms and environment. Indeed, bactericidal effect of AgNPs was reported to be in correlation with the amount of Ag^{+} released [50]. The intracellular oxidation and toxicity of CdSe quantum dots (QDs) was due to the release of Cd ions[51]. Interestingly, on the other hand, Larsen et al. showed the extracellular ion release of Au, an *inert*

metal, from surface of metallic gold implants reduced microgliosis, neuronal apoptosis and increased neural stem cell response after a brain injury[52]. This indicates that NP dissolution, better known for its side effect, can be exploited for applications. Clearly, increasing awareness of NPs dissolution in biological media helps to interpret better their biological response. Therefore, assessing dissolution and speciation is crucial and should be taken into account. However, there are challenges in assessment of dissolution of NPs including i) separation of dissolved species from the particles as well as species from each other due to the complexity of biological environment and ii) available techniques to measure dissolution. Therein, separation of NP from dissolved component is important since ineffective separation can lead to over/under representation of NP dissolution.

1.2. Characterization of nanoparticles: needs and challenges

Characterization, followed by synthesis, is a crucial stage in material preparation and indispensable in materials scientists´ dictionary. With it, materials scientists are able to unveil the properties of the materials to know if their synthesis was successful and reproducible. In addition, characterization is essential in providing information on the stability/reactivity of the materials and as a consequence, their safety. In this sense, characterization is not only needed in material science, but also in other sciences including biology, medicine and toxicology where the materials are applied.

Over decades, biologists and toxicologists keep using nanoparticles considering them as stable materials that experience no changes in their state or properties over processing and storage. Most of researches in biology or toxicology have been done using the nanoparticles as received from either commercial suppliers or collaborative nanotechnologists without re-examining their characteristics. The fact that nanoparticle properties may change when being aged with time or moved from one environment to another is too often ignored. Moreover, pre-treatments of the nanomaterials prior to the test such as sonication, UV-sterilization, which are used by

toxicologists, may alter the structure or the stability of the material. For instance, primary carbon nanotubes were found to be broken into much smaller units via sonication[53]. In this way, studies using such technique to resuspend the nanomaterials may have reported results on something totally different, unless the treated materials were characterized when and during being used. Krug and Wick pointed out that, for nanotoxicological researches, the quality of studies cannot be ensured unless two major aspects are considered: the investigated nanomaterials must be sufficiently characterized beforehand and the selected test methods must be validated[54].

The essential characterization not only applies for the pristine nanoparticles where size, shape and surface properties are usually determined, but also for their evolution with time and their stability in the storage and experimental media. Regarding medical applications, when being brought into the bloodstream, the precise form of the nanoparticles is still considered as a black box. In fact, it is not until the materials in these conditions are fully characterized that a nanomaterial-containing drug can be approved for administration[55]. Nanoparticles, with high surface energy, are extremely reactive. Therefore, without proper design, under the interactions with environment, the nanoparticles are ready to undergo changes as a function of time (as described in section 1.1). In another word, particles´ properties may have a lifetime and being able to follow their time dependence is needed to understand the reactivity and biological response of the particles. However, studies on biological response of nanomaterials which couple with the corresponding evolution of the materials are still rare[56]. Nevertheless, scientists, especially biologists who are applying the nanoparticles in biological media, have been increasingly aware of how important the adequate characterization for these materials is. This is due to a fact that inadequate characterization might result in conflicting results and/or misleading conclusions regarding nanoparticle behavior and reactivity. Renwick et al. showed the size effect to toxicity of nano-carbon black and nano-TiO_2 reporting that the nanomaterials were toxic while the corresponding bulk materials might not be when they were exposed directly into the rat lungs[57]. Working on the same materials, Barlow et al. reported only minor differences between small and large size in response to the L-2 type II cells

without providing the characterization of the materials either pristine or exposed to the medium[58].

It is clear that characterization for nanomaterials during their life cycle from creation through usage to disposal is important and vital for nanotechnology. However, on the viewpoint of toxicology, since the key characteristics that impact the toxicity of nanomaterials are not yet completely clarified, a consistent characterization is still missing, i. e. different studies give various characteristics of the materials. With this urge, specific groups have been established to examine characterization needs for nanostructured materials including the International Organization of Standards (ISO) Technical Committee (TC) 229 on Nanotechnology[59]. A list of the most crucial properties needed to be measured, particularly in association with toxicology studies has been identified (Table 1.1.) [60]. Nevertheless, with remarkable progress has been made in characterizing techniques, more and better characterization is expected for the nanomaterials.

Table 1.1. *Recommended minimum physical and chemical parameters for characterizing nanomaterials in toxicology studies* [60]

Interaction of nanoparticles with biological medium
What does the material look like? • Particle size/size distribution • Agglomeration state/aggregation • Shape What is the material made of? • Overall composition (including chemical composition and crystal structure) • Surface composition • Purity (including levels of impurities) What factors affect how a material interacts with its surrounding? • Surface area • Surface chemistry, including reactivity, hydrophobicity • Surface charge Overarching considerations to take into account when characterizing engineered nanomaterials in toxicity studies: • Stability – how do material properties change with time (dynamic stability), storage, handling, preparation, delivery, etc.? Include solubility, and the rate of material release through dissolution • Context/media – how do material properties change in different media; i.e., from the bulk material to dispersions to material in various biological matrices? (¨as administered¨ characterization is considered to be particularly important) • Where possible, materials should be characterized sufficiently to interpret the response to the amount of material against a range of potentially relevant dose metrics, including mass, surface area and number concentration.

1.3. Designing of nanoparticles

It is a fact that the NPs undergo transformation in biological media which in some case lead to unexpected changes on their original properties and identity, and the NPs then cannot execute their aimed mission. Understanding these transformations not only help to better interpret NP biological effect and fate as pointed out previously, but also assist in designing proper NPs for certain aims. For instance, to prevent undesired aggregation in a high ionic strength medium due to charge screening, sterically stabilized NPs should be used instead of the ones with electrostatic stabilization. In addition, strongly binding molecules which can form a dense layer generally stabilize the NPs better than weakly binding ones. In physiological conditions, NPs are ready to be coated with plasma proteins whose conformation could be altered due to the interaction and contribute to disease pathogenesis. Opsonization of NPs with specific functional group at their surface may result in nonspecific binding to receptors at cell surfaces. Additionally, dissolution of NPs in most of cases has been identified as the main mechanism for their toxicity. Therefore, the concept ´safe-by-design´, to produce more biocompatible nanomaterials, has been increasing aware of and applied. Several strategies have been proposed: i) coating NPs with suitable polymers such as polyethylene glycol (PEG) to prevent aggregation and their direct interaction with biomolecules[61]; ii) passivating NP surface to prevent ion release from the core[62] and iii) doping NPs to change the electronic structure and alleviate their dissolution potential[63].

In the same context of designing safer NPs, one must also take into account that the used NPs may be contaminated with toxins and the observed biological effect may not originate from the NPs or their transformation solely. It is reported by Vallhov et al. that AuNPs contaminated with lipopolysaccharides (LPS), naturally abundant endotoxins found in outer membrane of Gram-negative bacteria, can stimulate dendritic cells leading to increased expression of co-stimulatory molecules and production of cytokines[64]. Furthermore, by modifying the preparation procedure to produce cleaner AuNPs, they found a low impact on the functionality of the cells making them more suitable for medical applications. Thus, depending on the desired

function of NPs, the proper design of NP synthesis should be included. In this thesis, attempts to fabricate NPs with better resistance in biological media were done and will be discussed mainly in chapter 3 and 4.

References

1. Murthy, S. K., Nanoparticles in modern medicine: State of the art and future challenges. *International Journal of Nanomedicine* **2007,** *2* (2), 129-141.

2. Zhang, L.; Gu, F. X.; Chan, J. M.; Wang, A. Z.; Langer, R. S.; Farokhzad, O. C., Nanoparticles in medicine: Therapeutic applications and developments. *Clinical Pharmacology & Therapeutics* **2008,** *83* (5), 761-769.

3. Jain, P. K.; Huang, X. H.; El-Sayed, I. H.; El-Sayed, M. A., Noble Metals on the Nanoscale: Optical and Photothermal Properties and Some Applications in Imaging, Sensing, Biology, and Medicine. *Accounts of Chemical Research* **2008,** *41* (12), 1578-1586.

4. Babu, A.; Templeton, A. K.; Munshi, A.; Ramesh, R., Nanoparticle-Based Drug Delivery for Therapy of Lung Cancer: Progress and Challenges. *Journal of Nanomaterials* **2013**.

5. Bastus, N. G.; Casals, E.; Vazquez-Campos, S.; Puntes, V., Reactivity of engineered inorganic nanoparticles and carbon nanostructures in biological media. *Nanotoxicology* **2008,** *2* (3), 99-112.

6. Sakura, T.; Takahashi, T.; Kataoka, K.; Nagasaki, Y., One-pot preparation of mono-dispersed and physiologically stabilized gold colloid. *Colloid and Polymer Science* **2005,** *284* (1), 97-101.

7. Li, X.; Lenhart, J. J.; Walker, H. W., Aggregation Kinetics and Dissolution of Coated Silver Nanoparticles. *Langmuir* **2012,** *28* (2), 1095-1104.

8. Xia, T.; Kovochich, M.; Brant, J.; Hotze, M.; Sempf, J.; Oberley, T.; Sioutas, C.; Yeh, J. I.; Wiesner, M. R.; Nel, A. E., Comparison of the abilities of ambient and

manufactured nanoparticles to induce cellular toxicity according to an oxidative stress paradigm. *Nano Letters* **2006,** *6* (8), 1794-1807.

9. Casals, E.; Pfaller, T.; Duschl, A.; Oostingh, G. J.; Puntes, V., Time Evolution of the Nanoparticle Protein Corona. *Acs Nano* **2010,** *4* (7), 3623-3632.

10. Stebounova, L. V.; Guio, E.; Grassian, V. H., Silver nanoparticles in simulated biological media: a study of aggregation, sedimentation, and dissolution. *Journal of Nanoparticle Research* **2011,** *13* (1), 233-244.

11. Casals, E.; Gonzalez, E.; Puntes, V. F., Reactivity of inorganic nanoparticles in biological environments: insights into nanotoxicity mechanisms. *Journal of Physics D-Applied Physics* **2012,** *45* (44).

12. Rechberger, W.; Hohenau, A.; Leitner, A.; Krenn, J. R.; Lamprecht, B.; Aussenegg, F. R., Optical properties of two interacting gold nanoparticles. *Optics Communications* **2003,** *220* (1-3), 137-141.

13. Li, J.; Huang, Y.; Liu, X. D.; Lin, Y. Q.; Bai, L.; Li, Q., Effect of aggregates on the magnetization property of ferrofluids: A model of gaslike compression. *Science and Technology of Advanced Materials* **2007,** *8* (6), 448-454.

14. Rosicka, D.; Sembera, J., Influence of structure of iron nanoparticles in aggregates on their magnetic properties. *Nanoscale Research Letters* **2011,** *6*.

15. Jassby, D.; Budarz, J. F.; Wiesner, M., Impact of Aggregate Size and Structure on the Photocatalytic Properties of TiO2 and ZnO Nanoparticles. *Environmental Science & Technology* **2012,** *46* (13), 6934-6941.

16. Nel, A.; Xia, T.; Madler, L.; Li, N., Toxic potential of materials at the nanolevel. *Science* **2006,** *311* (5761), 622-627.

17. Tripathy, N.; Hong, T. K.; Ha, K. T.; Jeong, H. S.; Hahn, Y. B., Effect of ZnO nanoparticles aggregation on the toxicity in RAW 264.7 murine macrophage. *Journal of Hazardous Materials* **2014,** *270*, 110-117.

18. Albanese, A.; Chan, W. C. W., Effect of Gold Nanoparticle Aggregation on Cell Uptake and Toxicity. *Acs Nano* **2011,** *5* (7), 5478-5489.

19. Mirkin, C. A.; Letsinger, R. L.; Mucic, R. C.; Storhoff, J. J., A DNA-based method for rationally assembling nanoparticles into macroscopic materials. *Nature* **1996,** *382* (6592), 607-609.

20. Sastry, M.; Lala, N.; Patil, V.; Chavan, S. P.; Chittiboyina, A. G., Optical absorption study of the biotin-avidin interaction on colloidal silver and gold particles. *Langmuir* **1998,** *14* (15), 4138-4142.

21. Schofield, C. L.; Haines, A. H.; Field, R. A.; Russell, D. A., Silver and gold glyconanoparticles for colorimetric bioassays. *Langmuir* **2006,** *22* (15), 6707-6711.

22. Michaels, A. M.; Jiang, J.; Brus, L., Ag nanocrystal junctions as the site for surface-enhanced Raman scattering of single Rhodamine 6G molecules. *Journal of Physical Chemistry B* **2000,** *104* (50), 11965-11971.

23. Schwartzberg, A. M.; Grant, C. D.; Wolcott, A.; Talley, C. E.; Huser, T. R.; Bogomolni, R.; Zhang, J. Z., Unique gold nanoparticle aggregates as a highly active surface-enhanced Raman scattering substrate. *Journal of Physical Chemistry B* **2004,** *108* (50), 19191-19197.

24. Neurath, N.; Bull, H. B., The surface activity of proteins. *Chemical Reviews* **1938,** *23* (3), 391-435.

25. Hitchcock, D. I., Protein films on collodion membranes. *Journal of General Physiology* **1925,** *8* (2), 61-74.

26. Vroman, L., Effect of Adsorbed Proteins on Wettability of Hydrophilic and Hydrophobic Solids. *Nature* **1962,** *196* (4853), 476-&.

27. Dell'Orco, D.; Lundqvist, M.; Oslakovic, C.; Cedervall, T.; Linse, S., Modeling the Time Evolution of the Nanoparticle-Protein Corona in a Body Fluid. *Plos One* **2010,** *5* (6).

28. Lundqvist, M.; Stigler, J.; Cedervall, T.; Berggard, T.; Flanagan, M. B.; Lynch, I.; Elia, G.; Dawson, K., The Evolution of the Protein Corona around Nanoparticles: A Test Study. *Acs Nano* **2011,** *5* (9), 7503-7509.

29. Mahmoudi, M.; Lynch, I.; Ejtehadi, M. R.; Monopoli, M. P.; Bombelli, F. B.; Laurent, S., Protein-Nanoparticle Interactions: Opportunities and Challenges. *Chemical Reviews* **2011,** *111* (9), 5610-5637.

30. Prime, K. L.; Whitesides, G. M., Self-Assembled Organic Monolayers - Model Systems for Studying Adsorption of Proteins at Surfaces. *Science* **1991,** *252* (5009), 1164-1167.

31. Dobrovolskaia, M. A.; Patri, A. K.; Zheng, J. W.; Clogston, J. D.; Ayub, N.; Aggarwal, P.; Neun, B. W.; Hall, J. B.; McNeil, S. E., Interaction of colloidal gold nanoparticles with human blood: effects on particle size and analysis of plasma protein binding profiles. *Nanomedicine-Nanotechnology Biology and Medicine* **2009,** *5* (2), 106-117.

32. Cedervall, T.; Lynch, I.; Lindman, S.; Berggard, T.; Thulin, E.; Nilsson, H.; Dawson, K. A.; Linse, S., Understanding the nanoparticle-protein corona using methods to quantify exchange rates and affinities of proteins for nanoparticles. *Proceedings of the National Academy of Sciences of the United States of America* **2007,** *104* (7), 2050-2055.

33. Dutta, D.; Sundaram, S. K.; Teeguarden, J. G.; Riley, B. J.; Fifield, L. S.; Jacobs, J. M.; Addleman, S. R.; Kaysen, G. A.; Moudgil, B. M.; Weber, T. J., Adsorbed proteins influence the biological activity and molecular targeting of nanomaterials. *Toxicological Sciences* **2007,** *100* (1), 303-315.

34. Deng, Z. J.; Mortimer, G.; Schiller, T.; Musumeci, A.; Martin, D.; Minchin, R. F., Differential plasma protein binding to metal oxide nanoparticles. *Nanotechnology* **2009,** *20* (45).

35. Maiorano, G.; Sabella, S.; Sorce, B.; Brunetti, V.; Malvindi, M. A.; Cingolani, R.; Pompa, P. P., Effects of Cell Culture Media on the Dynamic Formation of Protein-Nanoparticle Complexes and Influence on the Cellular Response. *Acs Nano* **2010,** *4* (12), 7481-7491.

36. Lesniak, A.; Campbell, A.; Monopoli, M. P.; Lynch, I.; Salvati, A.; Dawson, K. A., Serum heat inactivation affects protein corona composition and nanoparticle uptake. *Biomaterials* **2010,** *31* (36), 9511-9518.

37. Hu, W. B.; Peng, C.; Lv, M.; Li, X. M.; Zhang, Y. J.; Chen, N.; Fan, C. H.; Huang, Q., Protein Corona-Mediated Mitigation of Cytotoxicity of Graphene Oxide. *Acs Nano* **2011,** *5* (5), 3693-3700.

38. Casals, E.; Pfaller, T.; Duschl, A.; Oostingh, G. J.; Puntes, V. F., Hardening of the Nanoparticle-Protein Corona in Metal (Au, Ag) and Oxide (Fe3O4, CoO, and CeO2) Nanoparticles. *Small* **2011,** *7* (24), 3479-3486.

39. Ruge, C. A.; Kirch, J.; Canadas, O.; Schneider, M.; Perez-Gil, J.; Schaefer, U. F.; Casals, C.; Lehr, C. M., Uptake of nanoparticles by alveolar macrophages is triggered by surfactant protein A. *Nanomedicine-Nanotechnology Biology and Medicine* **2011,** *7* (6), 690-693.

40. Jiang, X.; Weise, S.; Hafner, M.; Rocker, C.; Zhang, F.; Parak, W. J.; Nienhaus, G. U., Quantitative analysis of the protein corona on FePt nanoparticles formed by transferrin binding. *Journal of the Royal Society Interface* **2010,** *7*, S5-S13.

41. Kreuter, J., Nanoparticulate systems for brain delivery of drugs. *Advanced Drug Delivery Reviews* **2001,** *47* (1), 65-81.

42. Mortimer, M.; Kasemets, K.; Kahru, A., Toxicity of ZnO and CuO nanoparticles to ciliated protozoa Tetrahymena thermophila. *Toxicology* **2010,** *269* (2-3), 182-189.

43. Gunawan, C.; Teoh, W. Y.; Marquis, C. P.; Amal, R., Cytotoxic Origin of Copper(II) Oxide Nanoparticles: Comparative Studies with Micron-Sized Particles, Leachate, and Metal Salts. *Acs Nano* **2011,** *5* (9), 7214-7225.

44. Liu, J. Y.; Sonshine, D. A.; Shervani, S.; Hurt, R. H., Controlled Release of Biologically Active Silver from Nanosilver Surfaces. *Acs Nano* **2010,** *4* (11), 6903-6913.

45. Franklin, N. M.; Rogers, N. J.; Apte, S. C.; Batley, G. E.; Gadd, G. E.; Casey, P. S., Comparative toxicity of nanoparticulate ZnO, bulk ZnO, and ZnCl2 to a freshwater

microalga (Pseudokirchneriella subcapitata): The importance of particle solubility. *Environmental Science & Technology* **2007,** *41* (24), 8484-8490.

46. Osmond-McLeod, M. J.; Osmond, R. I. W.; Oytam, Y.; McCall, M. J.; Feltis, B.; Mackay-Sim, A.; Wood, S. A.; Cook, A. L., Surface coatings of ZnO nanoparticles mitigate differentially a host of transcriptional, protein and signalling responses in primary human olfactory cells. *Part Fibre Toxicol* **2013,** *10*.

47. Reed, R. B.; Ladner, D. A.; Higgins, C. P.; Westerhoff, P.; Ranville, J. F., Solubility of nano-zinc oxide in environmentally and biologically important matrices. *Environ Toxicol Chem* **2012,** *31* (1), 93-99.

48. Wang, Z. Y.; von dem Bussche, A.; Kabadi, P. K.; Kane, A. B.; Hurt, R. H., Biological and Environmental Transformations of Copper-Based Nanomaterials. *Acs Nano* **2013,** *7* (10), 8715-8727.

49. Gondikas, A. P.; Morris, A.; Reinsch, B. C.; Marinakos, S. M.; Lowry, G. V.; Hsu-Kim, H., Cysteine-Induced Modifications of Zero-valent Silver Nanomaterials: Implications for Particle Surface Chemistry, Aggregation, Dissolution, and Silver Speciation. *Environ Sci Technol* **2012,** *46* (13), 7037-7045.

50. Morones, J. R.; Elechiguerra, J. L.; Camacho, A.; Holt, K.; Kouri, J. B.; Ramirez, J. T.; Yacaman, M. J., The bactericidal effect of silver nanoparticles. *Nanotechnology* **2005,** *16* (10), 2346-2353.

51. Derfus, A. M.; Chan, W. C. W.; Bhatia, S. N., Probing the cytotoxicity of semiconductor quantum dots. *Nano Lett* **2004,** *4* (1), 11-18.

52. Larsen, A.; Kolind, K.; Pedersen, D. S.; Doering, P.; Pedersen, M. O.; Danscher, G.; Penkowa, M.; Stoltenberg, M., Gold ions bio-released from metallic gold particles reduce inflammation and apoptosis and increase the regenerative responses in focal brain injury. *Histochem Cell Biol* **2008,** *130* (4), 681-692.

53. Glory, J.; Mierczynska, A.; Pinault, M.; Mayne-L'Hermite, M.; Reynaud, C., Dispersion study of long and aligned multi-walled carbon nanotubes in water. *Journal of Nanoscience and Nanotechnology* **2007,** *7* (10), 3458-3462.

54. Krug, H. F.; Wick, P., Nanotoxicology: An Interdisciplinary Challenge. *Angewandte Chemie-International Edition* **2011,** *50* (6), 1260-1278.

55. Cressey, D., Tiny traits cause big headaches. *Nature* **2010,** *467* (7313), 264-265.

56. Editorial, Join the dialogue. *Nat Nanotechnol* **2012,** *7* (9), 545-545.

57. Renwick, L. C.; Brown, D.; Clouter, A.; Donaldson, K., Increased inflammation and altered macrophage chemotactic responses caused by two ultrafine particle types. *Occup Environ Med* **2004,** *61* (5), 442-447.

58. Barlow, P. G.; Baker, A. C.; Donaldson, K.; MacCallum, J.; Stone, V., Carbon black nanoparticles induce type II epithelial cells to release chemotaxins for alveolar macrophages. *Part Fibre Toxicol* **2005,** *2* (11).

59. Baer, D. R., Surface characterization of nanoparticles: critical needs and significant challenges. *Journal of Surface Analysis* **2011,** *17* (3), 163-169.

60. Boverhof, D. R.; David, R. M., Nanomaterial characterization: considerations and needs for hazard assessment and safety evaluation. *Analytical and Bioanalytical Chemistry* **2010,** *396* (3), 953-961.

61. Owens, D. E.; Peppas, N. A., Opsonization, biodistribution, and pharmacokinetics of polymeric nanoparticles. *Int J Pharm* **2006,** *307* (1), 93-102.

62. Loza, K.; Diendorf, J.; Sengstock, C.; Ruiz-Gonzalez, L.; Gonzalez-Calbet, J. M.; Vallet-Regi, M.; Koller, M.; Epple, M., The dissolution and biological effects of silver nanoparticles in biological media. *J Mater Chem B* **2014,** *2* (12), 1634-1643.

63. Xia, T. A.; Zhao, Y.; Sager, T.; George, S.; Pokhrel, S.; Li, N.; Schoenfeld, D.; Meng, H. A.; Lin, S. J.; Wang, X.; Wang, M. Y.; Ji, Z. X.; Zink, J. I.; Madler, L.; Castranova, V.; Lin, S.; Nel, A. E., Decreased Dissolution of ZnO by Iron Doping Yields Nanoparticles with Reduced Toxicity in the Rodent Lung and Zebrafish Embryos. *Acs Nano* **2011,** *5* (2), 1223-1235.

64. Vallhov, H.; Qin, J.; Johansson, S. M.; Ahlborg, N.; Muhammed, M. A.; Scheynius, A.; Gabrielsson, S., The importance of an endotoxin-free environment

during the production of nanoparticles used in medical applications. *Nano Lett* **2006,** *6* (8), 1682-1686.

Chapter 2

BEHAVIORS OF SILVER NANOPARTICLES IN MODEL BIOFLUIDS

2.1. Introduction

Nowadays, with the fast development of nanotechnology, a huge amount of nanoparticles (NPs) are being investigated and produced purposely for many applications including daily use[1-2]. According to USEPA (United States Environmental Protection Agency), nanomaterials have been incorporated in more than 1000 consumer products (data recorded by 2010). This number is definitely still growing and it is estimated that by 2015, nanomaterial-containing consumer products will value 1 trillion dollars on the world market. Consequently, ineluctable human exposure to NPs is increasing. NPs can enter human body via different routes, either by inhalation, ingestion, injection or skin contact. The fate and biodistribution of a chemical substance in the body is known to be extremely dependent on the portal of entry. This is also true for NPs, even more since their chemical reactivity is high. Therefore, NPs will experience different stories depending on how they do enter inside the body.

We choosed to work with silver nanoparticles (AgNPs) since among thousands of nanomaterials, they are of high interest for the following reasons: i) they are metallic with a strong surface plasmon resonance (SPR) which allows to monitor their fate as well as their environment as SPR is sensitive to size, shape, surface and aggregation state and the surroundings of the NPs[3-4]; ii) they are chemically reactive as catalysts[5]

and iii) they participate in redox processes, and can be corroded to release Ag cations which are themselves biologically active. Consequently, owing mainly to their antibacterial and antimicrobial properties, AgNPs have been increasingly manufactured and incorporated in a variety of commercial products such as food-packaging, bandages, clothes and socks[6]. Therefore, many studies have been performed to determine possible toxicity of AgNPs in cells[7-10] and there is still an ongoing debate on whether the AgNPs, their aggregates or their ions take responsibility for the detected toxicity. While AgNPs was found to induce higher level of ROS than Ag ions[11], there are also evidences indicating that the ions are more toxic than the NPs themselves[12-13]. Meanwhile, in other experiments, the role of AgNPs on their toxicity was ruled out by performing experiments in a way to prevent the oxidative dissolution or ion release[14]. However, several studies suggested that the particular toxicity profile of AgNPs might be attributed to a ´Trojan horse´ effect where the NPs act as a source of ions and release them further inside the biological system[15-16] or in another word, the NP is a carrier of Ag^+ that is released depending on the chemical environment the NP encounters. Consequently, it is accepted that the final biological response to NPs depends to a large extent on their chemical and physical states which are altered when NPs are brought into contact with the biological media[17]. These alterations include aggregation, agglomeration, protein corona formation and corrosion[18].

Despite a great deal of publications on biological impact of AgNPs, NP state after inoculation and during exposure, what determines its pharmacokinetics/pharmacodynamics and biodistribution, still has not been fully addressed due to its inherent difficulty. Therefore, acquiring knowledge of how NPs behave in different media is inevitable to better understand their induced biological effects. Another output of this understanding is that it would be possible to design the NPs fate.

In this chapter, the transformations of AgNPs in contact with various simulated body fluids corresponding to different potential internalization routes were investigated. These are saliva, gastric fluid, intestinal fluid and colonic fluid via ingestion, lung fluid

via inhalation, synovial fluid and serum via injection, tear and sweat via eye and skin contact. These fluids are synthetic and have been used by the pharmaceutical industry for decades to study the introduction of drugs inside the body. The evolution of the NPs through incubation time is followed by UV-Visible, Zeta-potential and Transmission electron microscope (TEM). The combination of these simple methods allows us to preliminary determine the complex behavior of NPs with the fast screening of a large number of samples.

2.2. Materials and methods

Reagents: silver nitrate ($AgNO_3$, ACS reagent ≥ 99%), sodium citrate tribasic dihydrate ($Na_3C_6H_5O_7.2H_2O$), sodium borohydride ($NaBH_4$, ReagentPlus 99%) were purchased from Sigma-Aldrich. Milli-Q water with a resistivity of 18.2 mΩ.cm was used throughout the experiments.

Synthesis: Citrate-coated AgNPs with an average diameter of 12nm were synthesized using Creighton method with some modification[19]. In a typical experiment, a 49ml solution of trisodium citrate (0.25mM) and $AgNO_3$ (0.25mM) was prepared in MilliQ water, then followed by a fast injection of 1ml of ice-cold prepared 0.1M $NaBH_4$ under vigorous stirring. The obtained yellow colloid was stored at 4^oC for later use.

Exposure to the media: the exposure experiments were done basically as what described in previous works of our group[20]. In particularly, AgNPs were dispersed in different body fluids (1:10 by volume) and kept in an incubator at 37^oC for various incubation time which are 0hr, 4hrs, 8hrs, 24hrs, 32hrs and 48hrs. Time point t=0hr is considered as the one done without incubation. Simulated body fluids including saliva, gastric fluid, intestinal fluid, colonic fluid, lung fluid, tear, sweat and synovial fluid are prepared using the formulations described by Marques et al.[21], traditionally used in pharmacology to test biocompatibility of drugs, as references with some modification. A detailed composition for the preparation can be found in the Appendix. Meanwhile, serum was purchased from Sigma-Aldrich and thawed without heat-inactivation for later use.

Purification: To minimize interference from the media in the characterization step, centrifugation was carried out in a way that incubated solutions (1.5ml) were spun for 15mins at 35000g. The obtained pellet was re-suspended in 0.2ml deionized H_2O or 2.2mM sodium citrate to get a stable colloid of NPs. The supernatants were kept for further experiments. To eliminate the possibility of aggregation due to processing of the NPs, the pristine AgNPs was spinned down under the same conditions. The obtained NPs showed a good dispersion which is displayed in UV-Visible spectrum and TEM image (Figure 1). Therefore, any observed aggregation is only attributed to the impact of the environment onto the NPs.

Characterization: Various techniques were applied to characterize the NPs and to follow the time evolution of their physical and chemical changes.

UV-Visible Spectrophotometry: UV-Visible spectra were recorded with a Shimadzu UV-2400 spectrophotometer. 0.2ml of NP suspension was added to a disposable low volume cuvette and spectra were achieved with scanning in the wavelength range from 300-800nm. The baseline is done with the dispersant in where the NPs are. Plasmonic NPs, such as gold and silver, exhibit a characteristic absorption band in the visible range so called surface plasmon resonance (SPR). This SPR is sensitive to the changes at the surface of the NPs or the interface of the NPs and the surrounding. Therefore, UV-Visible spectroscopy is a useful and quick analytical technique for our study.

Z-potential measurement: Measurements were performed with a Malvern ZetaSizer Nano ZS instrument. Prior to measurement, the colloidal solution of AgNPs was 5-time diluted with the correspondent dispersant to attain sufficient volume. A volume of 0.8ml sample was filled into a clear disposable Zeta cell and the data were recorded with specific parameters of refractive index and absorption coefficient of the material (silver and protein) and the viscosity of the dispersant. The values reported are the mean of three consecutive measurements with a standard deviation representing the reproducibility of the measurement. Z-potential is a common technique to predict the colloidal stability of NPs by surface charge. Normally, particles with surface charge

more negative than -30mV or more positive than +30mV are considered electrostatic stable.

Transmission Electron Microscopy (TEM): TEM images were taken with a JEOL 1010 electron microscope operated at low accelerating voltage (80 kV). Samples for TEM were prepared by drop casting of 10µL of NPs suspension after purification onto carbon-coated TEM grids. The grids were evaporated at room temperature. The samples were observed at different parts of the grid and with different magnifications. To obtain the size distribution of used AgNPs, more than 200 particles were analyzed and measured. TEM was used not only to perceive the morphology and primary size in dry state but also to observe the aggregation state of the nanoparticles exposed to different biological fluids.

Dissolution study: Recovery of Ag from the supernatant using a strong reducing agent. These experiments aim to detect the presence of active silver ions in the supernatant after incubation which implies the release of silver ion or the dissolution of the NPs. Typically, 0.1ml of 0.01M $NaBH_4$ was added to 1ml of every supernatant obtained from the purification of the samples incubated at 0hr and 24hrs. The mixture then was also centrifuged at 35000g for 15mins. The pellet was re-suspended in 0.2ml deionized H_2O or 2.2mM sodium citrate and the UV-Visible spectra of these suspensions were performed.

2.3. Results and discussion

2.3.1. Characterization of used materials

The pristine prepared sodium citrate AgNPs exhibits a characteristic absorption band centered at 392nm in the UV-Visible spectrum (Figure 2.1A). The NPs are spherical as seen in the TEM image (Figure 2.1B). The size distribution of these NPs was computer analyzed using ImageJ software giving an average diameter of 12.6±3.2 nm (Figure 2.1C). With this size, the estimated concentration of NPs is 10^{12} NPs per ml of solution. These citrate-coated AgNPs are negatively charged with a Zeta-potential value of -38mV in the synthesis medium (2.2mM sodium citrate).

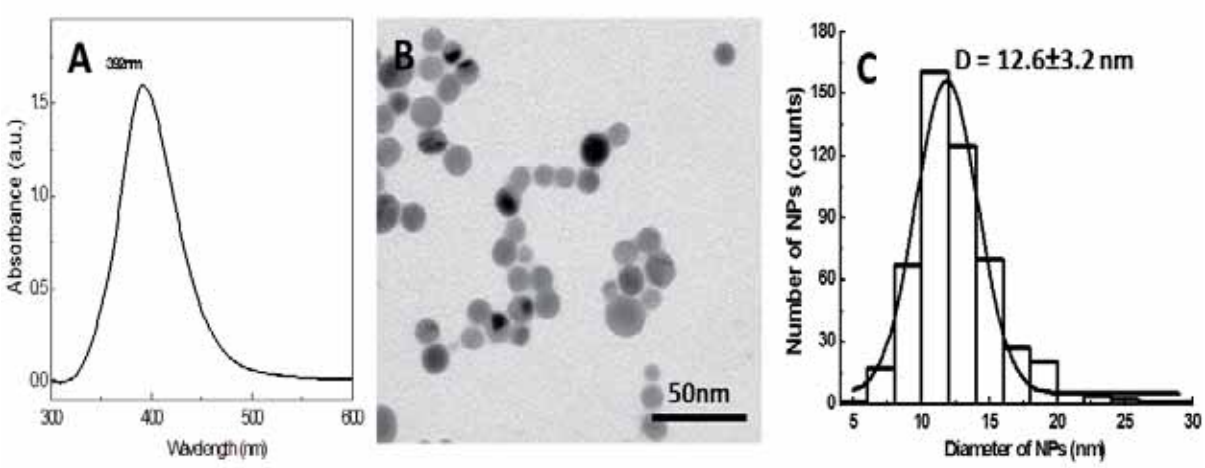

***Figure 2.1**. Characterization of citrate-coated AgNPs: (A) UV-Visible absorption spectrum, (B) TEM image and (C)histogram of size distribution obtained from computer processing of TEM images.*

The different media were prepared following pharmacological standards employed for the study of drug administration and pharmacokinetics[21].The main characteristics of these fluids including protein and saline content as well as pH are listed in Table 2.1 while their optical properties can be found in Figure 2.2.

Table 2.1. Main characteristics in composition of the fluids

Fluid	Protein concentration (mg/ml)	Others organic matters concentration (mg/ml)	Cl- concentration (mM)	Z-potential (mV)	pH
a. Saliva	3	0	21	-20.1	6.9
b. Gastric	1.515	0	154.2	-14.5	1.6
c. Intestinal	0	1.765	68.62	-5.91	6.5
d. Colonic	3	0.361	0	-15.8	7.8
e. Lung	15	0.2	112.8	-16	7.4
f. Synovial	15	3.2	139.4	-11.2	7.4
g. Serum	70	minor	100	-15.4	7.4
h. Tear	2.68	11.92	112.2	1.03	7.4
i. Sweat	0	0.01	40	1.97	4.9

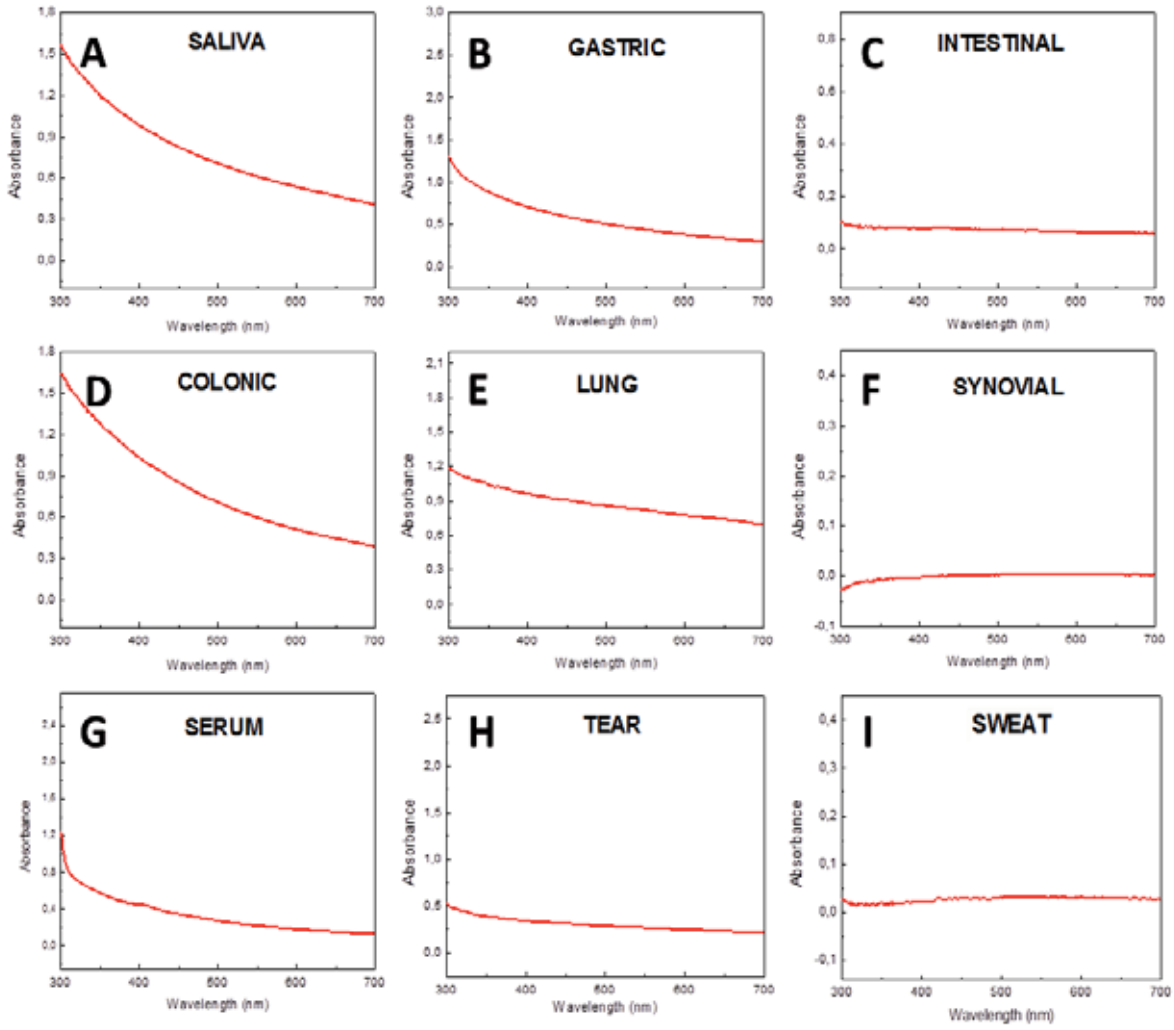

***Figure 2.2**. UV-Visible spectra of simulated body fluids: (A) saliva, (B) gastric fluid, (C) intestinal fluid, (D) colonic fluid, (E) lung fluid, (F) synovial fluid, (G) serum, (H) tear and (I) sweat.*

2.3.2. UV-Vis absorption of AgNPs vs. NP state

Once being brought into contact with a medium, NPs experience surface modifications (aggregation, protein adsorption, loose of atoms - dissolution) due to interactions between them and components from that medium. The NPs, to decrease their high surface energy, would go through dissimilar processes in different media. One should bear in mind that more than one process can happen at the same time and there might also be a competition between them. In fact, it is common to observe that NPs become unstable in the biological media and that they corrode while aggregate and

are coated by proteins, and then precipitate. Corrosion increases the ion concentration leading to aggregation[22], while aggregation, via total surface area decrease, reduces corrosion. What occur to the examined AgNPs in each investigated body fluids will be explored in this chapter focusing on i) biomolecules adsorption which readily happens in a protein-rich medium, ii) aggregation which takes place in highly saline media and iii) dissolution which is facilitated in reactive/oxidative environments.

For this purpose, we take advantage of the silver nanoparticle optical-plasmonic properties which are witnesses of their morphology, physical and chemical state and environment to track AgNP evolution with enough resolution. In general, the signatures of different states of the NP and their time evolution due to: i) aggregation (colloidal instability), ii) interaction with proteins and iii) dissolution and oxidation (chemical transformation) can be followed in the UV-Vis spectra as summarized in Figure 2.3 where theoretical plots and experimental results (in collaboration with Jordi Piella) for 20 and 50 nm spherical AgNPs corresponding to the different NP states are shown. It is true that the different optical response of the different NP states are highly convoluted, and only analysing the spectral evolution with time can the optical properties (peaks position and shape –Full width at half maximum (FWHM)-) be ascribed to the different NP composition (e. g. degree of oxidation), states and morphologies.

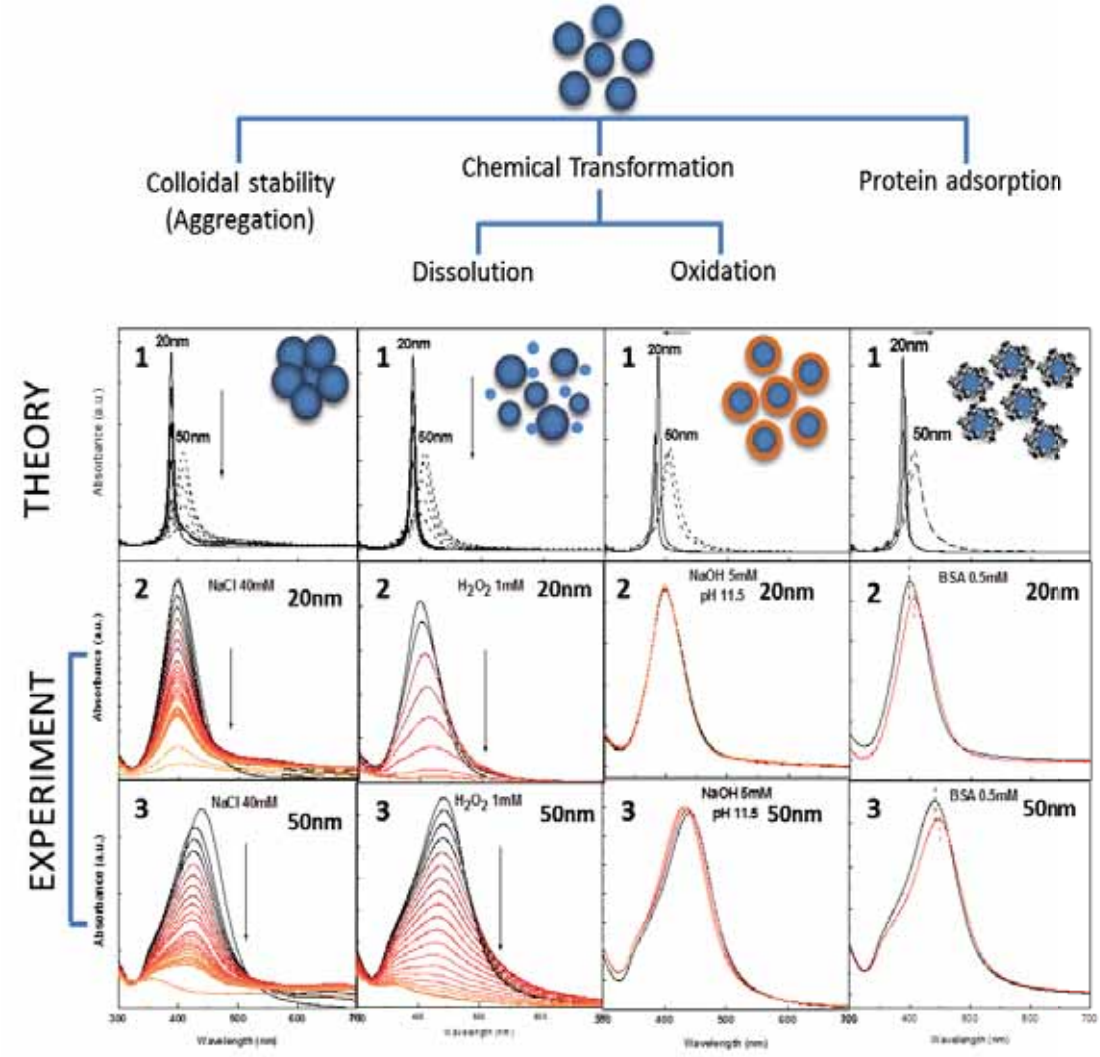

Figure 2.3. Observable modification of the UV-VIS spectra in different states of AgNPs*: Aggregation, Dissolution, Oxidation and Protein adsorption. These spectra were plotted theoretically (1) and experimentally (2-3) for AgNPs of 20nm (2) and 50nm (3). In which, aggregation study was done by exposing NPs (10^{12} NPs/ml) to 40mM NaCl while dissolution experiments were performed with H_2O_2 1mM and 2mM for 20nm and 50nm NPs, respectively. Additionally, oxidation of NPs was carried out in the presence of 5mM NaOH (pH 11.5). Finally, 0.5mM BSA was used in protein adsorption.*

Theoretical UV-Visible spectra of different NP states plotted using MiePlot software and MultiLayer NP simulation[23] showed different behaviours depending on NP state that in this work we use to monitor AgNP evolution. In the case of aggregation, a decrease in absorption intensity when the NPs aggregate heterogeneously, i. e.,

considering that the aggregation was slow and not all the particles aggregate at the same time (Figure 2.3), was observed. This is different then in the case of AuNPs where interaction leads to dramatic shifts and broadenings of the SPR peak due to the rapid decrease of the resonant absorption when the NPs aggregate. Additionally, an increase of the signal at lower energies (longer wavelengths) due to light scattering of large objects (above 50 nm), rather than just light absorption, also appears due to aggregation. Accordingly, the experimental temporal spectra obtained from exposing AgNPs of different sizes to 40mM NaCl exhibited a decrease in maximal absorption. They also displayed a shoulder in longer wavelengths (600-800nm) indicating the aggregation of the NPs. Alternatively, the aggregation can also be seen via an increase in size by Dynamic Light Scattering (DLS) as shown in Figure 2.4 and a drop in surface charge by Zeta-potential due to the charge screening that leads to aggregation. Protein corona (PC) formation (described in chapter 1) is observed with a modest peak shift (few nm) to longer wavelength while the peak shape is maintained. A small decrease in absorption intensity is also detected since the final object is larger and the extinction coefficient of larger NPs (in this range) is bigger[24]. Protein adsorption results in an increase in size by DLS (Figure 2.4) while the surface charge of the NPs evolves to the value of the protein. Using the same tool, theoretical UV-Visible absorption spectra of AgNPs with different sizes due to oxidation were also sketched. Contrary to a red-shift in the case of PC formation, a blue-shift is observed when the NPs are oxidized and generates a core-shell structure with an oxide layer as shell.

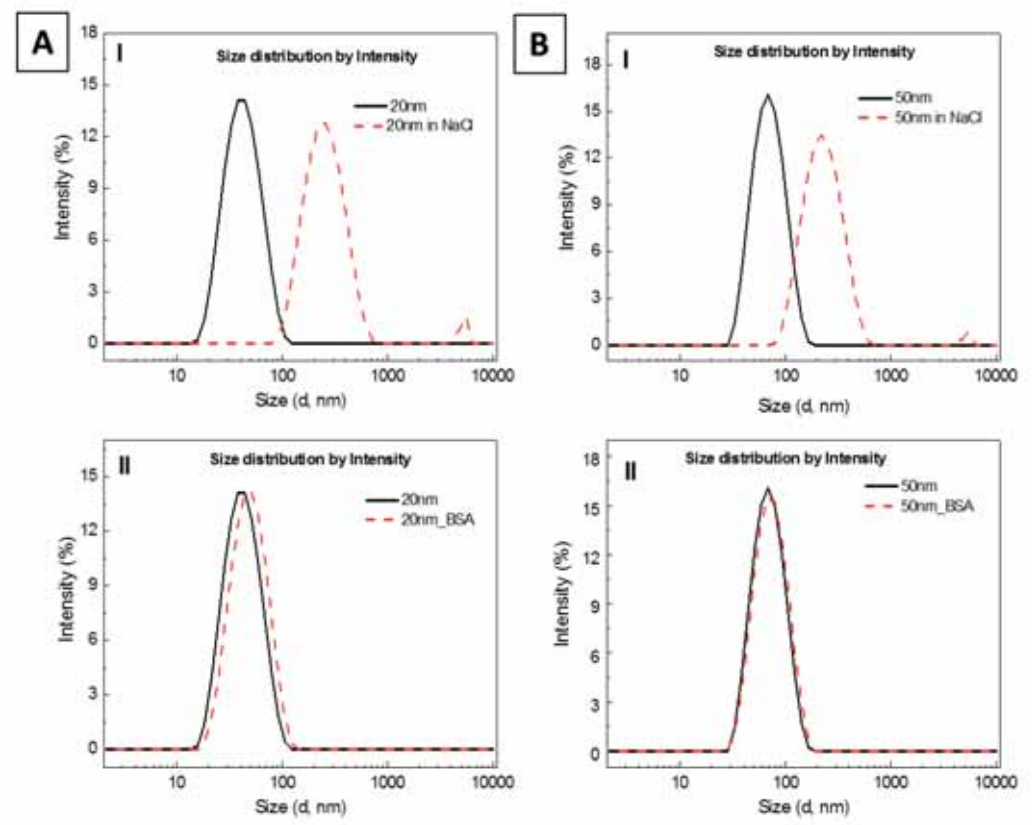

Figure 2.4. Changes in size distribution by Dynamic Light Scattering (DLS). *Size distribution by intensity of (A) 20nm and (B) 50nm AgNPs when being exposed to (I) 40mM NaCl for 30mins and (II) 0.5mM BSA at concentration of 10^{12} NPs/ml. DLS measurements were done with a Malvern Zetasizer Nano ZS Instrument operating at wavelength of 532nm as light source and 173^{o} as fixed scattering angle.*

Regarding dissolution, theoretical plots using MiePlot for AgNPs with different sizes demonstrated a decrease in peak absorbance over time. Additionally, a blue-shift was detected, more obviously in the case of larger NPs. Indeed, in a control experiment, the dissolution of AgNPs carried out by exposing them to H_2O_2 displayed the same damping in absorption intensity. An increase of the Full width at half maximum (FWHM) was also observed, attributed to Ostwald ripening occurring simultaneous to corrosion which resulted in the broadening of NP size distribution[25-26]. Ostwald ripening generates larger NPs that compensate the dissolution of others[27-28] impeding the observation of a net blue-shift as it would be expected in pure dissolving NPs, as discussed later.

The observed difference of behaviours becomes even more prominent when the UV-Visible spectra are measured as a function of time. i) Aggregation of NPs , once they are destabilized (e.g by screening of surface charge[29]), does never stop until the concentration of the NP is below the interaction limit (< 10^{10} NPs/ml)[30] since NPs have to meet in order to aggregate as mentioned in previous chapter. Therefore, the peak collapses once the aggregation of NPs grows too far and observable sedimentation occurs. In some cases, a residual signal may persist longer if the remaining unstable NPs are so diluted that they have no chance to meet and aggregate (below 10^{10} NPs/ml). Nevertheless, signal is often lost at these concentrations. In some few cases, NPs aggregation can be spontaneously stopped as the ratio of stabilizer versus NP surface increases during aggregation, this is however rare. ii) On the other side, if protein denaturation is not promoted (as it is in the most common cases) PC formation saturates quite fast and the protein stabilized NPs become very stable[20, 31]. Although small variations (a further red-shift) can be observed at longer times, they are no more than 10% of the initial red-shift. iii) Regarding dissolution as a function of time, it slows down as the number of NP ions increases in solution, and at some point stops when the solubility equilibrium is reached.

2.3.3. AgNPs in different body fluids

The UV-Visible spectra of AgNPs after being incubated in individual simulated body fluids for various periods of time are shown in Figure 2.5. In addition, time evolution of the maximal absorption (λ_{max}) is plotted in Figure 2.6.

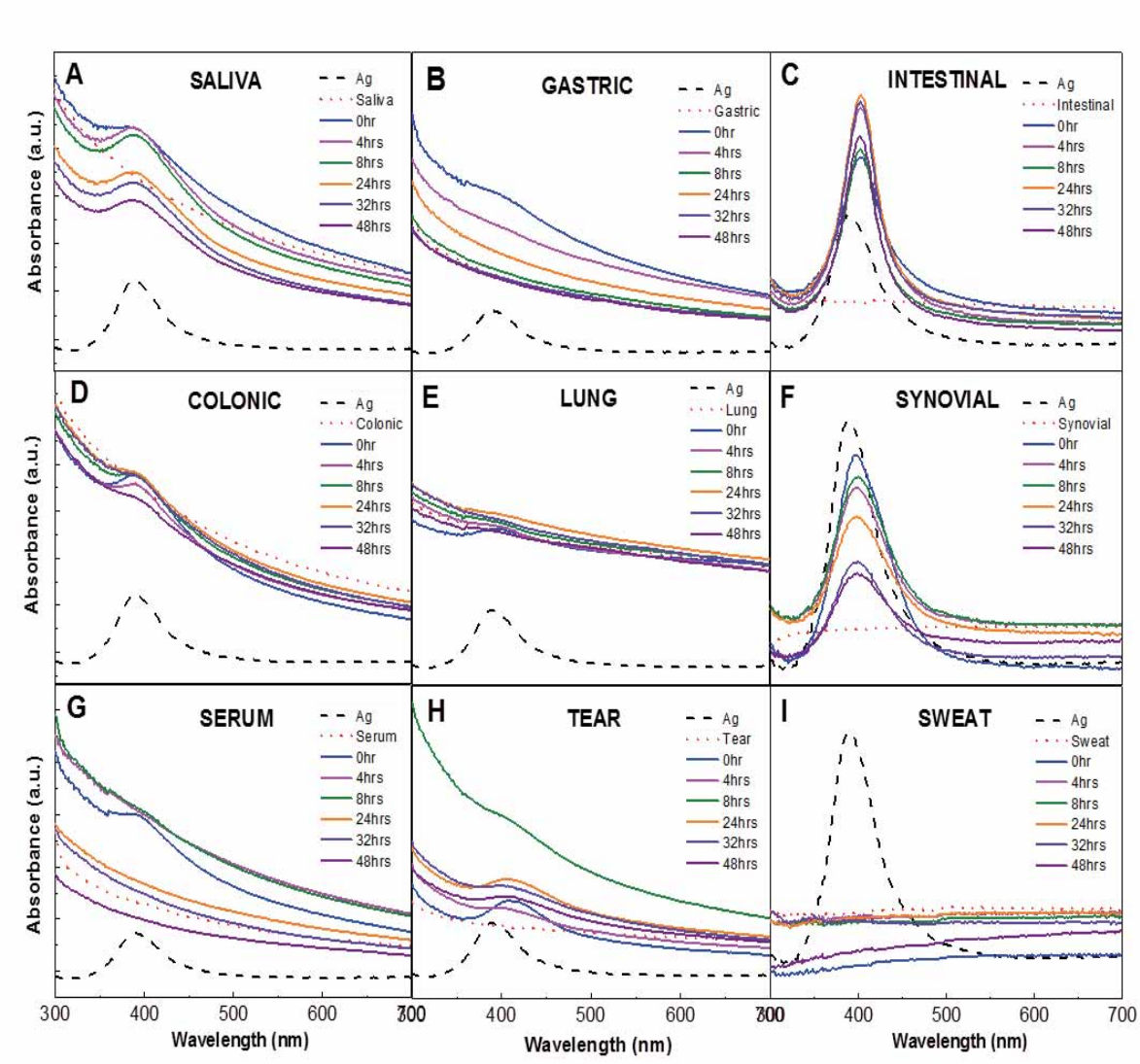

***Figure 2.5**. UV-Visible spectra of as-synthesized AgNPs (black dash curve), as-prepared fluids (red dash curve) and AgNPs after being exposed to simulated body fluids including (A) saliva, (B) gastric fluid, (C) intestinal fluid, (D) colonic fluid, (E) lung fluid, (F) synovial fluid, (G) serum, (H) tear and (I) sweat for different incubation times.*

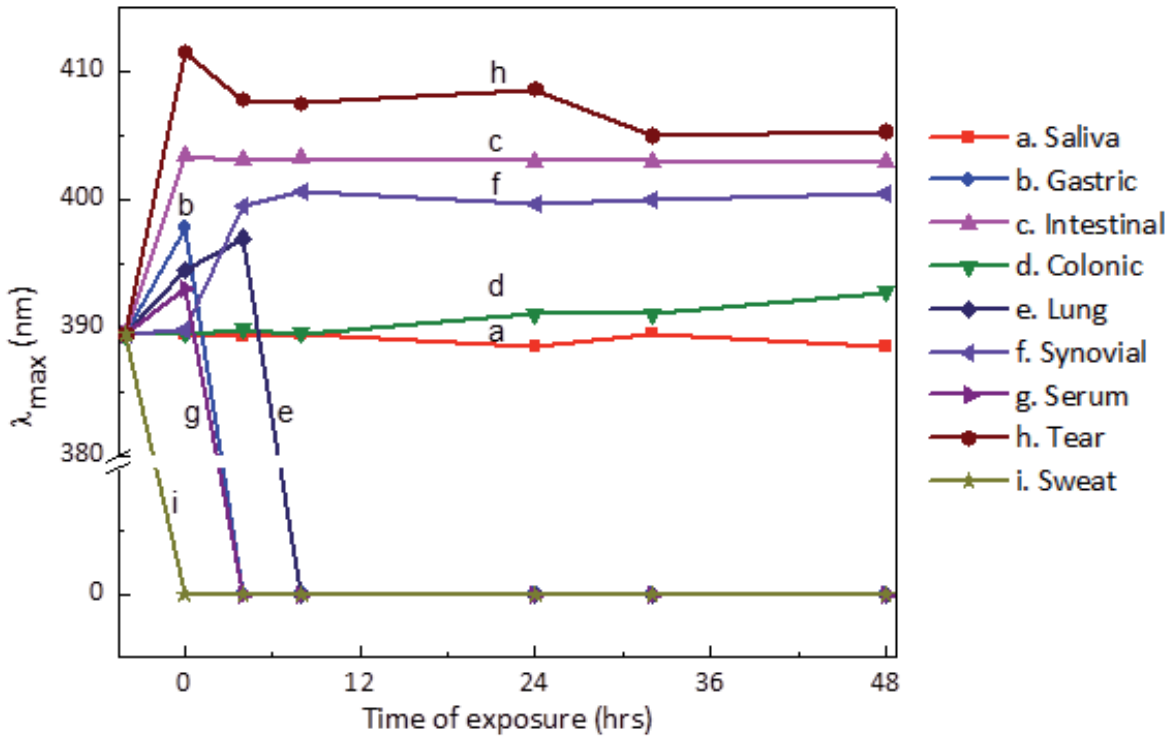

***Figure 2.6**. Time evolution of SPR absorption peak of AgNPs exposed to different body fluids a) saliva, b) gastric fluid, c) intestinal fluid, d) colonic fluid, e) lung fluid, f) synovial fluid, g) serum, h) tear and i) sweat. The flat lines in b, e, g and i mean absence of peak.*

2.3.3.1. Aggregation

As pointed out in chapter 1, there are several factors that cause the aggregation of colloidal NPs, for instance, initial concentration of NPs[32] and ionic strength of the medium (in the case of electrostatic stabilization), which is well described by the DLVO theory for colloidal stability[33-34]. The NPs concentration used in this study (10^{12} NP/ml) is similar to the one of gold nanoparticles reported previously which was proven to be stable in the tested conditions[20]. Hence, the aggregation detected here is due to the charge screening effect of salts or charge carriers in the media which causes a compression of the electrolytic double layer and a decrease in interparticle repulsion[34]. It is noticed that no aggregation occurred in media with high protein concentration including lung, synovial, serum and tear, despite the fact that they were highly saline fluids (the concentration of Cl^- is no lower than 100mM). The good dispersion of NPs in

these media can be seen in TEM images (Figure 2.7). Here, the stability of AgNPs was maintained thanks to the formation of proteins or organic molecule layers on their surface. In this case, the stabilizing mechanism changes from electrostatic to steric repulsion, and then the charge screening regarding colloidal stability becomes irrelevant.

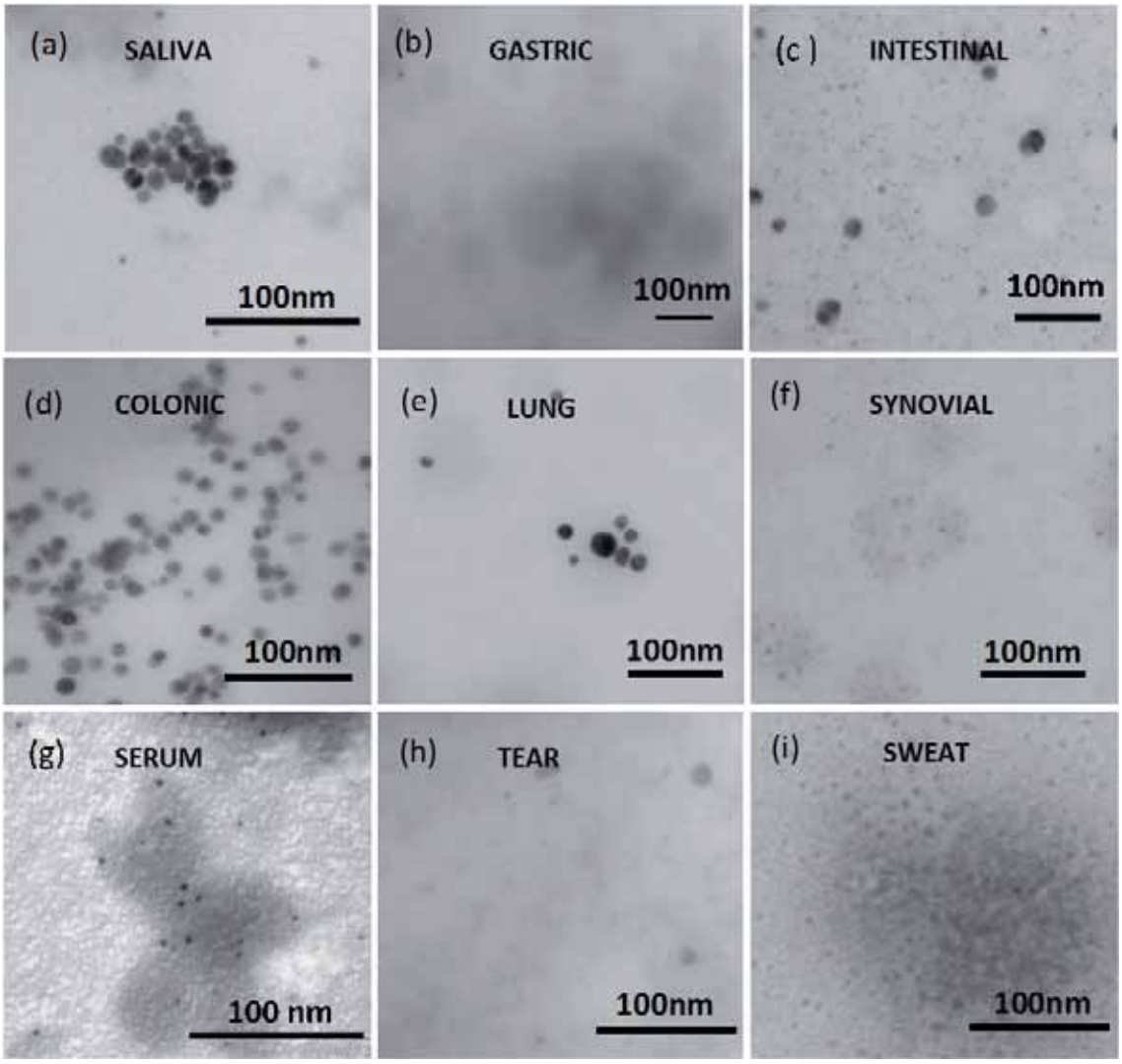

***Figure 2.7**. TEM images of silver nanoparticles after 24hrs of exposure in various body fluids (a) saliva, (b) gastric fluid, (c) intestinal fluid, (d) colonic fluid, (e) lung fluid, (f) synovial fluid, (g) serum, (h) tear and (i) sweat. The shadows observed on the TEM substrates correspond to organic matter residues.*

Moreover, it was reported previously that at the right concentrations, the coating of proteins on the NPs is faster than NPs aggregation[20]. Therefore, as expected, when the NPs were dispersed in sweat, a saline medium with very low organic matter content (Table 2.1), there was an instantaneous aggregation. This was shown by total vanishing of the plasmon band of AgNPs (Figure 2.5I) (also represented by λ_{max} =0 in Figure 2.6). Furthermore, the incubated NPs gave a low surface charge in this medium (Figure 2.8i) which is not enough to stabilize them electrostatically (absolute Zeta potential should be higher than 30mV to electrostatically stabilize a colloidal particle). The competition between aggregation induced by high ionic concentration and stabilization by protein absorption is well correlated to the relative amounts of both (ions and proteins).

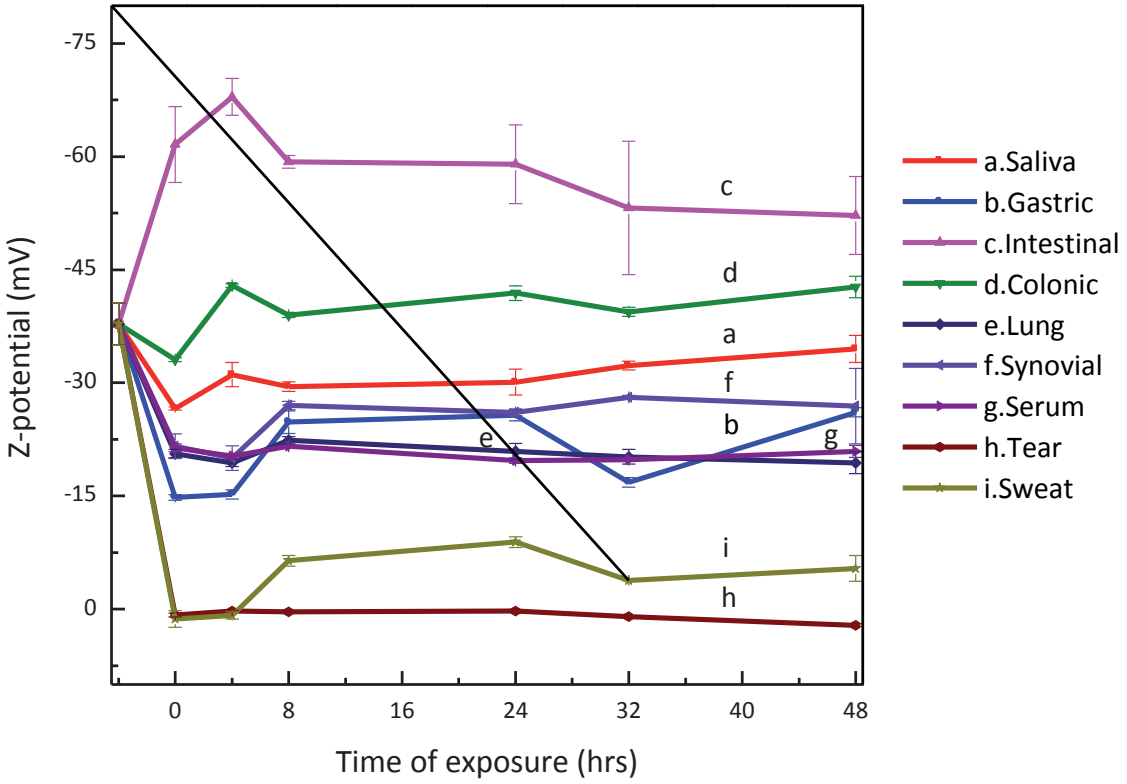

***Figure 2.8**. Time evolution of Z-Potential of citrate-coated AgNPs after being incubated in a) saliva, b) gastric fluid, c) intestinal fluid, d) colonic fluid, e) lung fluid, f) synovial fluid, g) serum, h) tear and i) sweat. The error bar is obtained from 3 measurements and each measurement was done with 13 runs. Flat line in h means Z-Potential equal to 0.*

2.3.3.2. Protein adsorption

Regarding protein adsorption, one has to note that most of body fluids contain proteins or biomolecules which have different affinity to the NP surface but normally higher compared to sodium citrate, the initial molecule at the NP surface. Therefore, when being exposed to such environments, the NPs easily undergo ligand exchange with the components of the media. The presence of this process can be primarily observed by a shift of few nm of SPR peak to higher wavelengths without changing peak shape. Additionally, the adsorption of proteins (protein corona) or the conjugation of molecules to the NPs withstands an increase in absorbance and a change in their surface charge as observed in our previous works[20, 31]. A more intense red-shift in the spectra of NPs was found when they were incubated in intestinal fluid (Figure 2.5C). This can be attributed to the conjugation of maleic acid, one of the main components of this fluid, to the NPs. This is accompanied by an increase of the negative Zeta-potential value of the NPs (Figure 2.8c) due to the fact that maleic acid (pKa1 = 1.9, pKa2 = 6.07) is deprotonated at the intestine pH, and it can form a more packed stabilizing layer exposing more surface charge[35]. A clear red-shift in UV-Visible absorption was also observed in the case of synovial fluid (Figure 2.5F) and tear (Figure 2.5H) which are protein- or organic matter-rich media. This can be seen clearly via the curves f and h in Figure 2.6 indicating the presence of biomolecules on the NP´s surface. Moreover, the Zeta-potential of the NPs in these fluids evolved toward the value of the corresponding fluid, reinforced this interpretation[20]. The protein corona also formed on the AgNPs after exposing to saliva and colonic fluid which displayed a small red-shift in the SPR peak (Figure 2.6a, d) along with a minor drop in their negative charge (Figure 2.8a, d), smaller than before corresponding to the lower protein concentration of the media. In all cases, there is a more or less marked evolution of the different UV-Visible spectra with time. The AgNPs after being incubated in lung fluid and serum also showed similar temporal evolution in surface charge (Figure 2.8e, g) indicating their surface modification by interactions with proteins. Finally, there was no sign of conjugation or protein absorption in sweat as expected since there are no organic or biological molecules present.

2.3.3.3. Dissolution

It is well-known that AgNPs can dissolve in certain dispersing media[29, 36-37]. The extent of their dissolution depends not only on their intrinsic properties such as size and shape, but also on Ag^+ concentration and characteristics of the surroundings, including pH and ionic strength, as well as the presence of organic matter, mainly proteins. The influence of these factors was observed in our study. Particularly, there was a very fast dissipation of the UV-Visible spectra (Figure 2.5B) of NPs in gastric fluid. This is attributed to the dissolution of AgNPs in an extremely low pH (1.6) and chlorine-rich environments rather than aggregation. Neither aggregates nor small NPs were found after 24hrs of incubation as shown in TEM image (Figure 2.7B). Unsurprisingly, to a certain degree, the dissolution was also observed when exposing citrate-coated AgNPs to media with high concentration of protein, or media with high content of organic matter, including lung fluid, synovial fluid, serum and tear (Figure 2.6e, f, g, h respectively). This can be attributed to strong interaction between proteins with Ag ions which favors AgNP dissolution. Additionally, these environments also contain a high amount of chlorine (higher than 100mM) which has been reported to facilitate the Ag dissolution forming insoluble AgCl[38-39]. In the case of lung fluid and serum, the SPR peaks also disappeared after 4hrs of incubation. Meanwhile in the case of tear and synovial fluid, the absorption intensity decreased gradually during 48hrs of incubation. The latter was also detected in NPs dispersed in colonic fluid indicating that minor dissolution might also occur. It is interesting that the tested AgNPs were more stable in colonic (chlorine-free medium with proteins) than in sweat (protein-free medium with chlorine) as seen in UV-Visible spectra and TEM images. Even though the decrease in UV-Visible absorption through incubation time was insignificant, still there might be minor dissolution in the case of saliva.

Dissolution was clearly observed in several simulated body fluids, for instance gastric fluid, lung fluid or serum. Meanwhile, there was no observable dissolution in intestinal fluid or sweat. It is straightforward to reason that if there was dissolution during the incubation, there would be presence of Ag ions in the supernatant after purification,

and that the concentration of these ions would increase through incubation time. To examine this, we utilized a simple methodology (described in Figure 2.9) based on UV-Vis technique. Particularly, a strong reducing agent ($NaBH_4$) was employed in an attempt to reduce the available Ag ions in supernatants obtained after purification of the samples after 0hr and 24hr incubation. This would produce derived AgNPs that will reveal the presence of an Ag source in those supernatants coming from the parental NPs. Initially, no color changes were observed in any of the supernatants which confirmed either low concentration of Ag or its absence. These solutions, after reduction, were centrifuged to concentrate the formed NPs, if there were any.

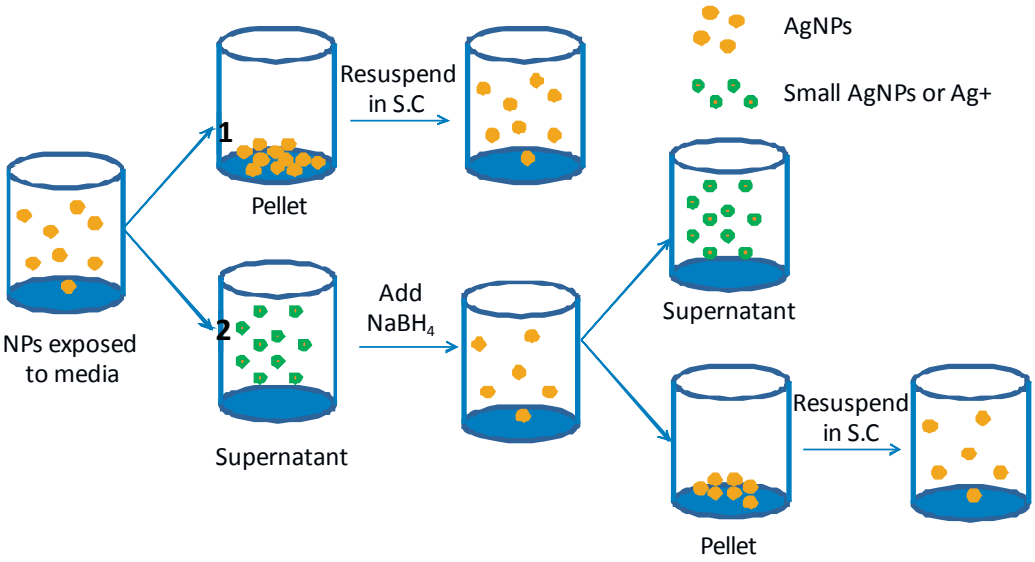

***Figure 2.9**. Schematic illustrations of the experiments. (1) The purification and characterization for the pellet. (2) The dissolution study*

The UV-Visible spectra from the suspension of purified supernatants showed 3 different states (Figure 2.10): (1) no absorption after processing supernatants from sweat and synovial fluid at 0hr or 24hrs (Figure 2.10F, I) suggesting that the temporal generation of ions was absent, or that the ions were transformed to other species; (2) a difference in absorption at various times of exposure, with missing SPR peaks, in those supernatants coming from gastric, colonic, lung fluids, serum and tear (Figure 2.10B, D, E, G, H) indicating that there might be ions complexed with organic matters

which are quite stable and (3) a clear SPR peak (Figure 2.10A, C) due to the presence of sufficiently Ag in the case of saliva and intestinal fluid, especially in intestinal. The observation here is quite consistent with the observed UV-Vis evolution of NPs in the different media. For instance, when putting the AgNPs into sweat, they aggregated and settled down, the free ions also formed precipitates as AgCl and as a result, there was almost no active silver (silver ready for reduction) in the supernatant. Meanwhile, in intestinal fluid, the NPs were stable (no aggregation, no dissolution) with the stabilization of maleic acid.

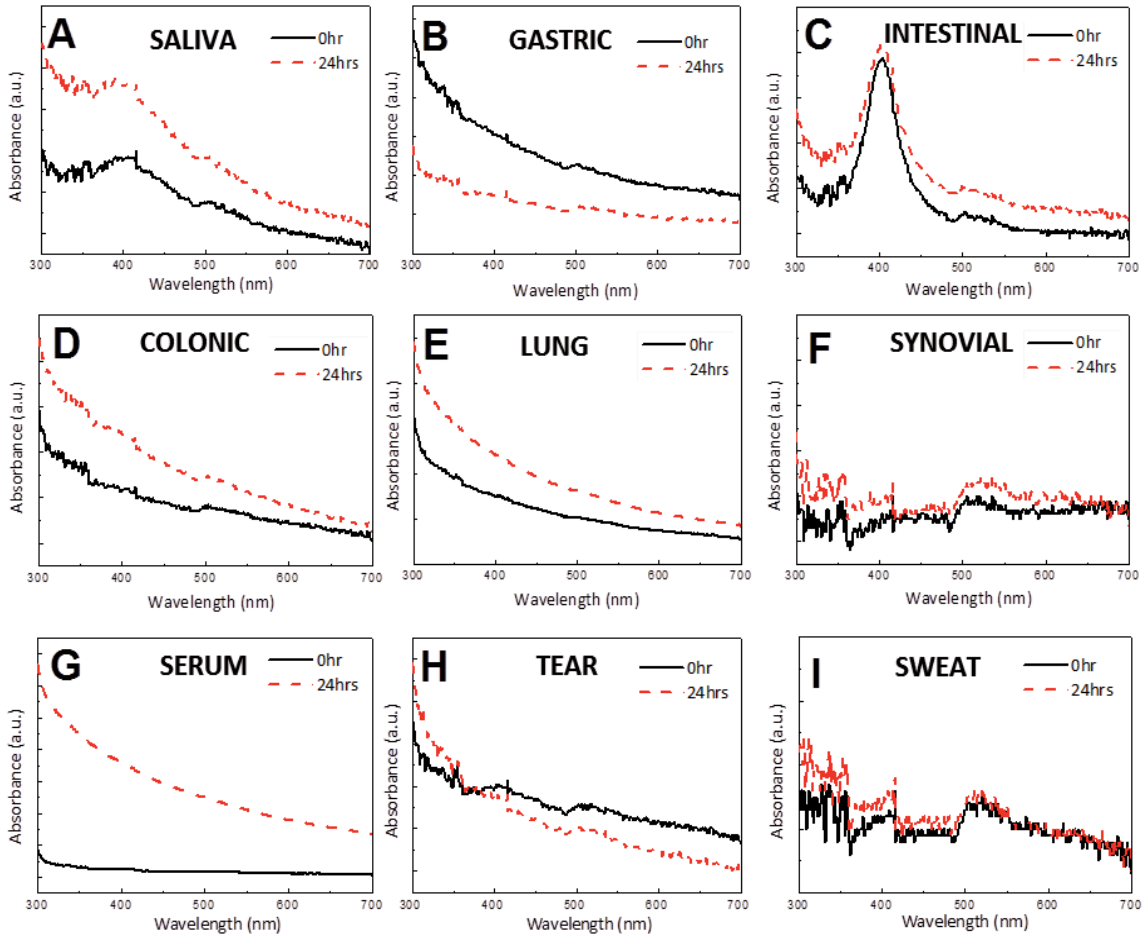

***Figure 2.10**. UV-Visible spectra of the dispersion of AgNPs obtained from the addition of $NaBH_4$ into the supernatant extracted after different time of incubation: 0hr and 24hrs in various body fluids: (A) saliva, (B) gastric fluid, (C) intestinal fluid, (D) colonic fluid, (E) lung fluid, (F) synovial fluid, (G) serum, (H) tear and (I) sweat.*

As a consequence, Ag dissolution can be tuned with surfactants as said before. For instance, in physiological media, incubation with thiol-containing molecules as MUA (mercapto-undecanoic acid) results in NPs which are less prone to corrosion and become more persistent, but still tend to aggregate in physiological environments, while AgNPs conjugated with PEG are very robust against aggregation and prevent protein absorption, but the resulting NPs are poorly protected against corrosion.

2.4. Conclusions

The behaviors of the tested AgNPs in the examined body fluids are summarized in Table 2.2.

Table 2.2. Summary of dominant AgNPs behavior in different fluids

Fluid	Dominant behavior		
	Protein corona / Conjugation	***Aggregation***	***Dissolution***
a. Saliva	X		x
b. Gastric			X
c. Intestinal	X		
d. Colonic	X		X
e. Lung	X		X
f. Synovial	X		X
g. Serum	X		X
h. Tear	X		X
i. Sweat		X	

Whether stable dispersion, aggregation, protein corona formation or dissolution dominates, it depends on the nature of the fluids, mainly driven by biomolecules content, ionic concentration and pH. Each factor has an impact to a different extent on the behavior of the NPs. Of course, more than one process can occur in a specific

medium and there might be a ´competition´ between them. For example, when NPs corrode (electrochemical dissolution), this increases the number of cations in solution what favours NP aggregation[22], especially when they possess negative Z-potential value. As the aggregates grow, and the total specific exposed surface area decreases, corrosion slows down and during the whole process, proteins interact with all these species: NPs, ions and aggregates. Additionally, this work also contributes to track the flow of NPs once they enter the body or helps to predict their possible biodistribution and fate which in turns, is useful for the designing more suitable NPs for different purposes. With this scheme, multiple incubations of NPs in different portals of entry are essential for the valid determination of the in vivo NPs response.

References

1. Faure, B.; Salazar-Alvarez, G.; Ahniyaz, A.; Villaluenga, I.; Berriozabal, G.; De Miguel, Y. R.; Bergstrom, L., Dispersion and surface functionalization of oxide nanoparticles for transparent photocatalytic and UV-protecting coatings and sunscreens. *Sci Technol Adv Mat* **2013**, *14* (2).

2. Powers, C. M.; Bale, A. S.; Kraft, A. D.; Makris, S. L.; Trecki, J.; Cowden, J.; Hotchkiss, A.; Gillespie, P. A., Developmental Neurotoxicity of Engineered Nanomaterials: Identifying Research Needs to Support Human Health Risk Assessment. *Toxicol Sci* **2013**, *134* (2), 225-242.

3. McFarland, A. D.; Van Duyne, R. P., Single silver nanoparticles as real-time optical sensors with zeptomole sensitivity. *Nano Lett* **2003**, *3* (8), 1057-1062.

4. Lee, K. S.; El-Sayed, M. A., Gold and silver nanoparticles in sensing and imaging: Sensitivity of plasmon response to size, shape, and metal composition. *J Phys Chem B* **2006**, *110* (39), 19220-19225.

5. Jiang, Z. J.; Liu, C. Y.; Sun, L. W., Catalytic properties of silver nanoparticles supported on silica spheres. *J Phys Chem B* **2005**, *109* (5), 1730-1735.

6. Chernousova, S.; Epple, M., Silver as Antibacterial Agent: Ion, Nanoparticle, and Metal. *Angew Chem Int Edit* **2013**, *52* (6), 1636-1653.

7. Asharani, P. V.; Wu, Y. L.; Gong, Z. Y.; Valiyaveettil, S., Toxicity of silver nanoparticles in zebrafish models. *Nanotechnology* **2008**, *19* (25).

8. AshaRani, P. V.; Mun, G. L. K.; Hande, M. P.; Valiyaveettil, S., Cytotoxicity and Genotoxicity of Silver Nanoparticles in Human Cells. *Acs Nano* **2009**, *3* (2), 279-290.

9. Lee, Y. J.; Kim, J.; Oh, J.; Bae, S.; Lee, S.; Hong, I. S.; Kim, S. H., Ion-release kinetics and ecotoxicity effects of silver nanoparticles. *Environ Toxicol Chem* **2012**, *31* (1), 155-159.

10. De Jong, W. H.; Van Der Ven, L. T. M.; Sleijffers, A.; Park, M. V. D. Z.; Jansen, E. H. J. M.; Van Loveren, H.; Vandebriel, R. J., Systemic and immunotoxicity of silver nanoparticles in an intravenous 28 days repeated dose toxicity study in rats. *Biomaterials* **2013**, *34* (33), 8333-8343.

11. Foldbjerg, R.; Dang, D. A.; Autrup, H., Cytotoxicity and genotoxicity of silver nanoparticles in the human lung cancer cell line, A549. *Arch Toxicol* **2011**, *85* (7), 743-750.

12. Bilberg, K.; Hovgaard, M. B.; Besenbacher, F.; Baatrup, E., In Vivo Toxicity of Silver Nanoparticles and Silver Ions in Zebrafish (Danio rerio). *Journal of Toxicology* **2012**, *2012*, 9.

13. Massarsky, A.; Dupuis, L.; Taylor, J.; Eisa-Beygi, S.; Strek, L.; Trudeau, V. L.; Moon, T. W., Assessment of nanosilver toxicity during zebrafish (Danio rerio) development. *Chemosphere* **2013**, *92* (1), 59-66.

14. Xiu, Z. M.; Zhang, Q. B.; Puppala, H. L.; Colvin, V. L.; Alvarez, P. J. J., Negligible Particle-Specific Antibacterial Activity of Silver Nanoparticles. *Nano Lett* **2012**, *12* (8), 4271-4275.

15. Limbach, L. K.; Wick, P.; Manser, P.; Grass, R. N.; Bruinink, A.; Stark, W. J., Exposure of engineered nanoparticles to human lung epithelial cells: Influence of chemical composition and catalytic activity on oxidative stress. *Environ Sci Technol* **2007**, *41* (11), 4158-4163.

16. Navarro, E.; Piccapietra, F.; Wagner, B.; Marconi, F.; Kaegi, R.; Odzak, N.; Sigg, L.; Behra, R., Toxicity of Silver Nanoparticles to Chlamydomonas reinhardtii. *Environ Sci Technol* **2008**, *42* (23), 8959-8964.

17. Buzea, C.; Pacheco, I. I.; Robbie, K., Nanomaterials and nanoparticles: Sources and toxicity. *Biointerphases* **2007**, *2* (4), Mr17-Mr71.

18. Liu, J. Y.; Wang, Z. Y.; Liu, F. D.; Kane, A. B.; Hurt, R. H., Chemical Transformations of Nanosilver in Biological Environments. *Acs Nano* **2012**, *6* (11), 9887-9899.

19. Creighton, J. A.; Blatchford, C. G.; Albrecht, M. G., Plasma Resonance Enhancement of Raman-Scattering by Pyridine Adsorbed on Silver or Gold Sol Particles of Size Comparable to the Excitation Wavelength. *J Chem Soc Farad T 2* **1979**, *75*, 790-798.

20. Casals, E.; Pfaller, T.; Duschl, A.; Oostingh, G. J.; Puntes, V., Time Evolution of the Nanoparticle Protein Corona. *Acs Nano* **2010**, *4* (7), 3623-3632.

21. Marques, M. R. C.; Loebenberg, R.; Almukainzi, M., Simulated Biological Fluids with Possible Application in Dissolution Testing. *Dissolut Technol* **2011**, *18* (3), 15-28.

22. Wang, D. W.; Tejerina, B.; Lagzi, I.; Kowalczyk, B.; Grzybowski, B. A., Bridging Interactions and Selective Nanoparticle Aggregation Mediated by Monovalent Cations. *Acs Nano* **2011**, *5* (1), 530-536.

23. Juluri, B. K.; Huang, J.; Jensen, L. *Extinction, Scattering and Absorption efficiencies of single and multilayer nanoparticles*, **2012**.

24. Evanoff, D. D.; Chumanov, G., Synthesis and optical properties of silver nanoparticles and arrays. *Chemphyschem* **2005**, *6* (7), 1221-1231.

25. Lamer, V. K.; Dinegar, R. H., Theory, Production and Mechanism of Formation of Monodispersed Hydrosols. *J Am Chem Soc* **1950**, *72* (11), 4847-4854.

26. Reiss, H., The Growth of Uniform Colloidal Dispersions. *J Chem Phys* **1951**, *19* (4), 482-487.

27. Ostwald, W., Studien über die Bildung und Umwandlung fester Körper. *Zeitschrift für physikalische Chemie* **1897**, *22*, 289-330.

28. Lorenz, R.; Voorhees, P. W., In *Growth and Coarsening: Ostwald Ripening in Material Processing*, Springer: **2002**; pp 117-118.

29. Li, X.; Lenhart, J. J.; Walker, H. W., Aggregation Kinetics and Dissolution of Coated Silver Nanoparticles. *Langmuir* **2012**, *28* (2), 1095-1104.

30. Keller, A. A.; Wang, H. T.; Zhou, D. X.; Lenihan, H. S.; Cherr, G.; Cardinale, B. J.; Miller, R.; Ji, Z. X., Stability and Aggregation of Metal Oxide Nanoparticles in Natural Aqueous Matrices. *Environ Sci Technol* **2010**, *44* (6), 1962-1967.

31. Casals, E.; Pfaller, T.; Duschl, A.; Oostingh, G. J.; Puntes, V. F., Hardening of the Nanoparticle-Protein Corona in Metal (Au, Ag) and Oxide (Fe3O4, CoO, and CeO2) Nanoparticles. *Small* **2011**, *7* (24), 3479-3486.

32. Bastus, N. G.; Casals, E.; Vazquez-Campos, S.; Puntes, V., Reactivity of engineered inorganic nanoparticles and carbon nanostructures in biological media. *Nanotoxicology* **2008**, *2* (3), 99-112.

33. Israelachvili, J., *Intermolecular and surface forces*. 2nd ed.; Academic Press: San Diego, CA, **1992**.

34. Bian, S. W.; Mudunkotuwa, I. A.; Rupasinghe, T.; Grassian, V. H., Aggregation and Dissolution of 4 nm ZnO Nanoparticles in Aqueous Environments: Influence of pH, Ionic Strength, Size, and Adsorption of Humic Acid. *Langmuir* **2011**, *27* (10), 6059-6068.

35. Ivanov, M. R. Covalently funtionalized gold nanoparticles: synthesis, characterization, and integration into capillary electrophoresis. University of Iowa, **2011**.

36. Geranio, L.; Heuberger, M.; Nowack, B., The Behavior of Silver Nanotextiles during Washing. *Environ Sci Technol* **2009**, *43* (21), 8113-8118.

37. Elzey, S.; Grassian, V. H., Agglomeration, isolation and dissolution of commercially manufactured silver nanoparticles in aqueous environments. *J Nanopart Res* **2010**, *12* (5), 1945-1958.

38. Liu, J. Y.; Sonshine, D. A.; Shervani, S.; Hurt, R. H., Controlled Release of Biologically Active Silver from Nanosilver Surfaces. *Acs Nano* **2010**, *4* (11), 6903-6913.

39. Liu, J. Y.; Hurt, R. H., Ion Release Kinetics and Particle Persistence in Aqueous Nano-Silver Colloids. *Environ Sci Technol* **2010**, *44* (6), 2169-2175.

Chapter 3

DISSOLUTION AND SPECIATION OF SILVER NANOPARTICLES IN BIOLOGICAL MEDIA

3.1. Introduction

We have observed in chapter 2 that nanoparticles (NPs) suffer different transformations when brought into contact with physiological media. Despite a general belief that NPs are as persistent as their bulk counterparts, small NPs are normally rather unstable and short-lived due to their high surface energy[1]. Atoms at the surface of a nanoparticle are quite unsettled: they do not benefit from the protection of the highly coordinated atoms as in the bulk, nor they dispose the high mobility of molecular species to dissipate energy. Small NPs have sizes close to the critical radius, which strongly depends on the monomer saturation and the NPs synthesis environment. When this environment is changed, then, the NP may enter into a critical zone where it became unstable and dissolves. The driving force behind NP dissolution mainly depends on the solubility of the constituent ions in a given environment and the concentration gradient of NPs in solution[2]. This phenomenon is referred to as the Gibbs-Thomson effect and in nanoparticles manifest as Ostwald ripening, where NPs dissolve or grow due to concentration gradients of reacting species. Indeed, it has been reported that generally, below 20-30 nm, changes in the crystal structure and crystal (surface) defects enhance NP dissolution[3]. Furthermore, the surface tension[2] and activation energy relevant to dissolution[4] are also size-

dependent for small NPs. Thus, for a given mass, the kinetics of dissolution will be proportional to the specific surface area and the coordination of the atoms at that surface. In fact, in geochemistry, a NP is considered as the intermediate state between the nuclei - which are being formed and dissolved as a function of ionic concentration- and corresponding larger particle or composites[5]. Additionally, if the released ions participate in competing reactions, their mobility is high and their concentration low, then the system is moved far away from the saturation point and the NPs tend towards complete dissolution. If during dissolution, the concentration of available ions brings the system to saturation, the ions will dissolve more slowly or not at all. Since the chemical potential of silver (4.26eV) is not high enough to resist oxidation, they suffer corrosion and other forms of reactive dissolution. As shown in previous chapter, AgNPs did dissolve in several biological fluids.

The biological effects of silver nanoparticles (AgNPs) to different organisms have been demonstrated in a great deal of studies[6-9] and it is well-known that the induced biological effects or potential toxicity of NPs are strongly dependent on their colloidal (aggregation) and chemical (interaction with proteins and corrosion) stability[10-12]. For instance, Kvitek et al. found a direct correlation between the aggregation state of AgNPs coated with various surfactants and their enhanced antibacterial activity[13]. The effects of AgNPs corrosion in physiological (in vivo and in vitro) conditions were also described recently[14]. It is considered that the release of silver ion is one of the main factors that cause their toxicity[6, 15]. However, there is no a single report about the species one may find in the cell culture media as a result of that dissolution. Thus, determining the modifications that AgNPs undertake when being exposed to environments, especially biological ones, is crucial to understand the associated biological responses and to design safer nanoparticles. In addition, Ag speciation, especially as a function of time, is necessary for a more comprehensive evaluation on its biological effects.

In this chapter, how standard AgNPs rapidly dissolves and transforms (partition and speciation) in cell culture media, challenging the understanding of the mechanisms of biological response to NP exposure, is shown. Several factors that influence the

dissolution of AgNPs were investigated and methodologies to control the dissolution were proposed.

3.2. Materials and methods

Reagents: silver nitrate ($AgNO_3$, ACS reagent ≥ 99%), sodium citrate tribasic dihydrate ($Na_3C_6H_5O_7.2H_2O$), sodium borohydride ($NaBH_4$, ReagentPlus 99%), sodium nitrate ($NaNO_3$, ReagentPlus ≥ 99%), hydrochloric acid (HCl, ACS reagent 37%), nitric acid (HNO_3, ACS reagent 70%), Dulbecco´s modified eagle´s medium (DMEM, with 4500mg/L glucose and sodium bicarbonate, without L-glutamine, sodium pyruvate, and phenol red, liquid, sterile-filtered), fetal bovine serum (FBS, sterile-filtered), human serum (HuS, from human male AB plasma, USA origin, sterile-filtered) and trypsin from bovine pancreas were purchased from Sigma-Aldrich. Standard grade regenerated cellulose dialysis membranes (3.5kD and 8kD MWCO) were supplied by SpectrumLabs. Milli-Q water with a resistivity of 18.2 mΩ.cm was used throughout the experiments.

Synthesis of AgNPs: Citrate-coated AgNPs with average diameter of 15nm, hereafter Ag15 were synthesized using the same procedure as described in chapter 2. Meanwhile, 50nm citrate-capped NPs (Ag50) were prepared mainly following Lee-Meisel method[16]. Indeed, 100ml of 1mM $AgNO_3$ aqueous solution was heated to boiling, then 10ml of 0.1M sodium citrate was dropped in continuously. The mixture was kept boiling for 30mins until a grey resultant solution was obtained before being cooled down. Concentrations of prepared NPs are 10^{12} and 10^{11} NP/ml respectively.

Exposure to the media: the exposure experiments were done following the procedure as described in our previous work[17]. In particularly, as-prepared AgNPs with proper concentration were added to complete cell culture medium (cCCM) (1:10 by volume) and incubated at 37°C for different incubation times. The cCCM was prepared under sterile conditions by mixing serum, either fetal bovine serum (FBS) or human serum (HuS), in DMEM. The media contain 10% in volume of serum. All materials are

provided by Sigma-Aldrich and serum was thawed without heat-inactivation before usage.

Purification: Prior to characterization, 1.5ml of incubation mixture was centrifuged for 15mins at 35000g. The collected pellet was re-suspended in 0.2ml deionized H_2O or 2.2mM sodium citrate to get a stable colloid of NPs. The supernatants were also kept for characterization.

Characterization: Various techniques including UV-Vis, Z-potential, TEM as described in chapter 2 were used to characterize the NPs as well as to follow the evolution of their physical and chemical changes over time.

Speciation of Ag: 15nm citrate-coated AgNPs were incubated with cCCM (DMEM supplemented with 10% FBS) for 8hrs prior to the partition. Ag species were separated either by dialysis or centrifugation coupled with stepwise treatments based on difference in solubility and chemical reactivity between different species.

X-ray Diffraction (XRD): Identification of insoluble species was performed with XRD. X-Ray measurement was acquired with PAnalytical MPD (multi-purpose diffractometer) operated at 45Kv/40mA. The measurement is Standard Theta/2Theta scanning with Cu X-ray tube (wavelength of 1,540598 Armstrong).

Separation by dialysis: The incubated mixture was first dialyzed with the cellulose membrane of 3.5KDa against MiliQ water to extract the fraction of Ag^+_Free in any forms (free here means without the attachment of the proteins). The mixture then was processed with trypsin digestion or $NaNO_3$ treatment followed by the second dialysis with 8KDa membrane to remove the Ag^+_proteins fraction. Prior to the third dialysis to obtain AgNPs segment, the solution was treated with concentrated HNO_3. Finally, the remained solution was digested with concentrated HCl preparing for quantification.

Separation by centrifugation: After the incubation, the mixture was centrifuged at 55000g for 30mins to separate soluble (Ag^+_Free and Ag^+_Proteins) from insoluble (AgNPs and AgCl) species. The soluble part was treated with $(NH_4)_2SO_4$ to precipitate Ag^+_Proteins and the two components were split by a mild centrifugation at 14000g

for 10mins. Meanwhile, the insoluble fraction was resuspended in HNO_3 to digest AgNPs out of AgCl. Then AgCl was removed by another centrifugation at 55000g in 30mins, followed by dissolving with HCl.

Quantification by Inductively Coupled Plasma-Mass Spectroscopy (ICP-MS): Mass spectra were done for aliquots collected from different fragments. Samples were prepared at an optimal concentration for ICP-MS analysis. Measurements were performed using an ICP-MS Agilent instrument (Model: 7500cx) with a detection limit of 0.0239 ppb. Ga was used as the internal standard with the integration time/point and time/mass of 0.1 and 0.3 sec, respectively.

3.3. Results and Discussions

3.3.1. Behaviors of AgNPs in cell culture media – Aggregation, Protein absorption and Dissolution

To properly study NP state by UV-Vis, interference with serum was avoided by purification of the NPs from the incubation media before analysis. As shown in Figure 3.1A, the SPR peak of AgNPs exposed to cCCM, which was impeded before purification, was revealed after purification. In order to rule out the possibility of aggregation due to NP purification process, control experiments for non-exposed NPs were also done at the same conditions for incubation in and purification from 2.2 mM sodium citrate (the initial medium after synthesis) instead of using cCCM. It is observed that there is no significant change in shape and intensity of AgNPs SPR absorption peak (Figure 3.1B). This experiment confirms that if there is any modification of the NPs which might be detected in UV-Visible spectra, it is due to the interaction between the NPs with the exposure medium, not because of the experimental procedure.

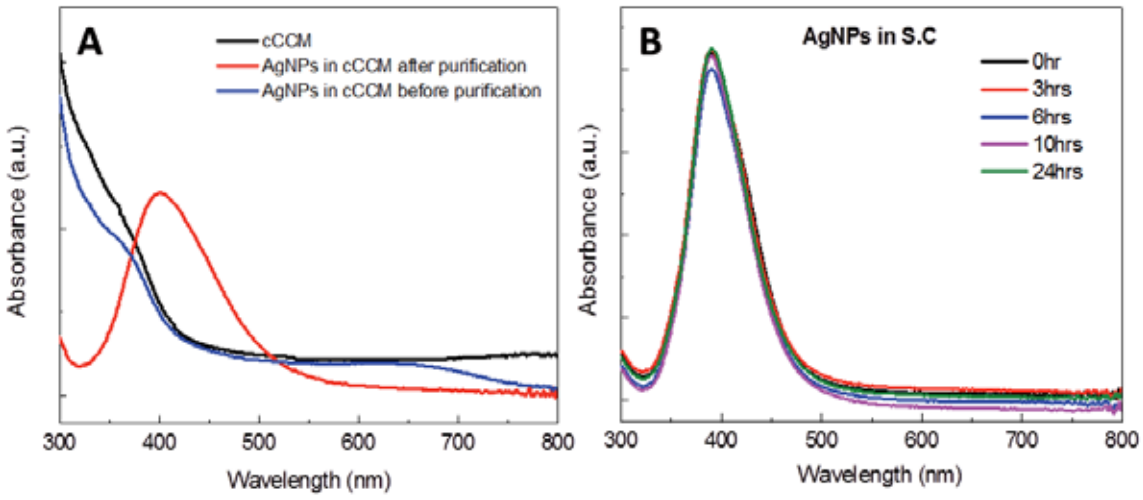

Figure 3.1. *(A) Interference of exposure medium to optical measurement of NPs. The characteristic SPR peak of AgNPs was not observable without centrifugation (blue line) which is contrary to the case with centrifugation to separate NPs out of exposed environment (red line). (B) Control experiment. UV-Visible spectra of centrifuged citrate-coated AgNPs obtained at different time of incubation without exposure.*

Herein, when incubating standard citrate-coated AgNPs with average diameter of 15nm, Ag15 (Figure 3.2A), in cCCM (DMEM supplemented with 10% FBS), one can observe the adsorption of proteins on the NP surface or the PC formation at short times. This is depicted by the 3nm red-shift in the SPR absorption band of AgNPs when increasing the incubation time (Figure 3.2C). Also, the gradually drop over time in the negative surface charge of the NPs from -44mV to -26mV towards the value of the serum which is around -10mV (Figure 3.2D) confirms the adsorption of proteins[17-18].

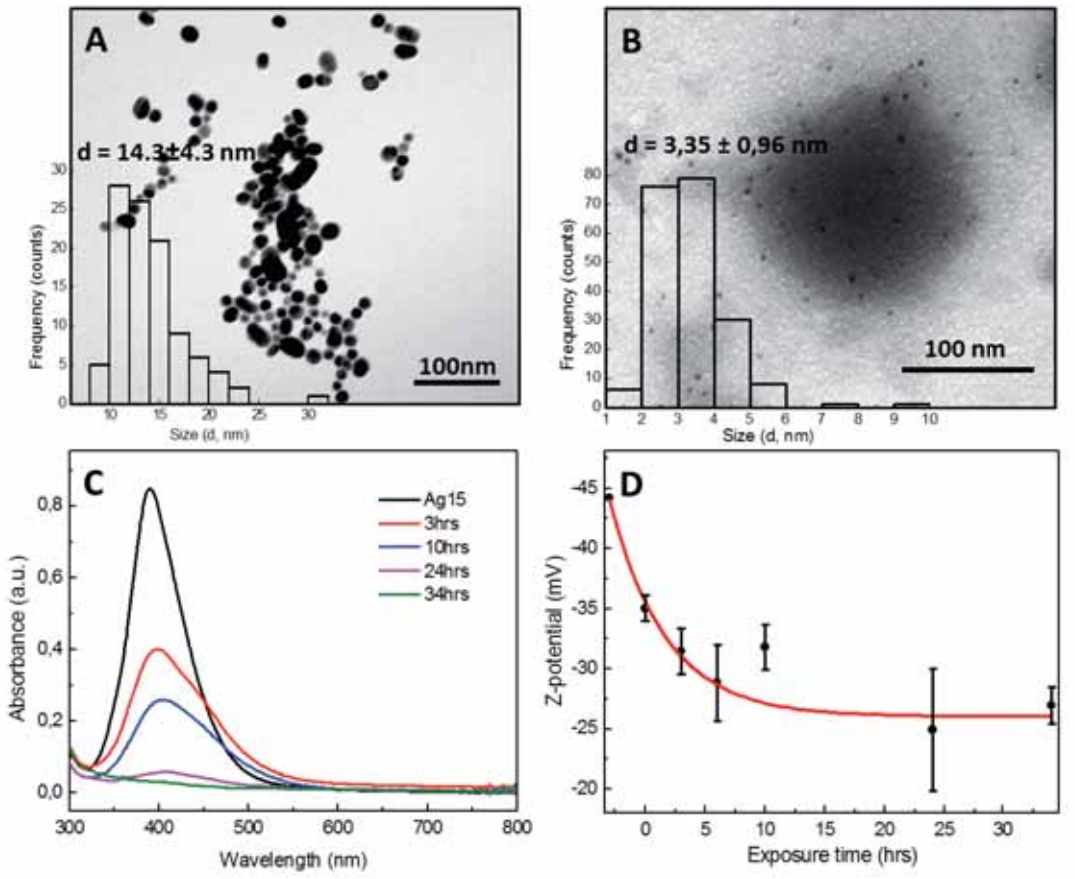

***Figure 3.2**. Characterization of Ag15: (A) TEM image and size distribution (inset) and characterization of Ag15 incubated in FBS/DMEM: (B) TEM image with size distribution (inset) of Ag15 after incubation for 24hrs; (C) UV-Visible spectra of AgNPs obtained at different time of exposure and (D) Temporal evolution in Z-potential of the NPs.*

Note that together with the protein adsorption, there are evidences of aggregation but only at short incubation time. Even though the aggregation can be inhibited by the protein adsorption which helps to stabilize the NPs by steric repulsion instead of electrostatic repulsion, the protein adsorption is a time-dependent process in which the proteins with higher mobility but lower affinity arrive first, and then are replaced by higher affinity but less abundant protein (Vroman effect)[19]. Interestingly, as time evolves, there was the decrease in absorbance of the AgNP SPR peak (Figure 3.2C) which initially could be attributed to the dissolution or sedimentation of the NPs. The latter is excluded since smaller NPs of less than 5nm in diameter were found in the

pellet of the sample incubated for 24hrs under TEM (Figure 3.2B), as a result of corrosion and dissolution. Besides, no signs of aggregation were observed at any time.

3.3.2. Dissolution. Effects of NP intrinsic properties

Among various other intrinsic properties of the NPs that affect their solubility such as surface area, surface morphology and crystallinity, size is considered as the physicochemical property that plays a major role on solubility of NPs. Auffan and her group concluded that 20-30nm is the critical size of NPs where they arise unique properties which are absent in the case of larger particles with the same chemical composition[1]. In our study, citrate-coated AgNPs of 2 different average sizes, below and above this threshold: 15nm (Ag15, smaller than critical size) and 50nm (Ag50, bigger than critical size) were investigated during incubation in DMEM supplemented with 10% FBS. The two particles were exposed at concentrations with the same specific surface area. Figure 3.3A and 3.3B show the temporal UV-Vis spectra obtained after exposing the NPs up to 48hrs.

It is clear that the large NPs are more stable. Assuming that the dielectric constant for AgNPs is basically the same for the explored sizes, to roughly evaluate and compare both NPs dissolution rate, the relative losses of absorption at a certain time-point T is determined by the ratio of integrated UV-Visible absorbance from 323 to 600nm at that time point to the correspondent one at 0hr. As expected, the disappearance of the signal is higher in the case of the smaller NPs comparing to the bigger ones (Figure 3.3C). Indeed, this is governed by the Gibbs-Thomson effect, by which the particles tend to minimize their surface energy and thus, the smaller NPs which possess a high surface energy are more reactive and dissolve faster[1, 3].

Surface coatings, obtained from the use of capping agents usually to enhance the dispersion of NPs, can also have critical effect on NPs´ solubility. Indeed, the dependence of NP solubility on capping agents has also been intensively investigated[20-21]. Herein, when coating AgNPs with MUA (11-mercaptoundecanoic acid), a thiol-containing capping agent which has stronger affinity to the metal surface than sodium citrate[22], there was no significant decrease in absorption intensity up to 48hrs of

incubation (Figure 3.3D). This could be attributed to the fact that NPs were better protected with MUA from the attack of corrosive agents (i.e. Cl^-).

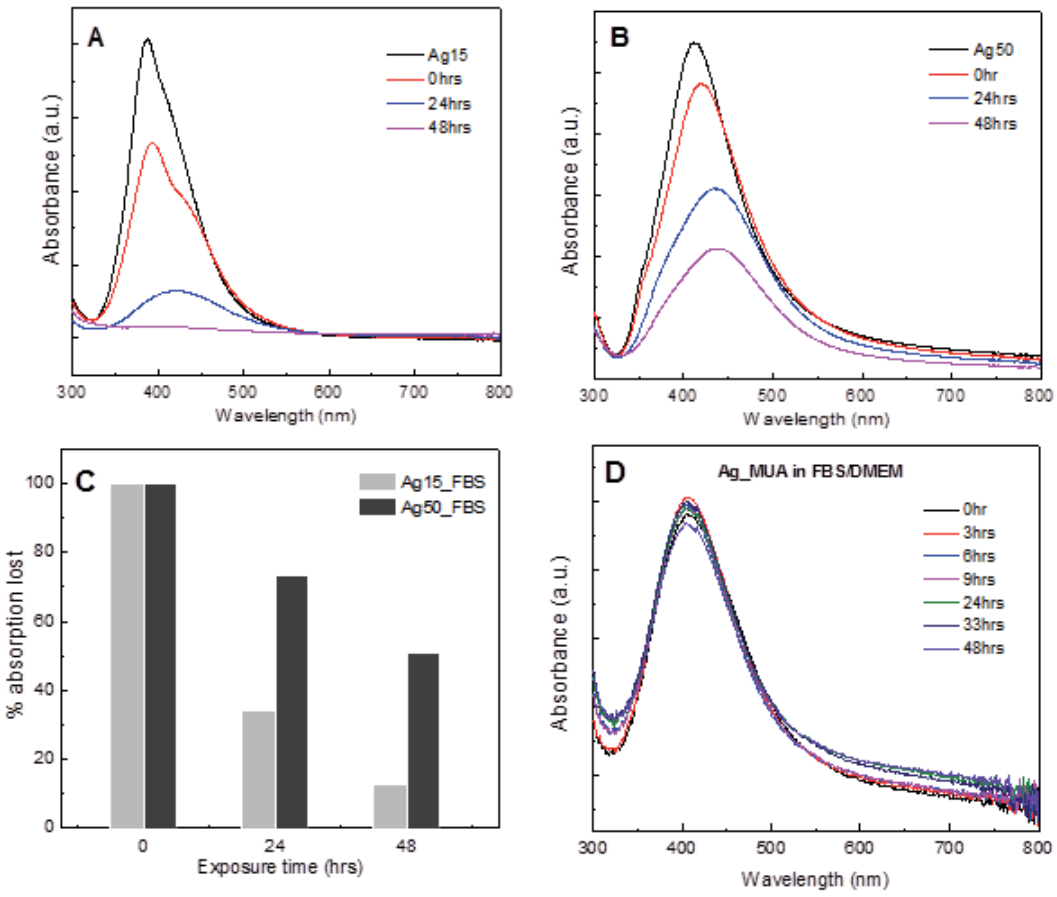

Figure 3.3. *(A, B) UV-Visible spectra obtained after different time of incubation in cCCM (DMEM supplemented with 10% FBS) of various size AgNPs: A) 15nm and B) 50nm. C) Percentage of lost absorption intensity through exposure time of AgNPs with different sizes and D) Temporal UV-Visible spectra of MUA-conjugated Ag15 NPs obtained after incubation in cCCM (DMEM supplemented with 10% FBS). There is no significant decrease in absorption intensity over investigated exposure time indicating that MUA is protecting the NP from dissolution.*

3.3.3. Dissolution. The role of media components

It is considered that during the dissolution, the dissolved ions of AgNPs are in equilibrium with the NPs at the proximity of NP surface. Therefore, factors that make the concentration of Ag ions on the NP surface decrease will shift this equilibrium

towards NP dissolution. It is well-known that the dissolution of AgNPs can be accelerated by Cl^- due to the formation of precipitated AgCl[23]. In addition, proteins or macromolecules which trap the ions by forming complex with them will do the same[24]. Therefore, cellular culture environments which are highly saline (Cl^-, present in physiological conditions at 150 mM in concentration) and rich in protein content are reservoirs of ion-scavengers where dissolution of Ag is facilitated (Figure 3.4). In our study, the impact of these ion scavengers was also investigated individually.

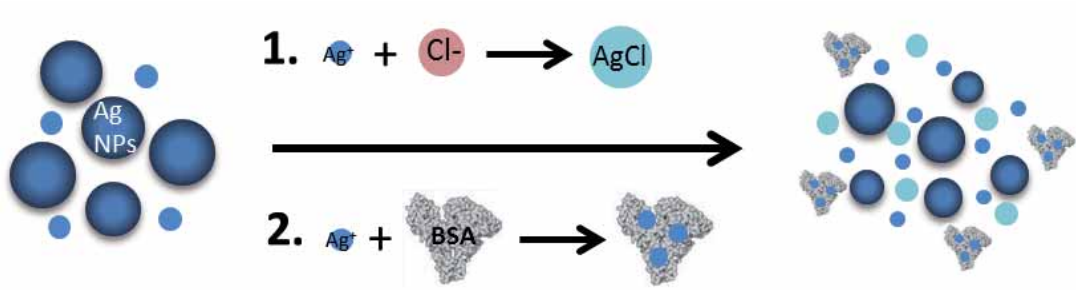

Figure 3.4. *Driving forces for dissolution of NPs in cCCM: 1. Formation of hydrophobic compound mainly AgCl; 2. Formation of Ag+_proteins complex.*

The role of Cl^- ions was studied by dispersing 10^{12} NPs/ml 15nm AgNPs (Ag15) in NaCl solutions of different concentration at a similar ratio in volume as in the main experiment (1:10). It is observed in the case of 1mM NaCl that the NPs are still stable as seen in the UV-Visible spectra as a function of time (Figure 3.5A). Particularly, there is no peak shift, decrease in the absorption intensity or increase of absorbance at the wavelength longer than 500nm. Moreover, the observed mild sharpening of the peak suggests that there might be changes in the NP morphology. This could be attributed to the fact that the NPs might be etched, ¨polished¨, by Cl^-[25]. On the contrary, at the concentration of 5mM, the observed decrease in absorbance of SPR peak suggests that the NPs are fully corroded by Cl^- (Figure 3.5B). Also, consistent to what described earlier on characteristics of UV-Vis spectra corresponding to various processes (chapter 2), there is no red-shift of the absorption band but the broadening of the peak suggesting that the size defocusing is happening as a result of the dissolution. With these observations, it is assumed that the Cl^- conducted first the etching, then the dissolution of the NPs.

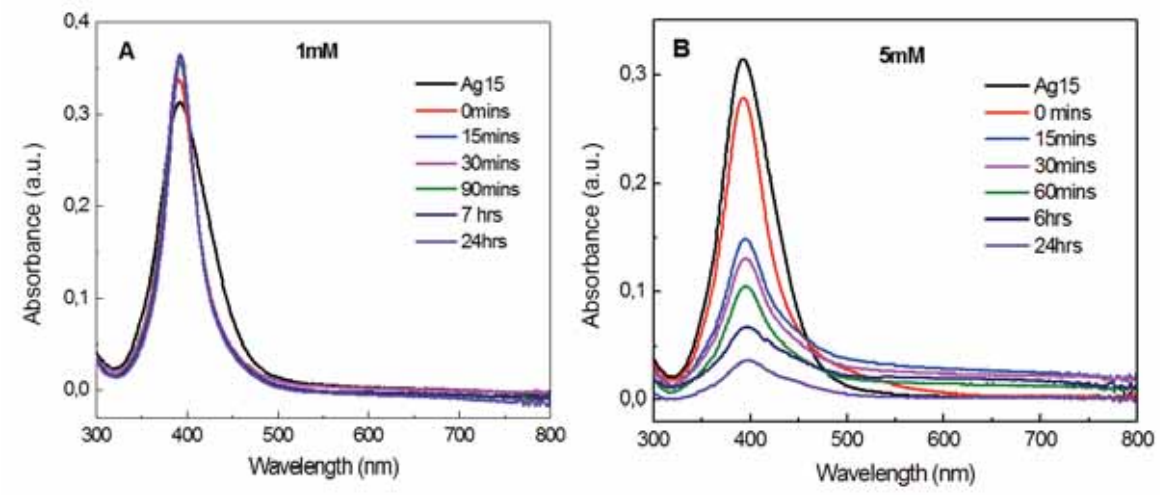

Figure 3.5. *UV-Visible spectra recorded at different period of time when exposing AgNPs to various concentration of NaCl: A) 1mM and B) 5mM.*

To examine the role of proteins in the dissolution of NPs, AgNPs were incubated with 0.5mM BSA (as a model protein and the most abundant one (~ 70%) in serum) in sodium citrate. As expected, a corona of albumins on the NPs was observed in the SPR shift (Figure 3.6A) and the evolution of the Z-potential (Figure 3.6B) as mentioned previously.

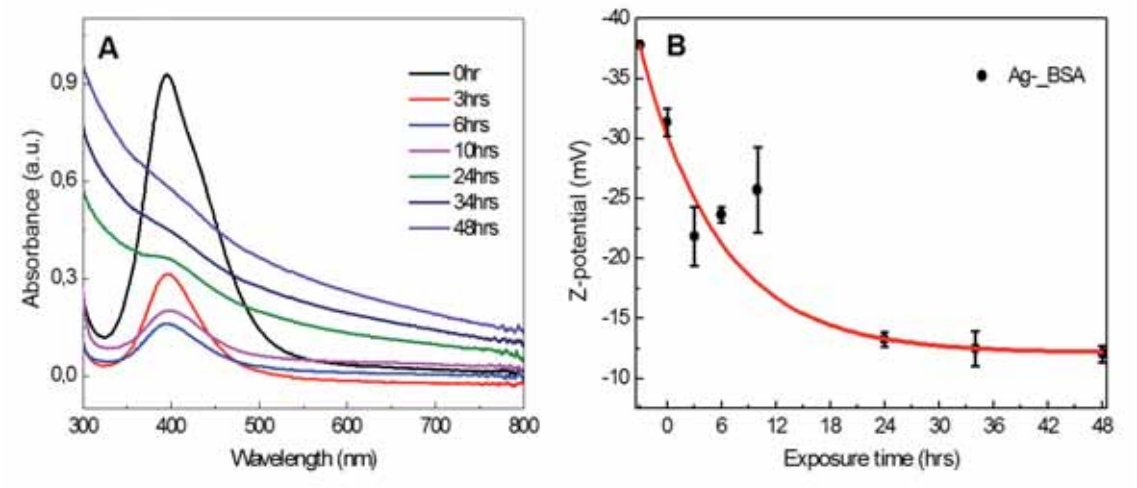

Figure 3.6*. Characterization of Ag15 incubated in 0.5mM BSA in S.C. (A) UV-Visible spectra of AgNPs obtained at different time of exposure and (B) Temporal evolution in Z-potential of the NPs.*

The dissolution of AgNPs was detected by a decrease in absorption intensity of SPR peak when increasing the incubation time. This finding confirmed that the proteins can give a hand to conduct the dissolution of AgNPs. The increased absorbance at longer wavelength and the final monotonous signal decrease from 300 to 800nm when increasing the incubation time might be attributed to the presence of molecular complex between Ag^+ and proteins (Figure 3.7) rather than aggregation since no large redshift or dramatic broadening were observed. All in all indicates a competitive protein protection (PC formation) at short times and protein-induced NP dissolution at longer times.

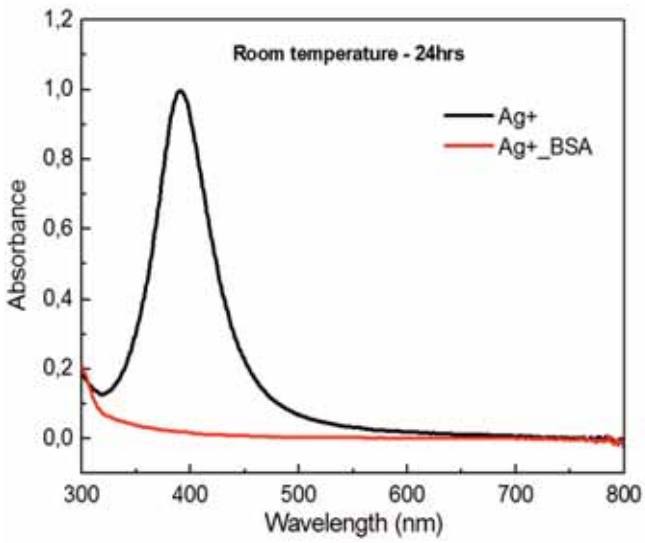

Figure 3.7. *UV-Visible spectra obtained after reduction by $NaBH_4$ of Ag^+ (final concentration of 0.025mM) incubated with (red line) and without (black line) BSA (7mg/ml) for 24hrs. In the presence of BSA, free Ag ions were separated from the mixture by BSA precipitation using ethanol followed by a centrifugation. The missing SPR peak in the case with BSA indicates that a high content of Ag^+ was trapped by BSA.*

Taking into account that the present biological entities or biomolecules may favour the dissolution of the NPs as discussed earlier, the effect of composition of exposure media is also investigated. Indeed, AgNPs were incubated with DMEM supplemented with FBS and human serum (HuS). Again, the changes in the UV-Visible peaks displaying the formation of a PC and the dissolution of the NPs were observed in both

studied media (Figure 3.8). The results show that signal loss when incubating 50nm AgNPs in the media with FBS is greater than in the one with HuS (Figure 3.8C) indicating that FBS is more reactive to the studied NPs than HuS, or in another word, the NPs are more stable in HuS than in FBS. Related results were observed when incubating SiO_2 NPs in different media as bovine and human serum supplemented DMEM[26]. This has strong implications on the translation from *in vitro* to *in vivo*, from animal models to human in medicine and toxicity.

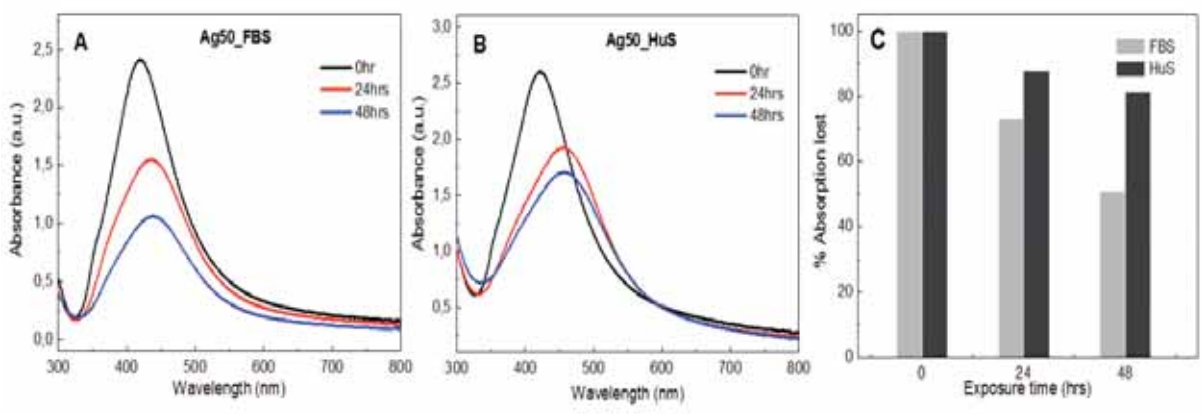

***Figure 3.8**. UV-Visible spectra (A, B) of Ag50 NPs obtained after different time of incubation in cCCM (DMEM supplemented with different serum): (A) FBS, (B) HuS, and corresponding percentage of lost absorption intensity (C).*

3.3.4. Ag speciation

It is obvious that the dissolution of AgNPs in cellular culture environments is happening to different extents depending on various factors including the size of NPs and the composition of the exposure media and the interactions of NPs and ions within it. Ag speciation was carried out to identify and quantify different generated Ag species coming from parental NPs. These studies are crucial for accurately determining the contribution of Ag species to AgNP related - detected biological effects. The main species which are supposed to be present include *soluble* Ag (Ag^+ with proteins, hereafter Ag^+_Proteins and Ag^+_Free which represents for any soluble form of Ag^+ and its soluble molecular forms but not with proteins) and *insoluble* Ag (AgNPs and

insoluble Ag compounds such as AgCl). Once identification of present Ag species is done, species separation is required prior to quantification.

The identification of insoluble Ag species was done by X-ray diffraction (XRD). XRD pattern taken for the dried sample after being incubated in cCCM (DMEM supplemented with FBS) for 8hrs (Figure 3.9) shows that Ag appeared mainly in the form of AgCl. This is indicated by the presence of characteristic peaks which are indexed to face centered cubic (fcc) structure of AgCl (JCPDS file No. 031-1238). There is also the existence of pure Ag observed with a low intensity peak at $2\theta = 38^0$ that will disappear with time. Herein, most AgCl is formed separately rather than deposited on AgNPs since there was no core-shell structures observed in TEM (Figure 3.2B). Even though both AgCl and Ag have the same fcc crystal structure, their lattice constant is quite far from each other. While the lattice constant of Ag is 408.53pm, the one of AgCl is 554.9pm. Thus, epitaxial growth is not expected. Moreover, due to the electrostatic interaction, it is not straightforward for Cl^- to approach negatively charged NP surface. Thus, AgCl is preferentially formed between diffused Ag^+ and Cl^- in solution[27]. Interestingly, there was no signal for Ag_2O or Ag_2S as it has been found after dispersion of AgNPs in the environment. It is worth to know that there is no free S^{2-} in cCCM and even though the media composition includes sulfur-containing components such as cystine, methionine or thiamine, the sulfidation might take hours to days[28] when Ag is already dissolved. Meanwhile, the precipitation of AgCl is immediate in media with such high content of Cl^-.

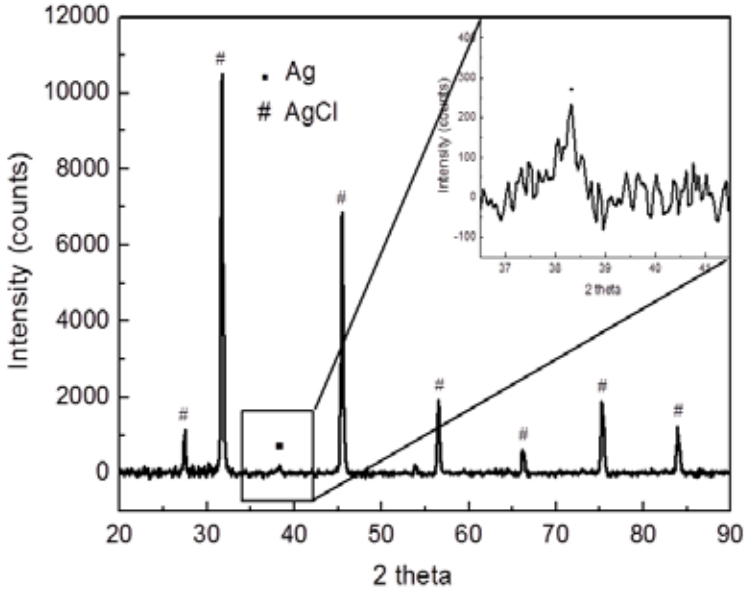

***Figure 3.9**. XRD pattern of centrifugated Ag15 after being incubated in FBS/DMEM for 8hrs.*

It is well-known that sample segmentation for subsequent proper classification and quantification analysis is challenging, especially when doing it in complex environments as biological media[29-30]. Herein, we develop a protocol to separate main Ag species generated when incubating AgNPs into complete cell culture medium. Two different techniques were applied to isolate the soluble from insoluble and the small from large species: centrifugation and dialysis. With centrifugation, soluble species as Ag^+ and Ag_Proteins are separated in the supernatant while insoluble species as AgNPs and AgCl are precipitated. With dialysis, ionic and small molecular species can be isolated first from AgNPs, AgCl and Ag_Proteins. Then, by protein digestion or cationic extraction, the Ag in the Ag_Proteins fraction can be assessed. Finally, the quantification of each fraction is performed by ICP-MS.

Regarding the quantification of the Ag in proteins, samples were treated with trypsin for digestion, or $NaNO_3$ to extract Ag^+ (Na^+ was reported as a competing cation of Ag^+ in the complexation with macromolecules[15]). Trypsin digestion, once soluble Ag species were removed, was used to cut proteins into smaller pieces which are able to cross the dialysis membrane while the other insoluble parts will not. Control

experiments were also done to make sure that with the used dialysis membrane, only Ag^+ or Ag^+ in complex with small fragment of proteins can pass through. Thus, after 8hrs of incubation, data obtained from ICP-MS show that about 70% of Ag in NP form was transformed to others species (Figure 3.10A) with a relative ratio of Ag^+_Free to Ag^+_Proteins to AgCl 1 : 6 : 7.5 (5%, 29% and 38%, respectively). With the assumption that the transformation ratios remain constant throughout the process and knowing the transformed amount of AgNPs from UV-Visible analysis, we estimated the distribution of different species at other time points as shown in Figure 3.10B.

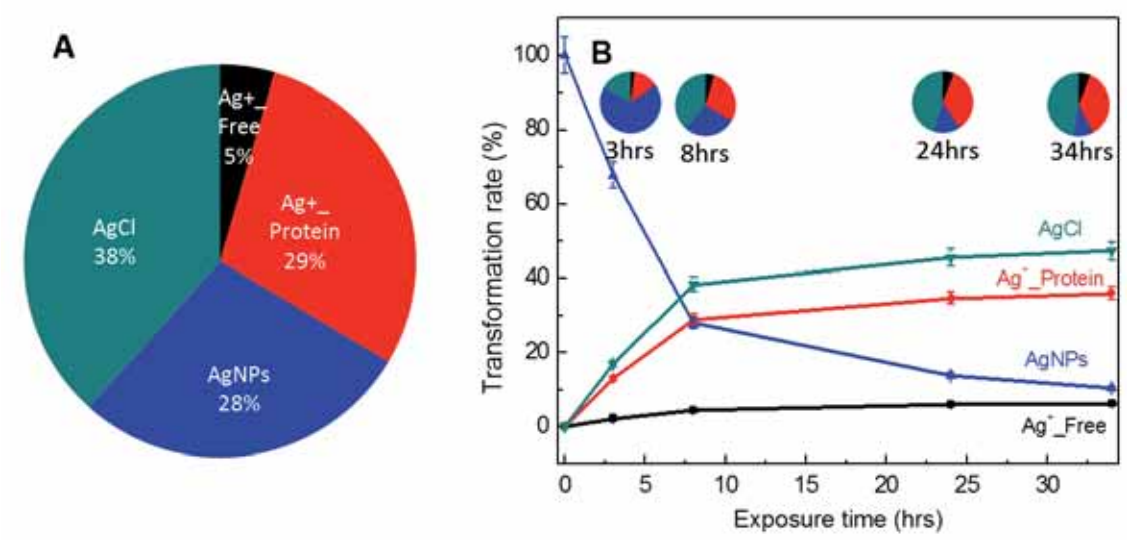

***Figure 3.10**. A) Contribution of different Ag species detected after 8 hours of incubating AgNP in DMEM supplemented with 10% FBS obtained from ICP-MS and B) Distribution of generated Ag species through incubation time.*

3.3.5. Controlled dissolution

Our observations are not only crucial for correct interpretation of data in nanotoxicology but also helpful in the safe design of NPs where dissolution of NPs should be controlled (accelerated or avoided). Since NPs dissolution in a certain environment is due to their high surface reactivity, one straightforward idea to govern it is to passivate their surface. Several environmental studies have reported that the presence of sulfur has induced the formation of an $Ag@Ag_2S$ core-sell structure which chemically passivates the NP surface and influence (block) the ion release[15, 31]. As

shown in the above section, it was observed that when coating the AgNPs with MUA, the NP dissolution was significantly reduced (Figure 3.3D). In this chapter, other solutions for controlling the dissolution of AgNPs in biological media, in addition to using a strongly binding surfactant, are also discussed, either by adding Ag^+ to AgNP solution prior to the exposure or ageing the NPs.

Thus, considering the NPs equilibrium with their ions, if there is an increase in the concentration of free Ag^+, the system, following Le Chatelier principle, will push the equilibrium towards creating AgNPs. As a result, dissolution is inhibited. In our experiment, prior to the exposure, different amounts of Ag^+ were added to Ag50 NPs solution. The amount of added Ag^+ is calculated as the percentage of initial Ag amount. Herein, we tried with the addition of low (6%) and high (20%) amount of Ag^+. Figure 3.11 shows the UV-Visible spectra of large size AgNPs after being incubated with FBS in DMEM without and with adding different amounts of Ag^+. As hypothesized, when increasing the added amount of Ag ions to the NP stock solution prior to the exposure, the evolution of UV-Visible spectra is less indicating that in an excess of Ag ions, before supersaturation, the NPs are more stable.

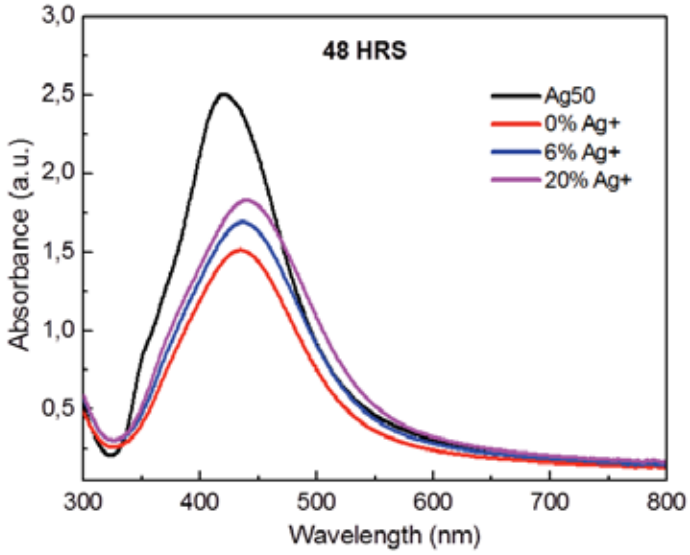

Figure 3.11. *UV-Visible spectra obtained after 48hrs incubation of Ag50 in FBS/DMEM without and with the addition of Ag+ (6% and 20%) prior to the exposure.*

To investigate the effect of ageing, AgNPs after being stored for 1 month were incubated in CCM supplemented with FBS. Contrary to the fresh prepared NPs, there was no significant dissolution of NPs observed in the time scale of the investigation. There was only a red shift in SPR band of the NPs due to the adsorption of the proteins instead of a dissipation of the peak (Figure 3.12).

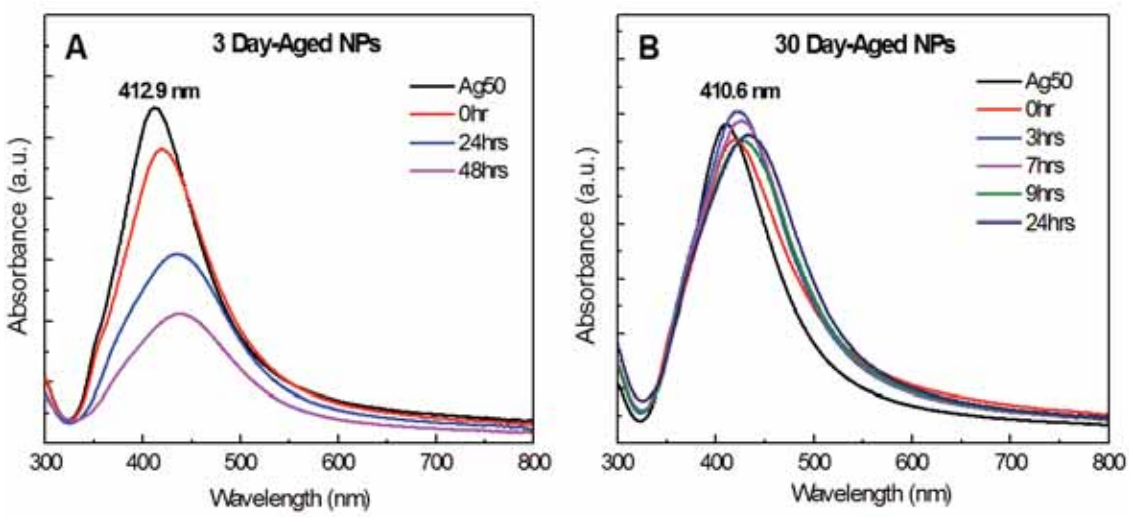

***Figure 3.11**. UV-Visible spectra obtained after different time of incubation in FBS of AgNPs (large size, 50nm) with different aging time: A) 3 days and B) 1 month.*

A possible explanation for these findings is that the AgNPs which are stored for a period of time got partially oxidized by the dissolved oxygen and formed an oxide layer on the surface which passivates the NP surface or reduce its surface reactivity, hence inhibits the dissolution. This oxidation is demonstrated by the blue-shift in SPR absorption peak before incubation from 412.9nm (at day 3) to 410.6nm (at day 30) which is attributed to the decrease in the size of the metallic Ag core[32].

3.4. Conclusions

The results presented in this chapter show that AgNPs of certain sizes dispersed in cell culture media supplemented with different types of serum experience transformations, mainly aggregation, protein adsorption and dissolution. The

significance of these processes, especially dissolution, depends on several factors including size of NPs and composition of media. The role of ion scavengers (Cl^- and biomolecules) to NP dissolution was confirmed in how they drive the equilibrium between NP and its corresponding ions towards dissolution. Then, various ways such as aging the NPs or doping NP solutions with their ionic counterparts, to inhibit or control the dissolution, were also presented. A developed protocol for identifying different Ag species generated during incubating NPs in biological media was shown in this chapter. These findings not only help to better evaluate the mechanism of NP toxicity but also contribute to the safer design of NPs.

References

1. Auffan, M.; Rose, J.; Bottero, J. Y.; Lowry, G. V.; Jolivet, J. P.; Wiesner, M. R., Towards a definition of inorganic nanoparticles from an environmental, health and safety perspective. *Nat Nanotechnol* **2009,** *4* (10), 634-641.

2. Borm, P.; Klaessig, F. C.; Landry, T. D.; Moudgil, B.; Pauluhn, J.; Thomas, K.; Trottier, R.; Wood, S., Research strategies for safety evaluation of nanomaterials, Part V: Role of dissolution in biological fate and effects of nanoscale particles. *Toxicol Sci* **2006,** *90* (1), 23-32.

3. Jolivet, J. P.; Froidefond, C.; Pottier, A.; Chaneac, C.; Cassaignon, S.; Tronc, E.; Euzen, P., Size tailoring of oxide nanoparticles by precipitation in aqueous medium. A semi-quantitative modelling. *J Mater Chem* **2004,** *14* (21), 3281-3288.

4. Talapin, D. V.; Rogach, A. L.; Haase, M.; Weller, H., Evolution of an ensemble of nanoparticles in a colloidal solution: Theoretical study. *J Phys Chem B* **2001,** *105* (49), 12278-12285.

5. Casals, E.; Gonzalez, E.; Puntes, V. F., Reactivity of inorganic nanoparticles in biological environments: insights into nanotoxicity mechanisms. *Journal of Physics D-Applied Physics* **2012,** *45* (44).

6. Navarro, E.; Piccapietra, F.; Wagner, B.; Marconi, F.; Kaegi, R.; Odzak, N.; Sigg, L.; Behra, R., Toxicity of Silver Nanoparticles to Chlamydomonas reinhardtii. *Environ Sci Technol* **2008,** *42* (23), 8959-8964.

7. Asharani, P. V.; Wu, Y. L.; Gong, Z. Y.; Valiyaveettil, S., Toxicity of silver nanoparticles in zebrafish models. *Nanotechnology* **2008,** *19* (25).

8. Choi, O.; Deng, K. K.; Kim, N. J.; Ross, L.; Surampalli, R. Y.; Hu, Z. Q., The inhibitory effects of silver nanoparticles, silver ions, and silver chloride colloids on microbial growth. *Water Res* **2008,** *42* (12), 3066-3074.

9. AshaRani, P. V.; Mun, G. L. K.; Hande, M. P.; Valiyaveettil, S., Cytotoxicity and Genotoxicity of Silver Nanoparticles in Human Cells. *Acs Nano* **2009,** *3* (2), 279-290.

10. Lazaro, F. J.; Abadia, A. R.; Romero, M. S.; Gutierrez, L.; Lazaro, J.; Morales, M. P., Magnetic characterisation of rat muscle tissues after subcutaneous iron dextran injection. *Bba-Mol Basis Dis* **2005,** *1740* (3), 434-445.

11. Xia, T.; Kovochich, M.; Liong, M.; Madler, L.; Gilbert, B.; Shi, H. B.; Yeh, J. I.; Zink, J. I.; Nel, A. E., Comparison of the Mechanism of Toxicity of Zinc Oxide and Cerium Oxide Nanoparticles Based on Dissolution and Oxidative Stress Properties. *Acs Nano* **2008,** *2* (10), 2121-2134.

12. Sharma, V. K., Stability and Toxicity of Silver Nanoparticles in Aquatic Environment: A Review. *Acs Sym Ser* **2013,** *1124*, 165-179.

13. Kvitek, L.; Panacek, A.; Soukupova, J.; Kolar, M.; Vecerova, R.; Prucek, R.; Holecova, M.; Zboril, R., Effect of surfactants and polymers on stability and antibacterial activity of silver nanoparticles (NPs). *J Phys Chem C* **2008,** *112* (15), 5825-5834.

14. Xiu, Z. M.; Zhang, Q. B.; Puppala, H. L.; Colvin, V. L.; Alvarez, P. J. J., Negligible Particle-Specific Antibacterial Activity of Silver Nanoparticles. *Nano Lett* **2012,** *12* (8), 4271-4275.

15. Liu, J. Y.; Sonshine, D. A.; Shervani, S.; Hurt, R. H., Controlled Release of Biologically Active Silver from Nanosilver Surfaces. *Acs Nano* **2010,** *4* (11), 6903-6913.

16. Lee, P. C.; Meisel, D., Adsorption and Surface-Enhanced Raman of Dyes on Silver and Gold Sols. *J Phys Chem-Us* **1982,** *86* (17), 3391-3395.

17. Casals, E.; Pfaller, T.; Duschl, A.; Oostingh, G. J.; Puntes, V., Time Evolution of the Nanoparticle Protein Corona. *Acs Nano* **2010,** *4* (7), 3623-3632.

18. Casals, E.; Pfaller, T.; Duschl, A.; Oostingh, G. J.; Puntes, V. F., Hardening of the Nanoparticle-Protein Corona in Metal (Au, Ag) and Oxide (Fe3O4, CoO, and CeO2) Nanoparticles. *Small* **2011,** *7* (24), 3479-3486.

19. Vroman, L., Effect of Adsorbed Proteins on Wettability of Hydrophilic and Hydrophobic Solids. *Nature* **1962,** *196* (4853), 476-&.

20. Li, X.; Lenhart, J. J.; Walker, H. W., Aggregation Kinetics and Dissolution of Coated Silver Nanoparticles. *Langmuir* **2012,** *28* (2), 1095-1104.

21. Chappell, M. A.; Miller, L. F.; George, A. J.; Pettway, B. A.; Price, C. L.; Porter, B. E.; Bednar, A. J.; Seiter, J. M.; Kennedy, A. J.; Steevens, J. A., Simultaneous dispersion-dissolution behavior of concentrated silver nanoparticle suspensions in the presence of model organic solutes. *Chemosphere* **2011,** *84* (8), 1108-1116.

22. Sperling, R. A.; Parak, W. J., Surface modification, functionalization and bioconjugation of colloidal inorganic nanoparticles. *Philos T R Soc A* **2010,** *368* (1915), 1333-1383.

23. Liu, J. Y.; Hurt, R. H., Ion Release Kinetics and Particle Persistence in Aqueous Nano-Silver Colloids. *Environ Sci Technol* **2010,** *44* (6), 2169-2175.

24. Gondikas, A. P.; Morris, A.; Reinsch, B. C.; Marinakos, S. M.; Lowry, G. V.; Kim, H. H., Cysteine-induced modifications of zero-valent Ag nanomaterials: implications for particle surface chemistry, aggregation, dissolution, and silver speciation. *Environ. Sci. Technol.* **2012,** *46* (13), 7037–7045.

25. An, J.; Tang, B.; Zheng, X. L.; Zhou, J.; Dong, F. X.; Xu, S. P.; Wang, Y.; Zhao, B.; Xu, W. Q., Sculpturing effect of chloride ions in shape transformation from triangular to discal silver nanoplates. *J Phys Chem C* **2008,** *112* (39), 15176-15182.

26. Izak-Nau, E.; Voetz, M.; Eiden, S.; Duschl, A.; Puntes, V. F., Altered characteristics of silica nanoparticles in bovine and human serum: the importance of nanomaterial characterization prior to its toxicological evaluation. *Part Fibre Toxicol* **2013,** *10*.

27. Levard, C.; Michel, F. M.; Wang, Y. G.; Choi, Y.; Eng, P.; Brown, G. E., Probing Ag nanoparticle surface oxidation in contact with (in)organics: an X-ray scattering and fluorescence yield approach. *J Synchrotron Radiat* **2011,** *18*, 871-878.

28. Liu, J. Y.; Pennell, K. G.; Hurt, R. H., Kinetics and Mechanisms of Nanosilver Oxysulfidation. *Environ Sci Technol* **2011,** *45* (17), 7345-7353.

29. Chao, J. B.; Liu, J. F.; Yu, S. J.; Feng, Y. D.; Tan, Z. Q.; Liu, R.; Yin, Y. G., Speciation Analysis of Silver Nanoparticles and Silver Ions in Antibacterial Products and Environmental Waters via Cloud Point Extraction-Based Separation. *Anal Chem* **2011,** *83* (17), 6875-6882.

30. Misra, S. K.; Dybowska, A.; Berhanu, D.; Luoma, S. N.; Valsami-Jones, E., The complexity of nanoparticle dissolution and its importance in nanotoxicological studies. *Sci Total Environ* **2012,** *438*, 225-232.

31. Levard, C.; Hotze, E. M.; Lowry, G. V.; Brown, G. E., Environmental Transformations of Silver Nanoparticles: Impact on Stability and Toxicity. *Environ Sci Technol* **2012,** *46* (13), 6900-6914.

32. Gorham, J. M.; MacCuspie, R. I.; Klein, K. L.; Fairbrother, D. H.; Holbrook, R. D., UV-induced photochemical transformations of citrate-capped silver nanoparticle suspensions. *J Nanopart Res* **2012,** *14* (10).

Chapter 4

ENHANCING CHEMICAL STABILITY OF SILVER NANOPARTICLES: CORE@SHELL STRUCTURE

4.1. Introduction

Noble metal nanoparticles (NPs) have been extensively investigated mainly due to their unique and fascinating optical properties which arise from a phenomenon so-called surface plasmon resonance (SPR). According to the Mie theory, this originates from the coherent oscillation of the conduction electrons at the surface of the NPs and their interaction with an external electromagnetic field[1]. These properties make them potential candidates for various applications in biosensors[2-3], surface-enhanced Raman scattering (SERS)[4], imaging[5] or biomedicine[6-7]. Among those NPs, gold and silver are of higher interest and have attracted considerable researches[8-9]. While gold is highly biocompatible, chemically stable, well-controlled synthesized and easy to be functionalized, silver shows higher plasmonic efficiency and superior electromagnetic enhancement in the visible range together with beneficially antibacterial properties. However, as reported in previous chapters, silver nanoparticles (AgNPs) suffer several transformations including dissolution when they are exposed to biological environments due to its ability of oxidation and corrosion. As a consequence, this can lead to loss of optical properties during analysis, NP disintegration and undesirable biological effects.

Au-Ag core-shell NPs have been focused more recently since combining these two metals offers the possibility to engineer their optical properties through continuously tuning the SPR by varying either the size of the core or the thickness of the shell[10-12]. Besides, AgNPs was recognized as a challenging material in obtaining a good monodispersity, especially in aqueous phase since it is very hard to control the nucleation of AgNPs[13]. Meanwhile, the preparation of uniform Au spherical NPs of different sizes is well-controlled[14] and the deposition of Ag on top of Au is facile due to their similar face-centered cubic (fcc) crystal structure and lattice constant. Therefore, using AuNPs as a template in fabricating the core-shell structures has been used to produce Ag-like monodispersed NPs[15]. Additionally to the improved morphology and optical properties tunability, with the support of highly noble Au core, we hypothesized that this approach would also bring about the opportunity to modify the Ag chemical potential, enhance its nobility, i.e. the potential to be oxidized, and therefore reduce its oxidative dissolution.

To synthesize bimetallic core-shell structures, successive reduction of two metal salt solutions is applied in which the NPs generated during the first reduction are used as seeds for the second one. This method is considered as the most suitable in comparison to simultaneous fabrication or co-reduction of precursor ions[16] which easily produce alloy structures that also serves to adjust the SPR and the chemical reactivity of Ag in a different way. Different preparation methods have been utilized to obtain Au-Ag core-shell NPs. For instance, the silver-coated gold NPs with controlled thickness of the shell were prepared using electrochemical synthesis[10] or in another case, UVA irradiation was applied to deposit Ag onto AuNP surface in the presence of a photoreducing ketone[17]. Selvakannan group synthesized aqueous Au-Ag core shell NPs using tyrosine as a pH-dependent reducing agent as well as the stabilizing agent[18]. Meanwhile, Lu et al. attempted to fabricate ¨stabilizer-free¨ NPs with ascorbic acid reduction[12], these ¨stabilizer free¨ NPs are preferred for sensing and further functionalization.

In this chapter, preparation of Au-Ag core-shell NPs by chemical reduction using sodium citrate as the only reducing agent in all the process is described. The optical properties of the NPs were tuned by changing Ag content in the shell, all monitored by UV-Visible spectroscopy. Then, chemical stability in biological environments of these NPs as a function of shell thickness was investigated via incubation in complete cell culture media for different times.

4.2. Materials and Methods

Materials. Gold (III) chloride trihydrate ($HAuCl_4$. $3H_2O$, ≥99.9% trace metals basis), sodium citrate tribasic dihydrate ($Na_3C_6H_5O_7.2H_2O$), silver nitrate ($AgNO_3$, ACS reagent ≥ 99%), sodium borohydride ($NaBH_4$, ReagentPlus 99%), Dulbecco´s modified eagle´s medium (DMEM, with 4500mg/L glucose and sodium bicarbonate, without L-glutamine, sodium pyruvate, and phenol red, liquid, sterile-filtered) and fetal bovine serum (FBS, sterile-filtered) were purchased from Sigma-Aldrich. Apart from FBS which was heat inactivated at 55^{o}C for 1hr before usage, all other reagents were used as received. Milli-Q water with a resistivity of 18.2 mΩ.cm was used throughout the experiments.

Synthesis of Au core. *Au seeds (10nm)*. Citrate-coated AuNPs of 10nm were prepared following Turkevich method[19]. Particularly, 1ml of 25mM $HAuCl_4$ aqueous solution was fastly injected to a boiling solution of sodium citrate (150ml, 2.2mM) in a three-neck round-bottom flask under vigorous stirring. After around 3 mins, the reaction mixture turned to wine-red color indicating the formation of nanoparticles. The solution was kept boiling for another 2 mins to make sure the reaction completed. The obtained nanoparticles would be used for the preparation of larger AuNPs or the growth of Ag shell.

Au core (~ 30nm). Citrate-stabilized AuNPs of around 30nm in diameter was prepared using the seed-mediated method developed by our group[14] with modification. Briefly, as-prepared Au seeds solution was first diluted 3 times by extracting 100ml of solution and adding 100ml of 2.2mM sodium citrate. Then, the mixture was heated to 90^{o}C under stirring. Subsequently, 1ml of 25mM $HAuCl_4$ was injected and after 30mins,

another 1ml was added. The process of dilution and injections was repeated again to yield 30nm AuNPs.

Synthesis of Au@Ag core-shell NPs.

With 10nm Au core. The deposition of Ag was carried out by added Ag precursor to the as-prepared Au seed solution. In a standard experiment, 1ml of 25mM $AgNO_3$ and 1ml of sodium citrate 60mM were added into 150ml of AuNPs solution at certain temperature under stirring. The reaction kinetics was followed by extracting an aliquot at different reaction times and the deposition was carried out for 30mins.

With 30nm Au core. 30ml of the as-prepared 30nm citrate-coated AuNPs was mixed with 60ml sodium citrate 2.2mM and the mixture was heated to 80^{o}C under stirring. Subsequently, 1ml of 1mM $AgNO_3$ was added and the mixture was kept stirring for 30mins in average. The addition of Ag precursor was repeated for certain times to get different Ag contents on the shell.

Synthesis of AgNPs *(12nm)*. Citrate-stabilized AgNPs were synthesized using the popular sodium borohydride reduction[20] with modification. In particular, 1ml of fresh ice-cold 0.1M $NaBH_4$ was quickly injected into a 49ml solution of trisodium citrate (0.25mM) and $AgNO_3$ (0.25mM) prepared in MilliQ water under vigorous stirring. The obtained colloids exhibit a bright yellow colour.

Characterization. The formation and evolution of the nanoparticles were detected by UV-Visible technique. UV-Visible spectra were recorded using a Shimadzu UV-2400 spectrophotometer. The morphology (size and shape) of the NPs was acquired using Transmission Electron Microscope (TEM) or Scanning Transmission Electron Microscope (STEM). TEM images were achieved with a JEOL 1010 electron microscope operating at a low accelerating voltage of 80 kV. Meanwhile, STEM images were obtained by a FEI Magellan 400L SEM using STEM mode. Hydrodynamic diameter of the NPs was measured by Dynamic Light Scattering performing on a Malvern ZetaSizer Nano ZS. Chemical mapping of core-shell NPs was done via Energy Dispersive X-ray

Spectroscopy (EDX) of a FEI Tecnai F20 microscope equipped with a high angle annular dark-field detector (HAADF) to determine their elemental composition.

Chemical stability in biological media studies. Chemical stability of Au and Au@Ag core shell NPs in biological environment was investigated by exposing these NPs to cellular culture medium. The NPs were dispersed in complete cell culture medium (cCCM, DMEM supplemented with 10% FBS) with the ratio 1:10 by volume. The mixture then was kept in an incubator at 37^{o}C for various incubation times. To prevent the interference of the serum to the characterization after incubation, the NPs were separated from the mixture by centrifugation at 19000rpm for 20mins. The particles were resuspended in deionized water prior to characterization.

4.3. Results and Discussions

4.3.1. Seed-mediated p*reparation of Au@Ag core-shell NPs*

The core-shell structures presented in this chapter were prepared using seeded growth method in which gold was used as seed and Ag shell was achieved by addition of the Ag precursor.

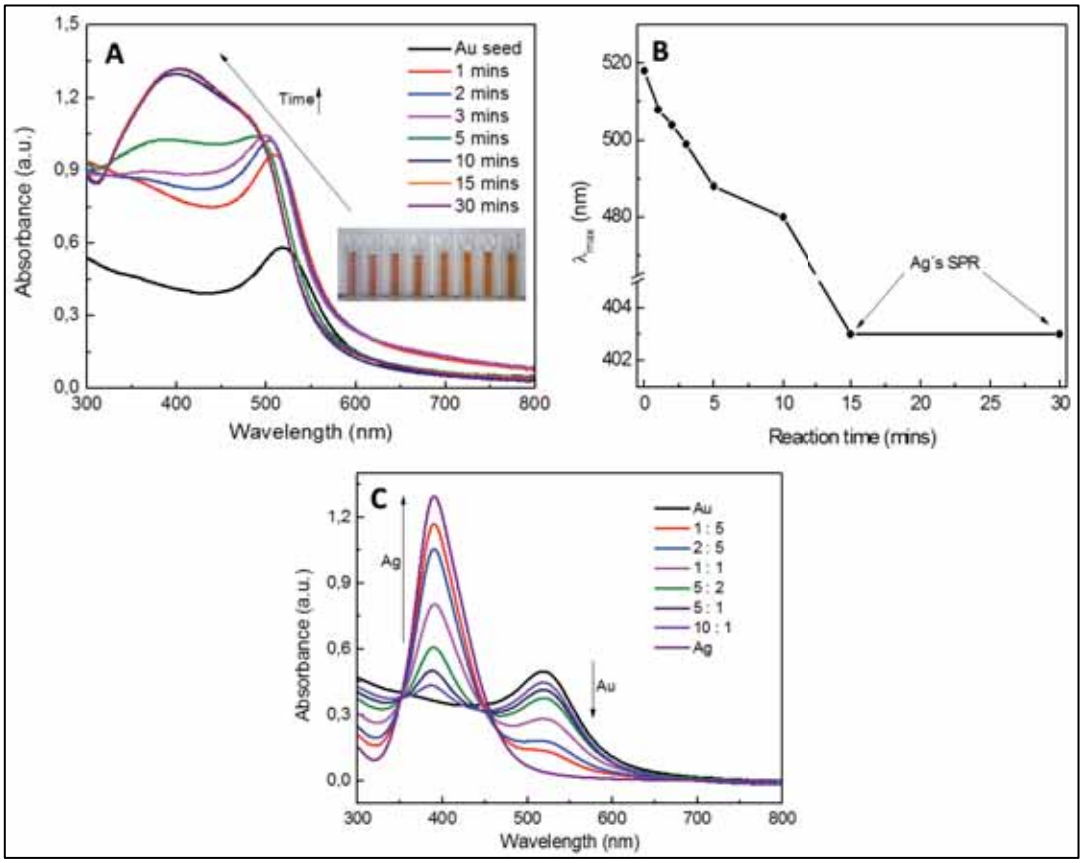

***Figure 4.1**. (A) UV-Vis temporal evolution of Ag shell growth on AuNPs in a single injection and (B) the corresponding evolution of maximal absorption over reaction time. (C) Dependence of UV-Vis spectra of Au-Ag NP mixture on different AuNP : AgNP molar ratios.*

In the present conditions, a large amount of Ag precursor is added so the growth of an increasing Ag shell in solution can be monitored. Figure 4.1A showed the evolution of AuNP spectrum towards AgNP´s one within single injection of Ag precursor.A gradual blue-shift from the characteristic absorption peak of AuNPs to the one of AgNPs as reaction time progress was observed as plotted in Figure 4.1B. This blue shift is attributed to the deposition of Ag onto Au surface which is consistent with previous reports[21]. In parallel, there is also an increase in absorption intensity due to the fact that compared to gold analogues, AgNPs have higher extinction coefficient[22]. In this condition, the deposition of Ag onto the Au surface finished after around 30mins.

To confirm that the added silver is deposited on Au surface instead of forming new individual AgNPs which might also lead to changes in detected optical properties, UV-Vis spectra for a mixture of presynthesized citrate-coated AuNPs (10nm in diameter) and AgNPs (12nm) at different ratio (in number of NPs) were taken as a control experiment. It is clear from Figure 4.1C that the SPR peak of AgNPs evolves when the amount of Ag in the mixture increases. However, the position of individual peaks (the one of gold and silver) stays the same and the final spectra is only a direct convolution of the two different contributions. There is no blue shift of the gold peak towards the absorption wavelength of silver as in the case of core-shell formation. Therefore, the SPR engineering is clearly seen in the core-shell structures.

Growing thick shells onto a NP is challenging since as the NP grows, more material is needed for each nm of the diameter growth. Adding a large amount of precursor normally yields to new nucleation, in such a way that tedious and time consuming multisteps growth is required to grow large shells, unless a fine kinetic control is achieved. It is reported previously that with seed-mediated method, the further growth of larger particles can be done using a lower concentration of seed NPs[14]. Thus, sequential dilution of the reaction solution and injection of Ag precursor were applied to deposit more Ag on Au's surface. In each growth step, 25ml of reaction mixture was first extracted, then 23ml DI H_2O, 1ml of 60mM sodium citrate and 1ml of 25mM $AgNO_3$ were added in that order. The mixture was stirred for 30mins in order to consume all the injected Ag. The evolution of absorption spectra of the reaction mixture through different generations (Figure 4.2B) showed that when continuing to provide Ag precursor, the SPR peak of Au dissipated and transformed completely to the peak of Ag. Moreover, once the peak of Ag has risen and was well-defined (centered at 397.5 nm at second growth step), the continuing addition of Ag precursor caused a gradually red-shift in the UV-Vis absorption of Ag (up to 405.2nm at the tenth growth step) indicating the further growth of the silver layer onto a buried AuNP which can be seen clearly in Figure 4.2B.

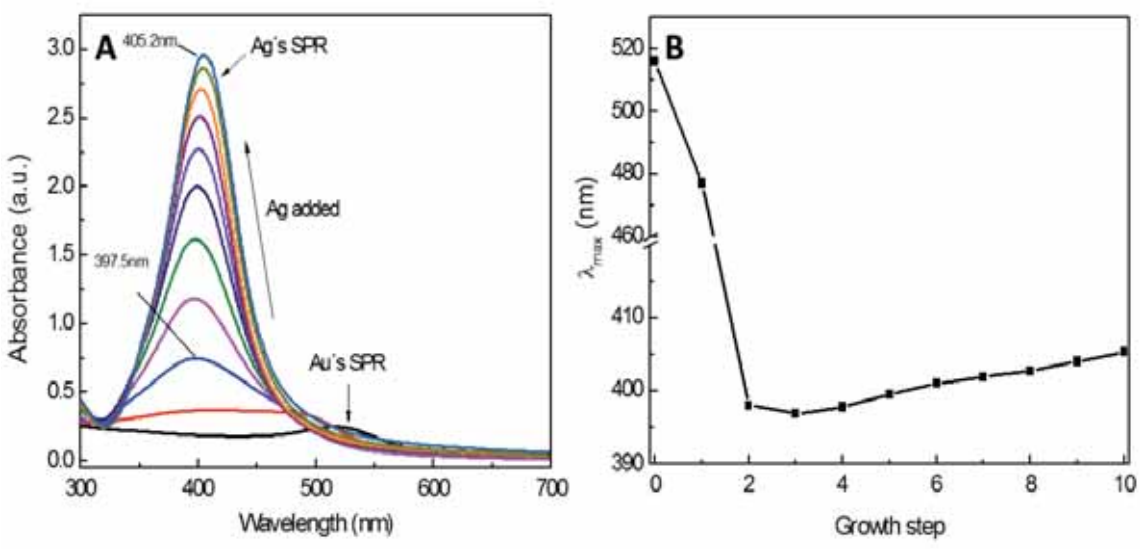

***Figure 4.2**. (A) UV-Vis spectra of NPs obtained after different growth steps by continuously adding of Ag precursor and (B) the corresponding evolution of SPR absorption peak.*

TEM images recorded for the NPs obtained at different growth step (Figure 4.3) displayed their corresponding morphology and confirm all the previous assumptions. Different from spherical seed NPs with well-defined edges (Figure 4.3A), a group of small clusters around parental NPs was observed in all growth steps (Figure 4.3B-D). These small AgNPs have low absorption properties and are not easily detected in the UV-Vis spectra, especially in the presence of strongly absorbent larger NPs. It is likely that in these conditions, the energy barriers for nucleation and growth are very similar. This observation might be due to either of two following possible processes or even both. The first one is that the added Ag was transformed to new separate AgNPs instead of growing onto the Au surface. The second one which has recently been reported as the oxidation of surface Ag when the drop of NPs solution is left evaporated on the TEM grid [23]. According to this hypothesis, it helps to confirm the existence of Ag layer on the surface of Au seed. It is also noticed that the Ag deposition is not homogenous all over the Au surface. Therefore, instead of a full-covered shell, Ag islands were formed as seen in Figure 4.3C. This observation suggested that the NPs conducted a Volmer-Weber island growth due to more preferable adatom-adatom (Ag-Ag) interactions rather than those of the adatom (Ag) with the surface (Au). In

addition, few big particles with *potato*-like shape, which is typical for silver, were also observed (Figure 4.3D). This might be due to the saturation of Ag ions in the reaction mixture at some point which resulted in the nucleation of separate AgNPs. Even though the deposition of Ag onto Au is facile due to their similar crystal structure and lattice constant, to get a well-defined homogeneous Ag shell, factors that control reaction kinetics need to be taken into account.

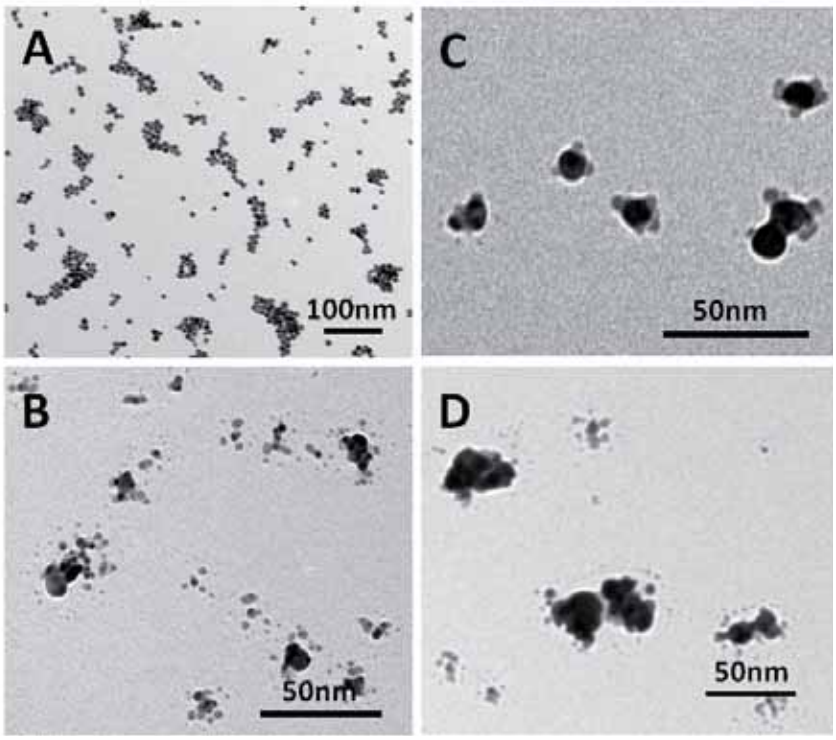

***Figure 4.3**. TEM images of Au seeds (A) and NPs obtained at different growth step: (B) third step, (C) sixth step and (D) nineth step.*

4.3.2. *Ag deposition. Effect of reaction temperature and adding mode of Ag precursor*.

To prevent the formation of the observed new Ag nuclei, the Ag deposition was carried out at milder conditions. In particular, after the seed preparation at boiling temperature, the reaction mixture was cooled down to 90^{o}C. Additionally, 0.2ml, instead of 1ml, of 25mM $AgNO_3$ was injected in each step to avoid the saturation of Ag ions. The corresponding evolution of UV-Vis absorption is shown in Figure 4.4.

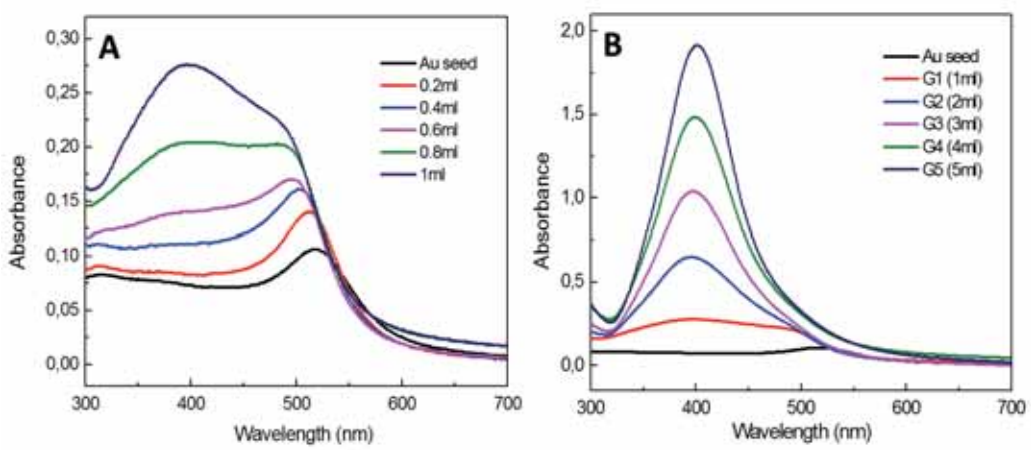

***Figure 4.4**. UV-Vis spectra of NPs obtained when injecting (A) from 0.2 to 1ml and (B) from 1 to 5ml of 25mM $AgNO_3$.*

Similar changes were observed over time as well as when adding more Ag precursor. However, it is noticed from TEM images taken from the aliquots extracted after injecting 0.2 (Figure 4.5A) and 1ml (Figure 4.5B) of 25mM $AgNO_3$ that at lower content of Ag, there is no formation of the small particles which was still found at higher content of Ag. This indicates that, in the latter case, the amount of Ag is in excess. In addition, the NPs tend to form the chain-like aggregates as what Lu and his group reported[12].

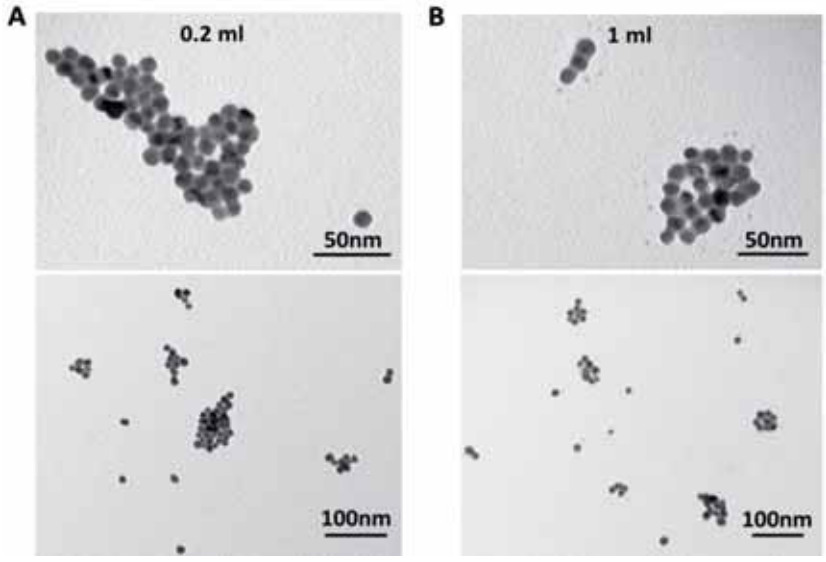

***Figure 4.5**. TEM images of NPs obtained when adding (A-B) 0.2ml and (C-D) 1ml of 25mM $AgNO_3$ to the seed solution.*

4.3.3. *Ag deposition. Effect of seed concentration*.

When growing NPs, especially larger ones, there is always a compromise between producing enough growth (large amounts of precursor needed) and avoiding new nucleation (small amounts of precursor required). Therefore, to produce significant growth of large NPs without generating new NPs, dilution of seed is necessary[14]. Herein, prior to the addition of Ag precursor, Au seed solution was diluted 1.5 times (extracting 50ml of seed solution and adding 50ml of H_2O). The reaction then was carried out at 90°C allowing a better synthesis control. It is obvious from the UV-Vis spectra obtained when adding different amount of Ag ions to the reaction mixture (Figure 4.6) that more Ag is provided, a monotonous evolution is detected.

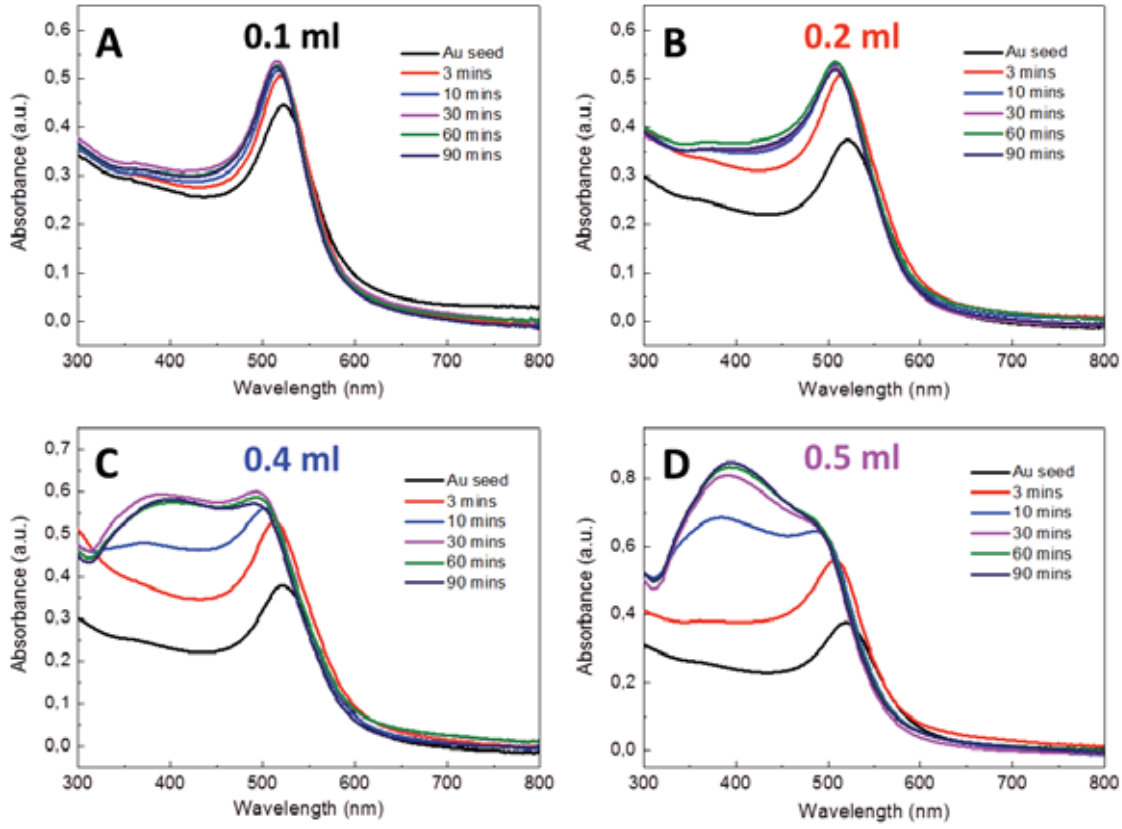

***Figure 4.6**. Temporal UV-Vis spectra obtained when injecting different amount of 25mM $AgNO_3$ (A) 0.1 ml, (B) 0.2 ml, (C) 0.4 ml and (D) 0.5 ml to the 1.5 time diluted Au seed solution.*

Details of this evolution were shown in the plot of SPR wavelength versus reaction time (Figure 4.7A) where a gradually blue shift was observed in all cases, and the shift was greater when more Ag ions were added. This indicates that the thickness of the Ag shell was increasing. In addition, at lower added Ag amount (0.1 to 0.4 ml), it takes around 30mins for all the Ag ions to be reduced, observed by a plateau in SPR evolution. Consistently with the blue shift, TEM images taken for NPs obtained when adding 0.1 and 0.5 ml of 25mM $AgNO_3$ (Figure 4.7B) showed that the latter NPs possess a thicker shell which is more evident and no new nucleation was observed.

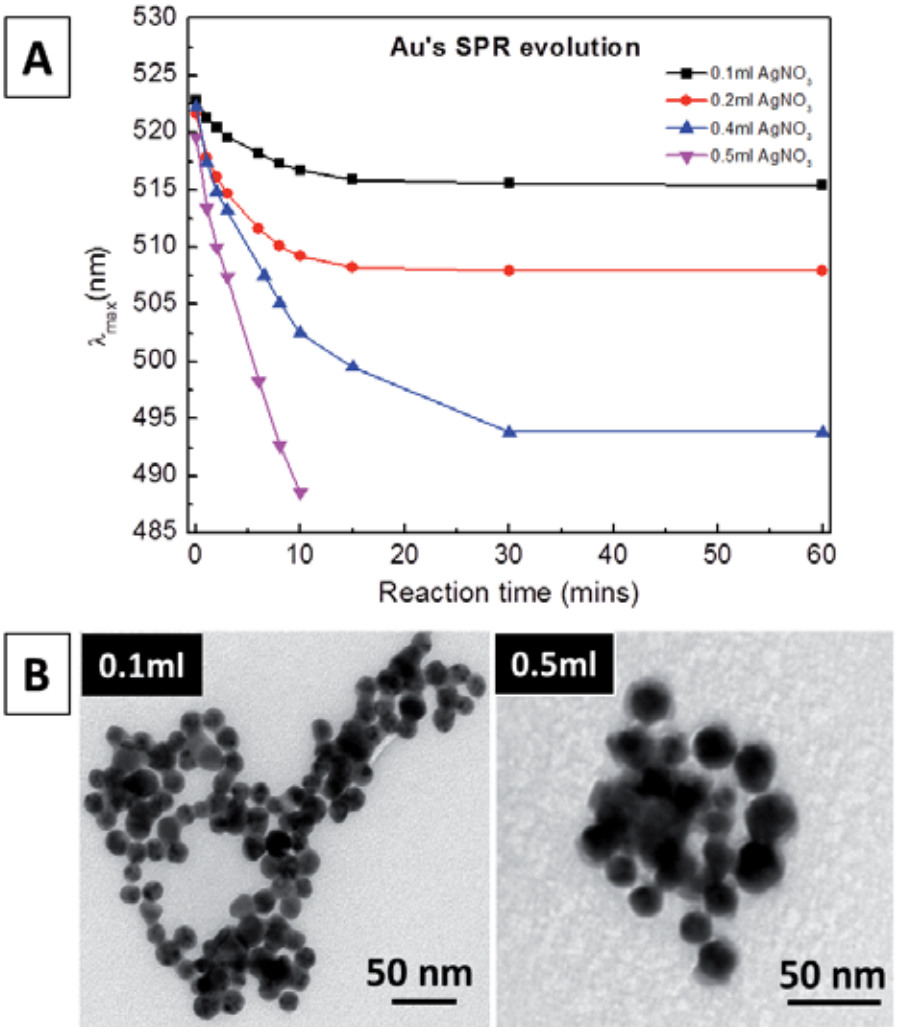

***Figure 4.7**. (A) Evolution of maximal absorption wavelength of AuNPs as a function of reaction time at different added amount of $AgNO_3$. (B) TEM images of NPs obtained when adding 0.1 and 0.5 ml of 25mM $AgNO_3$.*

4.3.4. *Growth of Ag shell on larger Au core (30nm)*

30nm AuNPs were first prepared following a seed-mediated method as previously reported[14] with modification (see experimental section 4.2). The growth of Ag shell then was done with several sequential injections of 1mM $AgNO_3$ (1ml each injection) to a solution of Au core at seed concentrations of 10^{11} NP/ml.

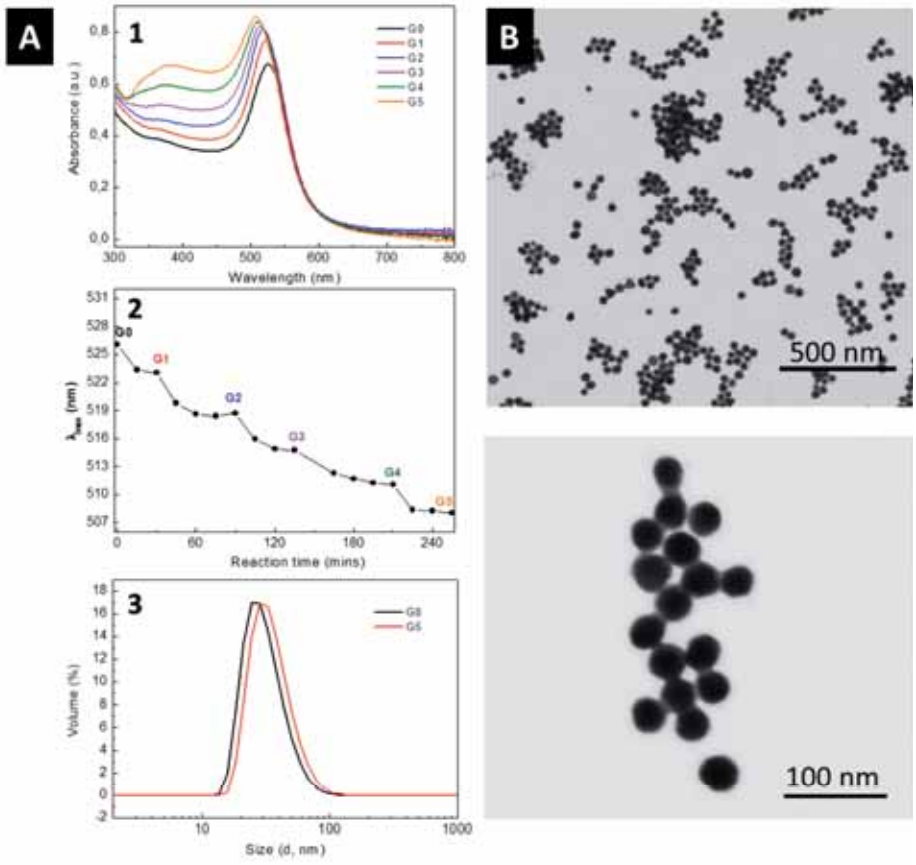

***Figure 4.8**. (A) Evolution in optical properties of Au@Ag core shell NPs with 30nm core through different growth step: 1) UV-Vis spectra; 2) SPR wavelength as a function of reaction time; 3) Dynamic Light Scattering (in volume) and (B) TEM images of NPs obtained at 5th growth step with different magnifications.*

As expected, the UV-Vis spectra obtained at different growth step (Figure 4.8A.1) show an evolution of SPR band from the peak of gold towards the one of silver accompanied with a gradual appearance of silver peak. This indicates that the Ag deposition is happening. The evolution of maximal absorption along with reaction time through

different growth steps is also presented in Figure 4.8A.2 where a clear blue-shift is always observed when adding more Ag. Importantly, new Ag precursor was added when there were no more changes in SPR peak position of the NPs to make sure the former added Ag was completely consumed and then, there would be no saturation of Ag ions. The Ag deposition is also clearly shown by an increase in hydrodynamic diameters of NPs analyzed by DLS (Figure 4.8A.3). The deposited Ag layer can be seen through TEM images as in Figure 4.8B where a shell is observed on top of the AuNPs.

The core-shell structure of Au@Ag nanoparticles is further confirmed by X-ray elemental mapping (Figure 4.9) where the uniform distribution of gold in the center and silver at the periphery of the particles is found. There is no fusion in the elemental distribution indicating that the obtained particles are pure core-shell rather than alloys.

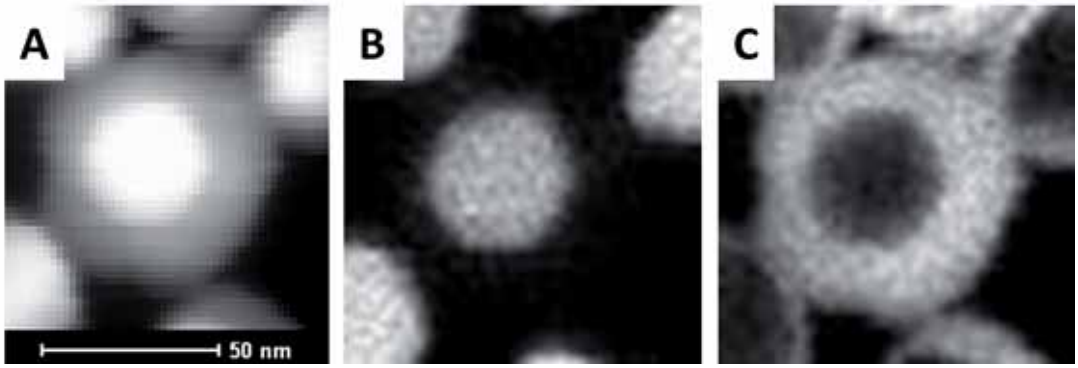

***Figure 4.9**. X-ray mapping of Au@Ag core shell NPs obtained after 5th growth step. STEM-HAADF image (A) and mapping analysis of NPs showing the distribution of gold (B) and silver (C) in the NPs. The scale bar in (A) is applied to (B) and (C).*

4.3.5. *Chemical stability of prepared core-shell NPs in biological media*

As reported in previous chapters, AgNPs suffer fast corrosion and dissolution when being exposed to biological media, particularly cell culture media. To verify if the Au core would affect the nobility of Ag on the shell, similar exposures were carried out for Au@Ag core-shell NPs. Note that the change in Ag nobility which may render the material less prone to oxidation could be due to the proximity effect, i.e. the

reorganization of electrons on Au and Ag atoms when they are at their proximity. In particular, Au@Ag NPs with different content of Ag deposited and the corresponding Au core NPs were incubated in complete cell culture media (DMEM supplemented with 10% FBS) and the evolution of their optical properties was followed. Figure 4.10 shows the UV-Vis spectra of these NPs after incubation for different periods of time.

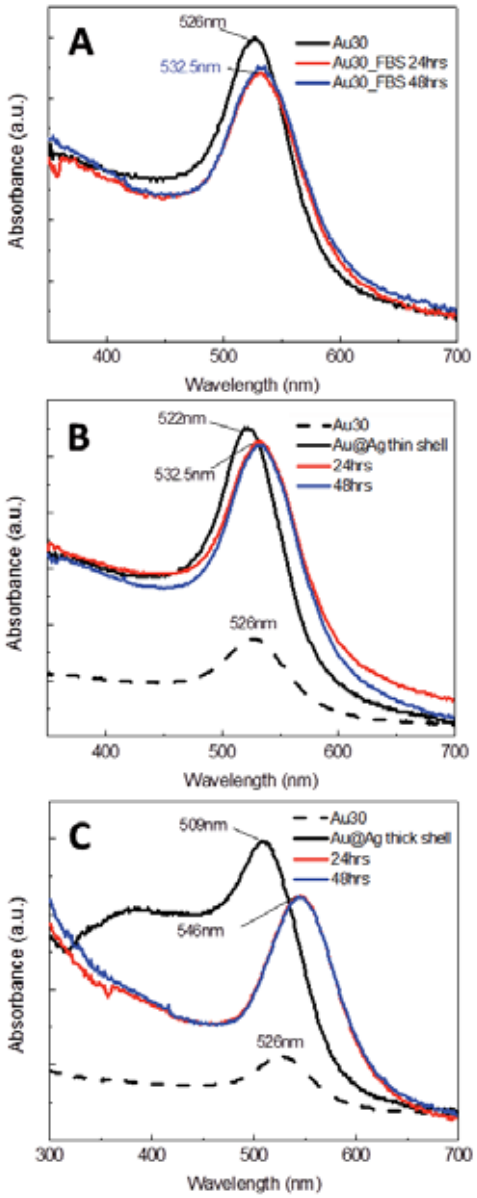

***Figure 4.10**. UV-Vis spectra obtained after incubating in complete cell culture media (FBS/DMEM) for different incubation time of (A) 30nm Au core, (B) Au@Ag core shell with less Ag content (1ml injection) and (C) Au@Ag core shell with more Ag content (5ml injection).*

As expected, there is a red-shift of the SPR peak in the case of AuNPs which is attributed to the protein adsorption or the formation of protein corona[24]. Similarly, a red-shift is also detected in the case of core-shell nanoparticles. In these cases, this shift can be the contribution of either the protein adsorption or the dissolution of the Ag shell and as a result, the SPR band of Au is recovered at higher wavelengths, or a combination of both processes. However, it is noticed that there is no change when continuing the incubation up to 48hrs indicating that the transformation of NPs has finished within the investigated timescale.

In principle, if the Ag shell was completely dissolved, the final appearance of UV-Vis spectra for core-shell NPs obtained after the incubation should be the same as the corresponding Au core, both the position and the intensity of the peak. After 24hrs of incubation, while the total shift of pure AuNPs peak is around 6.5nm from 526nm to 532.5nm (Figure 4.10A) solely resulted from the protein adsorption, this turns to 10.5nm (from 522nm to 532.5nm) in the case of the core-shell ones with lower content of Ag as shown in Figure 4.10B. Even though the final position after exposure in the case of less Ag in the shell is the same as the Au core, the decrease in absorption intensity is missing in the former, indicating that there might be still Ag on the Au surface. The dissolution of Ag is clearly observed in core-shell NPs with higher content of Ag in the shell where there is the disappearance of the shoulder around 400nm and the reduction in intensity of the SPR peak accompanied with a significant red-shift (Figure 4.10C). Similarly to core-shell NPs with low content of Ag, the Ag shell in this case is not completely corroded demonstrated by a huge red-shift of 20nm after 24hr-incubation and remarkably high intensity in UV-Vis in comparison with the pure Au core. It is contrary to the case of pure silver where complete dissolution can be observed with the same incubation conditions (chapter 2 and 3). This indicates that the Ag which stays closer to the Au surface is more chemically stable in biological environment. In another word, Au helps to increase the nobility of Ag at its proximity.

The presence of remain Ag on top of the Au core surface after being incubated in cCCM is confirmed by the STEM-based EDX line scanning. It can be seen from the

profile containing information about Au and Ag content in Figure 4.11B that a reduced Ag shell still exists.

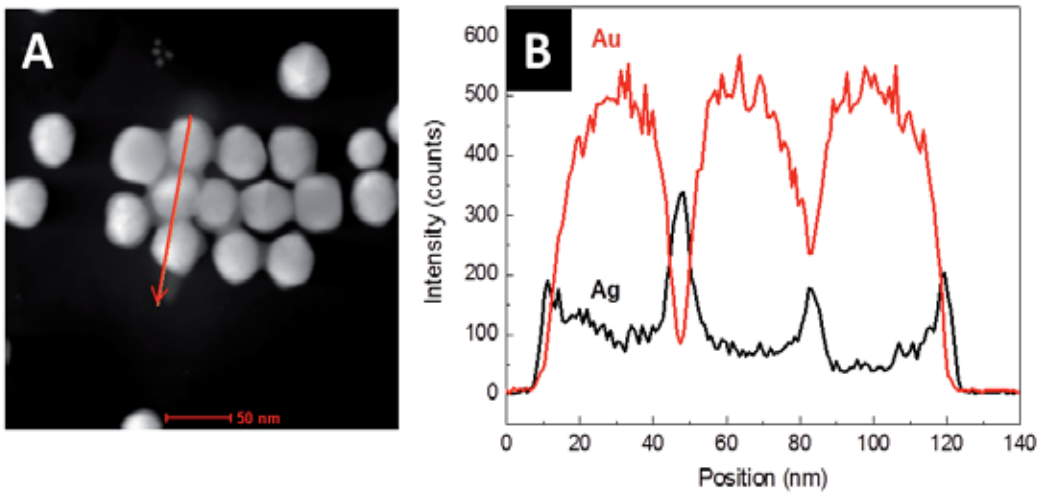

Figure 4.11. *EDX line scan for the core-shell NPs after incubation in cCCM: (A) STEM image of the obtained NPs (the red arrow shows the length and the direction of the scan); (B) EDX line scan across the NPs reveals the presence of the Ag shell.*

A similar finding is achieved when carrying out the EDX line scanning for the core shell NPs with lower content of Ag in the shell after 24hr incubation (Figure 4.12). It is worth to mention that the low intensity of Ag profile is consistent due to its thinness. Noticeably, it was extracted from the line scanning spectra of core-shell NPs obtained before incubation that the thickness of the Ag shell is about 3.8 nm while the one from after incubation showed a ´noble´ Ag layer approximate 2 to 2.3 nm thick. This nobilization phenomena has also been observed in Au-Ag multilayered thin films[25].

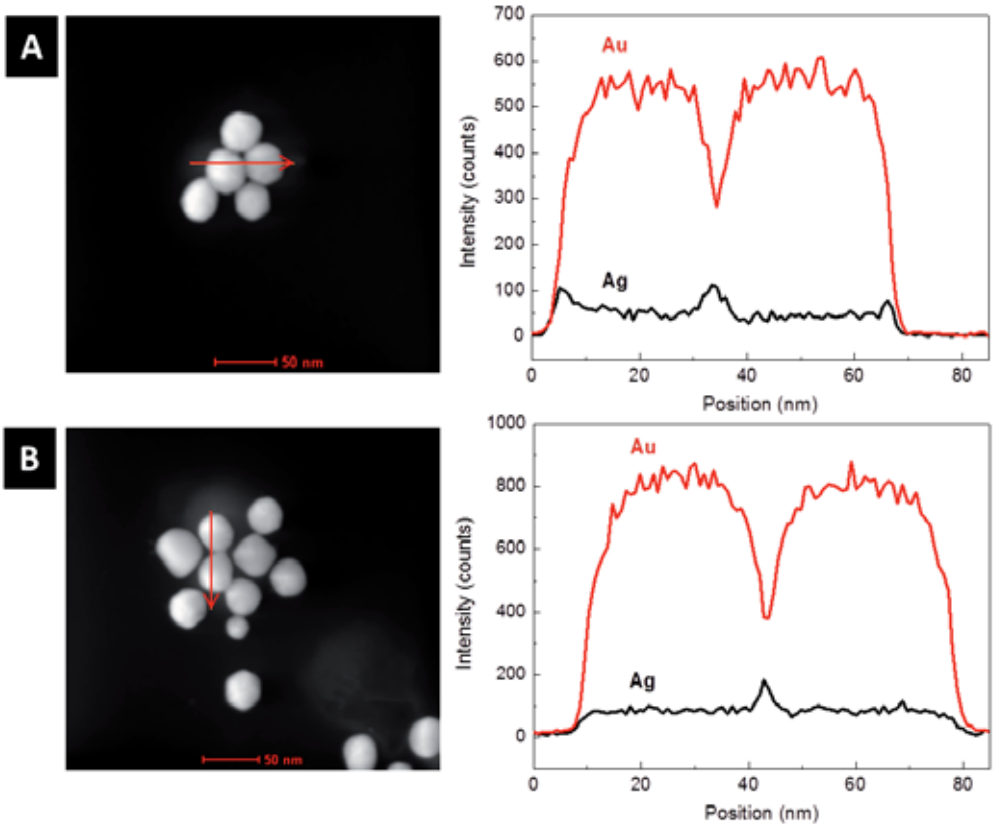

Figure 4.12. *EDX line scan for the core-shell NPs with less content of Ag before (A) and after (B) incubation in cCCM in which, Left: STEM image of the obtained NPs (the red arrow shows the length and the direction of the scan); Right: EDX line scan across the NPs shows the presence of the Ag shell.*

4.4. Conclusion

Gold-silver core-shell nanoparticles of different optical properties were obtained with a seed-mediated approach by varying the size of gold core as well as the thickness of silver shell. Silver shell morphology and thickness can be tuned with kinetic control on several factors including the reaction temperature, seed concentration and manner in adding silver precursor. The prepared core-shell structures showed an enhanced chemical stability in biological environment in comparison with the monometallic silver while maintaining Ag-like optical properties. Indeed, a noble silver layer of approximate 2-2.3nm was found remained on gold surface after being exposed to

complete cell culture medium. These findings are helpful in designing nanomaterials with desirable persistency and anticipated biological responses that trigger.

References

1. Mie, G., Articles on the optical characteristics of turbid tubes, especially colloidal metal solutions. *Ann Phys-Berlin* **1908,** *25* (3), 377-445.

2. Anker, J. N.; Hall, W. P.; Lyandres, O.; Shah, N. C.; Zhao, J.; Van Duyne, R. P., Biosensing with plasmonic nanosensors. *Nat Mater* **2008,** *7* (6), 442-453.

3. Doria, G.; Conde, J.; Veigas, B.; Giestas, L.; Almeida, C.; Assuncao, M.; Rosa, J.; Baptista, P. V., Noble Metal Nanoparticles for Biosensing Applications. *Sensors-Basel* **2012,** *12* (2), 1657-1687.

4. Pustovit, V. N.; Shahbazyan, T. V., Microscopic theory of surface-enhanced Raman scattering in noble-metal nanoparticles. *Phys Rev B* **2006,** *73* (8).

5. Thurn, K. T.; Brown, E. M. B.; Wu, A.; Vogt, S.; Lai, B.; Maser, J.; Paunesku, T.; Woloschak, G. E., Nanoparticles for applications in cellular Imaging. *Nanoscale Res Lett* **2007,** *2* (9), 430-441.

6. Tran, N. T. T.; Wang, T. H.; Lin, C. Y.; Tsai, Y. C.; Lai, C. H.; Tai, Y.; Yung, B. Y. M., Direct Synthesis of Rev Peptide-Conjugated Gold Nanoparticles and Their Application in Cancer Therapeutics. *Bioconjugate Chem* **2011,** *22* (7), 1394-1401.

7. Liao, H. W.; Nehl, C. L.; Hafner, J. H., Biomedical applications of plasmon resonant metal nanoparticles. *Nanomedicine-Uk* **2006,** *1* (2), 201-208.

8. Evanoff, D. D.; Chumanov, G., Synthesis and optical properties of silver nanoparticles and arrays. *Chemphyschem* **2005,** *6* (7), 1221-1231.

9. Sardar, R.; Funston, A. M.; Mulvaney, P.; Murray, R. W., Gold Nanoparticles: Past, Present, and Future. *Langmuir* **2009,** *25* (24), 13840-13851.

10. Zhu, J.; Wang, Y. C.; Lu, Y. M., Fluorescence spectra characters of silver-coated gold colloidal nanoshells. *Colloid Surface A* **2004,** *232* (2-3), 155-161.

11. Shore, M. S.; Wang, J. W.; Johnston-Peck, A. C.; Oldenburg, A. L.; Tracy, J. B., Synthesis of Au(Core)/Ag(Shell) Nanoparticles and their Conversion to AuAg Alloy Nanoparticles. *Small* **2011,** *7* (2), 230-234.

12. Lu, L.; Burkey, G.; Halaciuga, I.; Goia, D. V., Core-shell gold/silver nanoparticles: Synthesis and optical properties. *J Colloid Interf Sci* **2013,** *392*, 90-95.

13. Bastus, N. G.; Merkoci, F.; Piella, J.; Puntes, V., Synthesis of Highly Monodisperse Citrate-Stabilized Silver Nanoparticles of up to 200 nm: Kinetic Control and Catalytic Properties. *Chem Mater* **2014,** *26* (9), 2836-2846.

14. Bastus, N. G.; Comenge, J.; Puntes, V., Kinetically Controlled Seeded Growth Synthesis of Citrate-Stabilized Gold Nanoparticles of up to 200 nm: Size Focusing versus Ostwald Ripening. *Langmuir* **2011,** *27* (17), 11098-11105.

15. Lu, L. H.; Wang, H. S.; Zhou, Y. H.; Xi, S. Q.; Zhang, H. J.; Jiawen, H. B. W.; Zhao, B., Seed-mediated growth of large, monodisperse core-shell gold-silver nanoparticles with Ag-like optical properties. *Chem Commun* **2002,** (2), 144-145.

16. Anandan, S.; Grieser, F.; Ashokkumar, M., Sonochemical synthesis of Au-Ag core-shell bimetallic nanoparticles. *J Phys Chem C* **2008,** *112* (39), 15102-15105.

17. Gonzalez, C. M.; Liu, Y.; Scaiano, J. C., Photochemical Strategies for the Facile Synthesis of Gold-Silver Alloy and Core-Shell Bimetallic Nanoparticles. *J Phys Chem C* **2009,** *113* (27), 11861-11867.

18. Selvakannan, P. R.; Swami, A.; Srisathiyanarayanan, D.; Shirude, P. S.; Pasricha, R.; Mandale, A. B.; Sastry, M., Synthesis of aqueous Au core-Ag shell nanoparticles using tyrosine as a pH-dependent reducing agent and assembling phase-transferred silver nanoparticles at the air-water interface. *Langmuir* **2004,** *20* (18), 7825-7836.

19. Turkevich, J.; Stevenson, P. C.; Hillier, J., A study of the nucleation and growth processes in the synthesis of colloidal gold. *Discuss. Faraday Soc.* **1951,** *11*, 55.

20. Creighton, J. A.; Blatchford, C. G.; Albrecht, M. G., Plasma Resonance Enhancement of Raman-Scattering by Pyridine Adsorbed on Silver or Gold Sol Particles

of Size Comparable to the Excitation Wavelength. *J Chem Soc Farad T 2* **1979,** *75*, 790-798.

21. Xu, S.; Zhao, B.; Xu, W.; Fan, Y., Preparation of Au–Ag coreshell nanoparticles and application of bimetallic sandwich in surface-enhanced Raman scattering (SERS). *Colloids and Surfaces A: Physicochem. Eng. Aspects* **2005,** (257–258), 313-317.

22. Thompson, D. G.; Enright, A.; Faulds, K.; Smith, W. E.; Graham, D., Ultrasensitive DNA detection using oligonucleotide-silver nanoparticle conjugates. *Anal Chem* **2008,** *80* (8), 2805-2810.

23. Glover, R. D.; M., M. J.; E., H. J., Generation of metal nanoparticles from silver and copper objects: nanoparticle dynamics on surfaces and potential sources of nanoparticles in the environment. *ACS Nano* **2011,** *5* (11), 8950-8957.

24. Casals, E.; Pfaller, T.; Duschl, A.; Oostingh, G. J.; Puntes, V., Time Evolution of the Nanoparticle Protein Corona. *Acs Nano* **2010,** *4* (7), 3623-3632.

25. Roy, R. K.; Mandal, S. K.; Pal, A. K., Effect of interfacial alloying on the surface plasmon resonance of nanocrystalline Au-Ag multilayer thin films. *Eur Phys J B* **2003,** *33* (1), 109-114.

Chapter 5

BIOLOGICAL EFFECTS OF NANOPARTICLES

5.1. Introduction

Being a fellow of NanoTOES (Nanotechnology: Training of experts in safety) project, I had chances to do different secondments to various collaborators´ labs who work in biology to get insights in the biological field. The obtained data during these short visits will be presented in this chapter.

It is straightforward that to be applicable in daily products, a material must bring no risks to human health and environment or in another word, they must be safe. Historically, there have been hazardous products being accepted too readily, from the use of lead in paint and children toys to the introduction of thalidomide as painkiller. More recent, zinc oxide, an ingredient commonly found in cosmetics, sunscreens and classified as GRAS (generally recognized as safe) by FDA (Food and Drug Administration), was found to cause neural stem cell apoptosis in its nanoparticulate format in in vitro experiments[1]. Therefore, prior to being manufactured and incorporated in consumable products, biological effects of a material should be carefully determined.

As mentioned over and over, nanomaterials are increasingly being used for commercial purposes due to their useful properties. However, at the same time, these small size materials may also possess potential adverse interactions with biological systems and the environment. Nanoparticles (NPs) can have similar dimensions as biological molecules such as proteins which results in the immediate adsorption of

biomolecules in living systems when they enter tissues and fluids of the body. These NP-protein interactions may modify the biodistribution of NPs and assist in the cell membrane penetration. Such type of activities consequently could cause disorders in cellular functions or even cell damages. For instance, alteration of macrophage functions (inflammation mediators) and damage to the pulmonary epithelium were found greater when administrating 20nm TiO_2 particles to rats via inhalation in comparison with the same mass of 250nm particles[2]. However, this difference was due to unproper dosing where no difference was found when concentration was normalized to surface area instead of mass. Cytotoxicity of bare superparamagnetic iron oxide nanoparticles (SPIONs) to fibroblast was also reported where 20% loss of cell viability was observed at test concentration of 0.05mg/mL[3] while others are safe and used in the clinic including MRI and ferumoxytol[4]. ZnO NPs were found to exert cytotoxicity on mice liver and kidney cells via induction of oxidative stress, DNA damage and apoptosis related to its dissolution and pH alteration in physiological conditions[5].

NPs, once enter human body, are expected to be recognized as a foreign object by immune system and eliminated by it. In case the NPs are designed in a way that they are not seen as a danger by immune system, destruction of NPs is not triggered and their *in vivo* retention time is prolonged. This is sometimes assisted by the adsorption of protein which creates a new biological identity for NPs as mentioned in previous chapters. Under such circumstance, NPs could induce unwanted immune/inflammatory response that may be harmful to the body and cause pathologies. Particularly, NPs could (i) activate the complement cascade that removes pathogens, and platelets; (ii) interact with immune cells including macrophages, monocytes, lymphocytes; (iii) trigger non-specific inflammatory responses; (iv) facilitate antigen-specific hypersensitivity reactions and release of chemokines and immunoregulatory cytokines. On the other hand, NPs can also suppress inflammatory responses or induce no immunomodulatory activities. As an example, engineered carbon nanotubes (CNTs) were reported to activate the complement system. While both single-walled (SWNTs) and double-walled (DWNTs) nanotubes stimulate the

classical pathway (activated by antigen-antibody complexes), only DWNTs triggered the alternative pathway (antibody independent)[6]. In addition, immunosuppression of CNTs via suppression of B cell function was observed by Mitchell et al.[7]. However, LPS contamination was not discarded in those works.

Due to the remarkable introduction of NPs into the environment including ambient air, water and soil, an increasing number of studies have also focused on the assessment of the ecotoxicity of the NPs. Various trophic levels including microorganisms, plants, invertebrates and vertebrates have been chosen for ecotoxicity determination and test systems have been standardized for some organisms under some exposure conditions[8]. To name few among others, silver nanoparticles, well-known for their antibacterial properties, were found to be toxic to algae, plants, fungi, bacteria like nitrogen fixing heterotrophic and soil forming chemolithotrophic bacteria[9]. They are also harmful to fish as they disrupt the Na^+, K^+-ATPase preventing osmoregulation[10]. In another study, Barrena et al. conducted germination (cucumber and lettuce), bioluminescent (Photobacterium phosphoreum) and anaerobic toxicity tests for Au, Ag and Fe_3O_4 NPs and found that low or zero toxicity was observed at the tested concentration[11].

In this chapter, attempts on investigating some of the above mentioned biological effects of NPs were performed. Concretely, cytotoxicity of Au and AgNPs with different surface properties was studied via cell viability by CellTiter blue (CTB) and membrane integrity by Lactose Dehydrogenase (LDH). Measurements of ROS production were also carried out. In addition, ecotoxicity of AgNPs of various sizes was examined on soil nematodes *Caenorhabditis elegans* using synthetic soil pore water. Finally, immune responses to AuNPs exposure were investigated and the role of contaminated endotoxin is also discussed.

5.2. Materials and Methods

5.2.1. Cytotoxicity and ROS production of NPs (in collaboration with Paris Lodron University of Salzburg (PLUS))

Tested nanoparticles

The tested NPs include AuNPs of negatively charge (10nm citrate-coated synthesized following protocol in chapter 4) and positively charge (obtained by quickly injecting 1ml of ice cold $NaBH_4$ 0.1M into a 49ml aqueous mixture containing 0.25mM $HAuCl_4$ and 0.1% chitosan under vigorous stirring), AgNPs of negatively charge (15nm citrate-coated as in previous chapters) and positively charge (achieved from the addition of 1ml of ice cold 0.1M $NaBH_4$ into a 49ml aqueous mixture containing 0.25mM $AgNO_3$ and 0.1% chitosan under vigorous stirring). The corresponding human plasma and human serum coated NPs were also investigated. The coating was done by incubating NPs with the fluids at 37^oC for 24hrs.

Exposure conditions

10µl of NPs at stock concentration (0.033mg/L for Au and 0.027mg/L for Ag) were exposed to 1ml of U937 (human leukemic monocyte lymphoma) or A549 (Human lung adenocarcinoma epithelial) cells (cell density: 10^5cells/ml). For the analysis of cytotoxicity including CellTiter Blue (CTB) and Lactose Dehydrogenase (LDH), cells grown in 96 well plates were exposed to the NPs for either 24 or 48 hours once they formed a confluent monolayer. Meanwhile, ROS production was measured in 24-well plates where the cells were exposed to NPs for 4 hours.

Cytotoxicity assays

CellTiter blue (CTB)

Cell viability was determined using the CellTiter Blue Cell viability kit (Promega, Madison, USA) after exposure to NPs. In all incubations, 0.1% Triton X-100 was used as a positive control. Fluorescence was measured at 590 nm upon excitation at 560 nm using a plate reader (Infinity 200 Pro, Tecan, Groedig Austria).

In house lactose dehydrogenase (LDH)

A modified lactate dehydrogenase assay was used to determine cytotoxicity via cell membrane integrity. Particularly, 50 µl of a solution containing 1mg/ml NADH and 0.75mM pyruvate was added to 10 µl test supernatant obtained after exposure by spinning down at 300g for 5mins, in triplicates and the mixture was incubated at 37°C for 30 minutes. Then, 50 µl of 2, 4 dinitrophenylhydrazine dissolved in 1M HCl was added to all wells following by the incubation at room temperature (RT) for 20 minutes. Finally, 50 µl of 4M sodium hydroxide (NaOH) was added and the absorbance at 540 nm was measured using a Tecan plate reader (Tecan infinity 200 pro) after leaving the plate to incubate for 5 minutes at RT.

Detection of reactive oxygen species *(Cell-based DCFH-DA assay)*

Cell-mediated ROS production was detected by dichloro-dihydro fluorescein diacetate (DCFH-DA) assay as manufacturer's instructions (Sigma-Aldrich, St. Louis, USA). Briefly, 5µl carboxy-DCFHDA (1 mM) was added to each tested well 60 minutes before the end of the exposure. Cells only exposed to cell culture medium acted as negative controls while 500µM H_2O_2 was used as a positive control. Once the exposure period ended, cells were washed twice with 500µl phosphate buffer saline (PBS) and harvested using 75 µl Trypsin. The trypsin reaction was neutralized by adding 425 µl cell culture medium (PBS supplemented with FCS). Cells were then immediately analysed using a flow cytometer (FACSCanto^{TM}, Becton Dickinson). All steps were performed in reduced light conditions due to the light sensitivity of the dye.

5.2.2. Immune response of NPs (in collaboration with Consiglio Nazionale delle Ricerche (CNR))

Monocyte isolation

Human monocytes were obtained from discarded buffy coats of healthy blood donors. Monocytes were obtained by isolating PBMC (peripheral blood mononuclear cells) on Ficoll-Paque PLUS gradients (GE Healthcare, Bio-Sciences AB, Uppsala, Sweden) and subsequent separation with Monocyte Isolation kit II (Miltenyi Biotec, Bergisch-Gladbach, Germany). Only preparations with >95% purity (determined by differential staining on cytocentrifuge smears) and viability (trypan blue dye exclusion) were used.

Isolated monocytes were finally suspended in 2 ml of RPMI 1640+Glutamax-I Medium (GIBCO, Life Technologies, Paisley, UK) supplemented with 50 mg/ml Gentamicin (GIBCO) and 5% heat-inactivated human AB serum (Sigma-Aldrich Inc., St. Louis, MO) at $2x10^6$ cells/well in 8-well plates (Costar, Corning Inc., Corning, NY).

Exposure conditions

Monocytes were exposed to i) LPS (from E.coli serotype 055:B5; Sigma-Aldrich) at 0.01, 0.1, 1. 10 and 100ng/mL; ii) 10nm citrate coated AuNPs (synthesized following protocol described in chapter 4) at 0.25, 0.5, 1, 2 (cm^2/mL) and iii) LPS contaminated AuNPs at similar concentration as NPs (AuNPs were incubated with 200ng/ml LPS for 1hr at room temperature. The collected contaminated NPs then were incubated in plasma at 37^{o}C for another 1hr prior to the exposure). Exposed cells were incubated over night at 37^{o}C in moist air with 5% CO_2. Then, supernatants were collected by centrifuging the plates at 5000rpm for 5mins for detection of protein production and cells were harvested in 400µl of Qiazol (Qiagen, Hilden, Germany) for gene expression analysis.

Gene expression analysis by qPCR

cDNAs were reverse transcribed from total RNA (100 ng) according to the QuantiTect Reverse Transcription Kit (Qiagen) instructions. Three separate reverse transcriptions were performed for each samples and an identical reaction without the reverse transcriptase was also run as negative control. Taqman polymerase chain reaction was performed by an Rotor-Gene™ 3000 (Corbett Research, Doncaster Victoria, Australia), using the QuantiTect SYBR Green PCR master Mix (Qiagen).The final reaction mixture with a total volume of 25µl contained 12.5µl 2x QuantiTect SYBR Green PCR Master Mix, 0.3 µM of each primer and 2.5µl of cDNA. PCR conditions included 95°C for 15min, followed by 45 cycles of 95°C for 15s, 50-60°C for 30s and 72°C for 30s. Primer sequences were supplied by Qiagen both for target and housekeeping genes.

Protein detection by ELISA

IL-1β and IL-1Ra protein production were detected on supernatants collected after incubation by enzyme - linked immunosorbent assay (ELISA). ELISA kits for IL-1β, IL-1Ra were purchased from R&D Systems (Minneapolis, USA) and assays were performed

according to the manufacturers' instructions. Each sample was assayed in duplicate, and detection was carried out with a JUPITER microplate spectrophotometer (Asys Hitech GmbH, Eugendorf, Austria).

5.2.3. Ecotoxicity of AgNPs on soil nematode *Caenorhabditis elegans* (in collaboration with Centre for Ecology and Hydrology (CEH))

Preparing the synthetic soil pore water

The synthetic soil pore water (SSPW) was prepared by adding the following components: $NaHCO_3$, anhydrous KNO_3, $Ca(NO_3)_2$, $MgSO_4 \cdot 7H_2O$, $Na_2HPO_4 \cdot 12H_2O$, and HNO_3 (all provided by Sigma Aldrich); Fe 1 g/L and Al 1 g/L atom absorption spectroscopy standard (VWR International) with amounts per liter shown in Table 5.1 into 750 mL of deionized water. The solution was then filled with water up to 1L. The obtained solution was first bubbled overnight with air to obtain a stable pH of 8.2.

Table 5.1. Composition of synthetic soil pore water

Component	Stock concentration (M)	Volume (mL) per liter of SSPW
$NaHCO_3$	0.1	40
KNO_3	0.1	10
$Ca(NO_3)_2$	0.1	12.5
$MgSO_4$	0.1	5
Na_2HPO_4	0.1	0.01
HNO_3	0.1	10
Iron standard	0.0179 (g/l)	0.559
Aluminium standard	0.037 (g/l)	0.27

Tested NPs

Synthetic spherical citrate/tannic acid coated AgNPs of different sizes (15, 23 and 48nm) were used. To obtain these NPs, 20 mL of 6.8 mM aqueous solution of tri-sodium citrate, containing increasing amounts of tannic acid (0.0047, 0.047 and

0.47mM) corresponding to increasing size of obtained NPs, was heated to 60°C and added with vigorous stirring to 80 mL of 0.74 mM $AgNO_3$ preheated to 60°C. The mixture was kept at 60°C for 3 min, or until its color turned yellow, boiled for 20 mins and cooled down to room temperature[12].

Toxicity test of AgNPs

Ecotoxicity of AgNPs was examined by C. elegans assay using SSPW in a 6-well plate format. Stock solution of tested species was prepared by dispersing the corresponding species into SSPW at a concentration twice the maximum tested concentration. 5 doses of each NPs (0.625, 1.25, 2.5, 5 and 10mg/L) were tested while 10 times lower doses were applied for control Ag ions ($AgNO_3$). Each dose or treatment was carried out with 6 replicates which were distributed randomly among exposure plates. For each test replicate, 1 mL aliquot of stock solution was mixed with another mL of SSPW containing E. coli to 1000 Forzamin attenuation units to yield the desired test concentration in a 2-mL volume and an appropriate food density. After the test solutions were added to the wells, an adult nematode was added to each and incubated at 20^{o}C for 72 h. Then, adult survival and reproduction was measured. Particularly, offspring were first stained with 1% Rose Bengal solution (1ml/well) and plates were then incubated at 55^{o}C to kill laid eggs and hatched juveniles before counting.

5.3. Results and Discussions

5.3.1. Cytotoxicity and ROS production of nanoparticles.

5.3.1.1. Cell membrane integrity

There are different ways to examine cytotoxicity. One of the most common ways is to determine the integrity of the cell membrane. When the membrane is compromised or damaged, lactate hydrogenase (LDH), a protease only active in cells with healthy membrane, will be released into the external environment. Therefore, by measuring released LDH in the supernatant, cell membrane integrity, i. e. cytotoxicity, can be

determined. Cytotoxicity of gold and silver NPs, in which the effects of NP surface charge is of high interest, has been widely investigated using the LDH assay. Herein, we studied the impact of protein adsorption on cytotoxicity of charged NPs.

When exposing immortalized U937 cells (10^5cells/ml) to gold and silver NPs of negative and positive charges for 24 hrs, there was no significant difference in LDH release of charged AuNPs (-60mV and +67mV) while there was an increased release in positive charged AgNPs (+57mV) in comparison with negative charge (-48mV) (Figure 5.1A, B). This is due to the fact that positively charged components can interact more easily and stronger with negatively charged plasma membrane of the cells which can result in its damage. Similar results were observed when the exposure was prolonged up to 48hrs (Figure 5.1C, D) and the positively charged AgNPs were found to induce even higher relative LDH release in respect to other types of NPs.

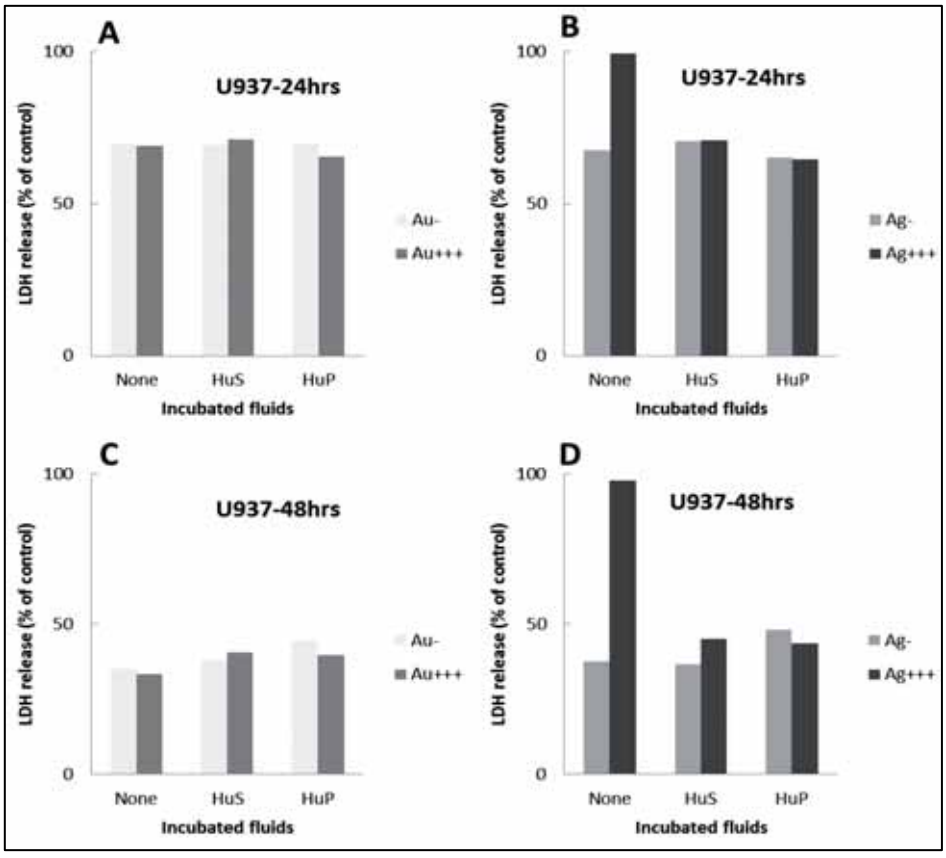

Figure 5.1. *Percentage LDH release from U937 cells after 24 (A, B) and 48 hour (C, D) treatments with AuNPs (A, C) and AgNPs (B, D) of negative and positive charge with and without preincubation with biofluids including human serum and human plasma.*

As discussed previously, protein corona of NPs is known to affect their interaction with cells[13]. In our study, pre-incubation of positive and negative AuNPs as well as negatively charged AgNPs in human serum (HuS) or human plasma (HuP) did not make any significant changes in LDH release of the cells (Figure 5.1). However, interestingly in the case of positively charged AgNPs, LDH release was clearly decreased, around twice when the exposure was carried out for 48hrs (Figure 5.1.D). This observation implies that pre-incubating NPs, especially positively charged ones, with proteins may help to bio-compatibilize them. The improved biocompatibility of positively charged AgNPs might result from the decrease in their surface charge due to the protein adsorption. Indeed, pre-incubated NPs possessed a surface charge of approximately 15mV instead of around 60mV of the original NPs (Figure 5.2D). This charge drop reduced the possibility to approach the cells of AgNPs where they could release ions which are toxic.

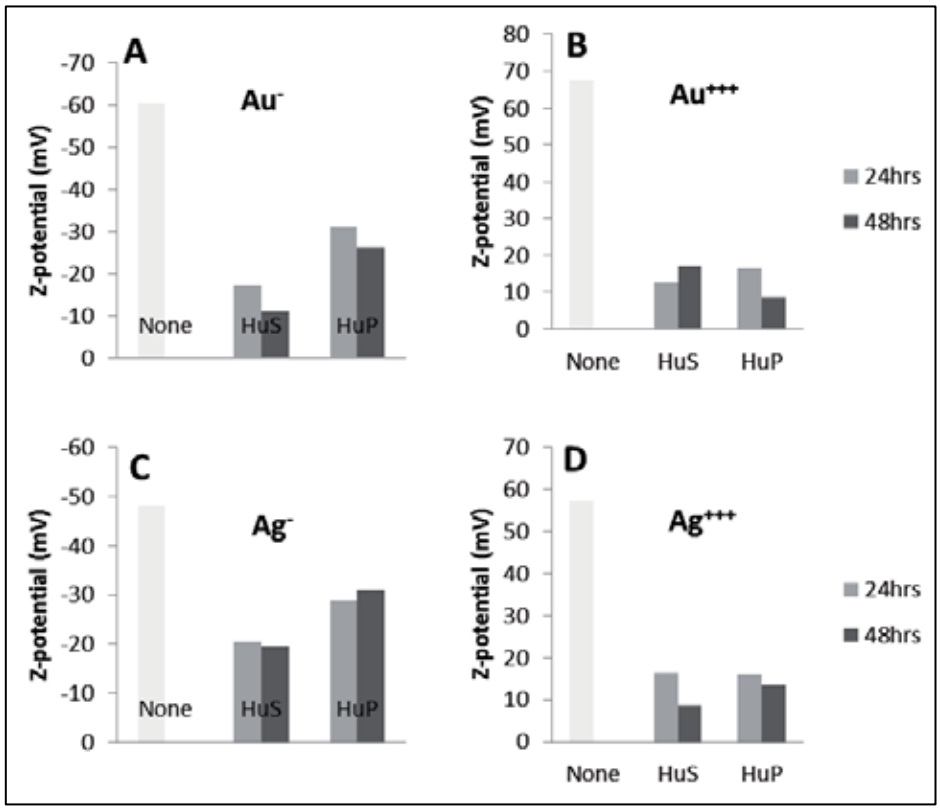

Figure 5.2. *Zeta-potential before and after incubation for 24 and 48hrs in different fluids of negatively (A) and positively (B) charged AuNPs as well as negatively (C) and positively (D) charged AgNPs.*

5.3.1.2. Cell viability

The cytotoxicity of NPs was also assessed using the CTB assay which measures the cell viability by metabolism. The assay is based on the ability of living cells to convert a redox dye (resazurin, blue color) into a fluorescent product (resorufin, pink color). Nonviable cells rapidly lose metabolic capacity and thus do not exhibit fluorescent property.

Similar to what were observed in membrane integrity assessment, at our exposure concentration (0.33µg/L for Au and 0.27µg/L for Ag), charged AuNPs and negatively charged AgNPs induced no significant effects on cell viability (Figure 5.3). Meanwhile, a remarkable decrease in cell viability was found when exposing U937 cells to positively charged AgNPs for 24 and 48hrs (Figure 5.3B, D). The toxicity of AgNPs with positive surface charge was also found to decrease after incubation with biofluids. Indeed, pre-incubated NPs induced significantly higher cell viability in comparison with the non-preincubated ones.

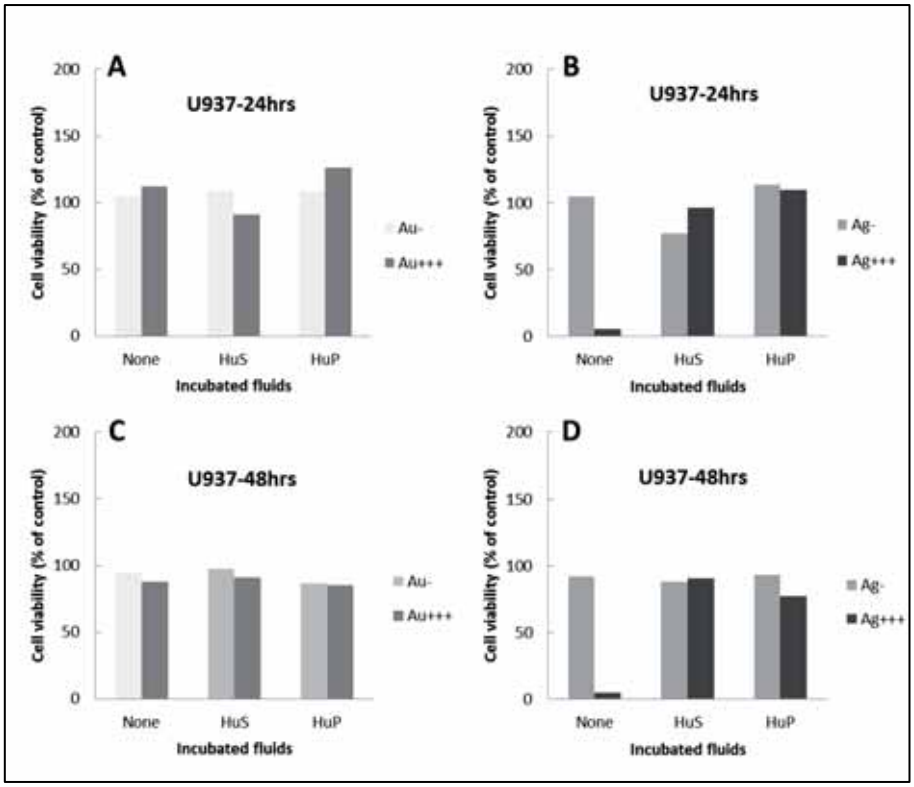

***Figure 5.3**. Cell viability of U937 cells from 24 hour (A, B) and 48 hour (C, D) exposures to charged gold (A, C) and silver (B, D) NPs.*

5.3.1.3. Oxidative stress

Oxidative stress is a state where the normal defense mechanisms of the cells cannot handle the overwhelmed generation of reactive oxygen species (ROS) due to stress conditions. Even though it may bring benefits to the immune system as a weapon to attack pathogens, oxidative stress conditions enhance the production of ROS including superoxide anion, hydrogen peroxide and hydroxyl radical which can cause damage to components of our cells including DNA. Oxidative stress has been considered as a universal mechanism of cellular stress caused by inorganic NPs[14-15]. Hence, apart from cell viability assays, ROS generation is indeed a convenient parameter to measure toxicity.

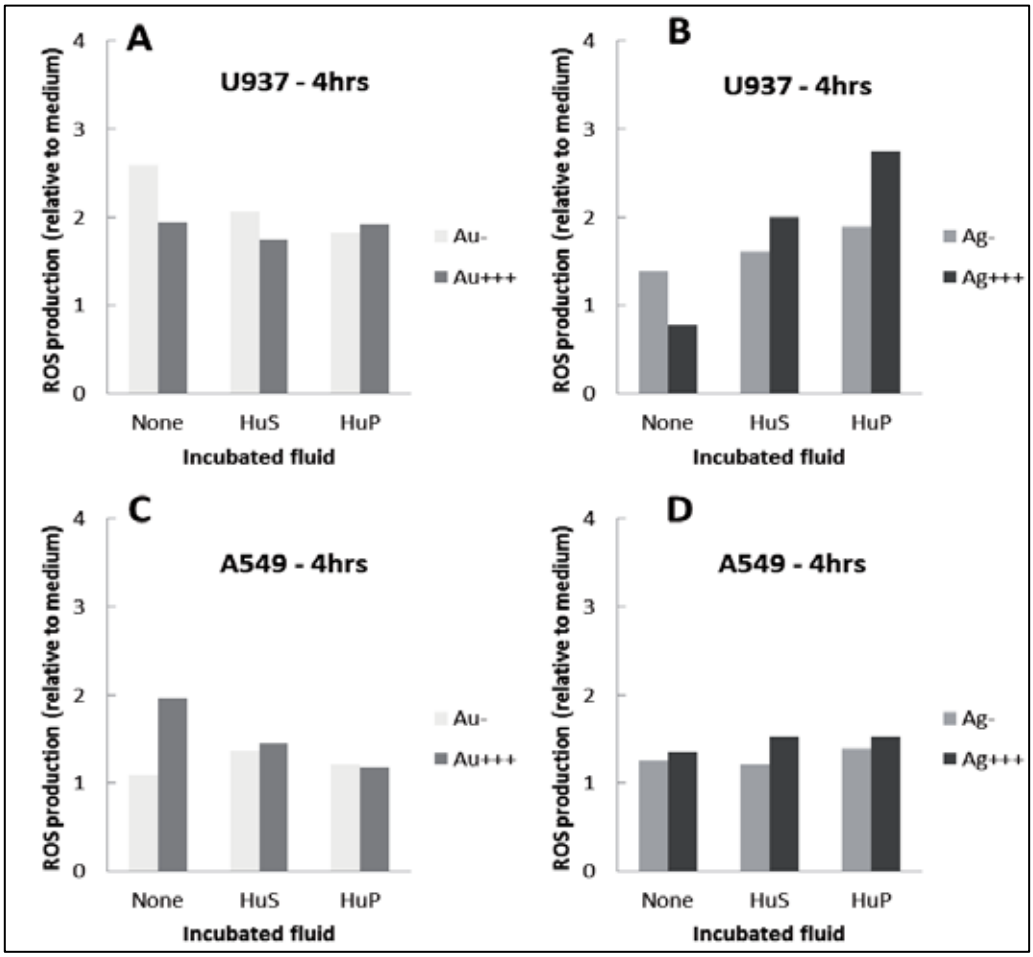

Figure 5.4. *ROS production measured using the DCFH-DA assay following a 4 hour exposure of U937 (A, B) and A549 (C, D) cells to charged gold (A, C) and silver (B, D) NPs.*

The role of exposed cell types in detected ROS production was proven when different cell lines (human monocyte U937 and human lung epithelial A549) behaved differently to the same NPs and dissimilar patterns were observed depending on the composition of the NPs. Particularly, when exposing U937 cells to charged AuNPs for 4hrs, negative NPs induce slightly more ROS production than positive ones while the contrary was seen when exposing A549 cells (Figure 5.4 A, C). In addition, there was no significant difference in ROS production of U937 cells after exposing to positively charged AuNPs pre-incubated with biofluids, whereas pre-incubation cause a decrease in production of ROS from A549 cells. Uneven behaviors to various cell lines were even clearer in the case of charged AgNPs (Figure 5. 4B, D). Different from the increase of ROS production when exposing U937 to pre-incubated AgNPs, A549 cells did not induce any excess ROS production after the pre-incubation. The difference in oxidative stress between these two cell lines could be attributed to the fact that the NPs incubated with human serum and human plasma are more recognizable by monocytes U937 (more sensitive to oxidative stress due to their immune function) than lung cells A549. Therefore, a deeper interaction of NPs with U937 in comparison with A549 is expectable. This comment contributes to the recognition of the effect of used cell lines in testing cytotoxicity of inorganic NPs.

5.3.2. Immune response to NP exposure.

5.3.2.1. ¨Cleanliness¨ of NPs. LAL assay

Innate inflammation is an immediate defense reaction of the immune system to identify and destroy foreign entities which may be dangerous to the host. However, excessive inflammatory reactions may lead to tissue damage and pathology. The ability of NPs to trigger inflammation which is potentially harmful to human health has been reported in various studies[16-17]. Nevertheless, lipopolysaccharide (LPS), the Gram-negative endotoxin, a major component in the outer membrane of Gram-negative bacteria which is ubiquitously present, can contaminate the NPs and interfere with the correct evaluation on inflammatory response of NPs. The inflammatory activities of LPS

on mammalian cells usually include ROS production, gene upregulation, synthesis and secretion of inflammatory factors such as cytokines IL-1β and TNF-α (tumor necrosis factor alpha). Oostingh et al. mentioned that only 0.1EU/ml of endotoxin can induce significant gene expression on human monocytes[18]. Therefore, to ensure if the observed effects are NP-induced, the endotoxin contamination should be determined since LPS cannot be easily removed (even sterilization). Otherwise, the investigated NPs should be *clean* enough.

To detect contaminated endotoxin of investigated AuNPs, either traditional or modified chromogenic Limulus Amoebocyte Lysate (LAL) assay can be used. While the traditional assay detects 4-nitroaniline (pNA), the endotoxin-stimulated LAL end-product, at 405nm, the new assay shifts the readout wavelength to 540nm using diazo coupling reagents. Prior to application, optical interference of the NPs to the assay was also tested and it was found that there was no significant NP interference to the reading up to 10cm^2/ml corresponds to 10^{12} NPs/ml (the concentration obtained from the synthesis) as shown in Figure 5.5 indicating the suitability of the assays for detecting endotoxin of AuNPs.

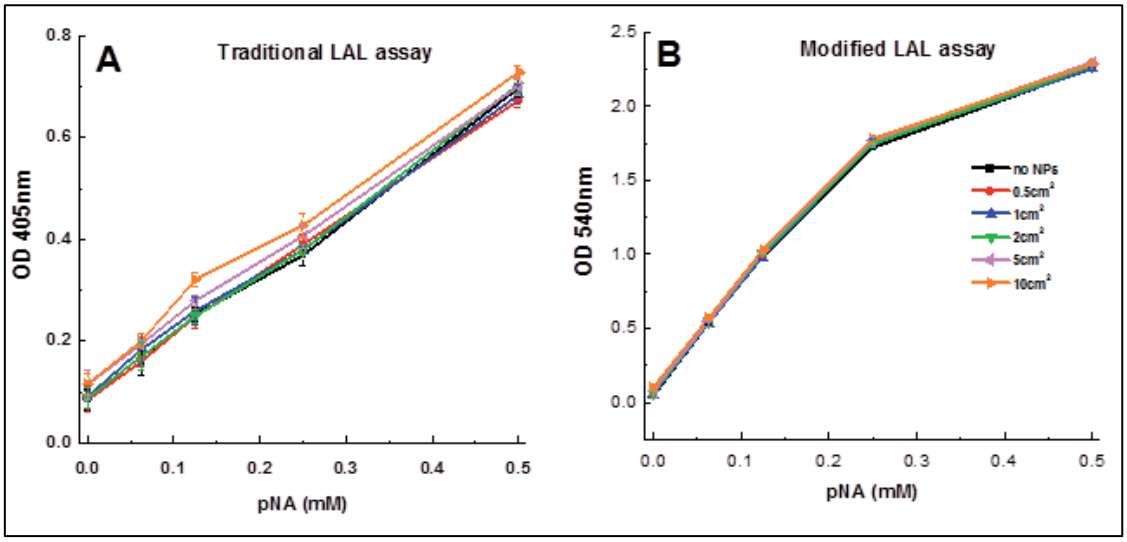

Figure 5.5. NP interference with the LAL assays' readouts*. Interference by Au NPs was tested on the reading of (A) pNA at 405 nm and (B) azo dye (obtained by adding diazo reagents to pNA) at 540 nm.*

Results from LAL test (Figure 5.6A) showed that the solution of investigated AuNPs contained a considerable amount of endotoxin, higher than 0.8EU, at synthesized concentration ($10cm^2$/ml). This contamination was found to be dose-dependent where lower concentrations of NPs (obtained by diluting the NPs with free-endotoxin water) contain less endotoxin. Thus, to minimize the interference of contaminated endotoxin, dilution of stock NPs was done to obtain proper concentration prior to the immune response test. In addition, incubation of NPs with LPS was carried out to know how the endotoxin interacted with them, whether they attached to the NPs. Particularly, as-prepared AuNPs were mixed with LPS at room temperature and the time evolution of SPR peak position of NPs was followed by UV-Vis. The immediate red-shift (λ_{max} increase) of the SPR wavelength at the first minutes, usually caused by the change in dielectric constant of NP surrounding, indicated the conjugation of LPS to NP surface (Figure 5.6B). When a higher concentration of LPS was used, the saturation of the peak shift was faster attained (less than 10 minutes), in comparison with lower concentration (around 30 minutes) as shown in Figure 5.6B. In short, the NPs prepared and stored in non-sterile conditions are potentially contaminated with endotoxin LPS and these LPS do attach to the NP surface.

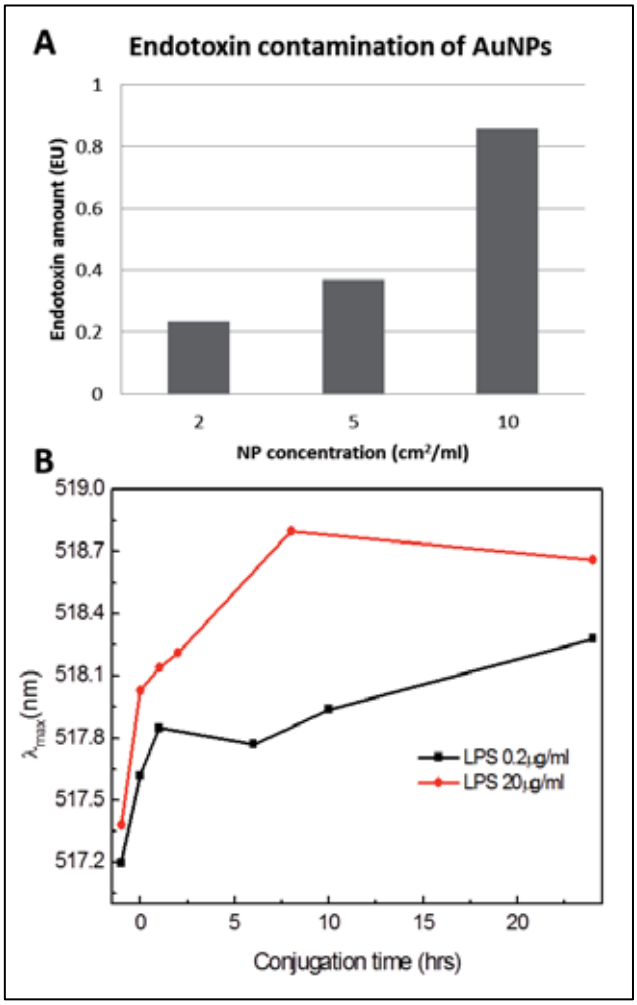

Figure 5.6. LPS contamination of synthesized NPs. *(A) Endotoxin detection in 10nm citrate coated AuNPs by Limulus Amoebocyte Lysate (LAL) assay. (B) Conjugation of LPS to AuNPs. Time evolution of maximal absorption wavelength (λ_{max}) of AuNPs upon incubation with LPS indicating the ability to attach to NPs of endotoxin.*

5.3.2.2. Impact on immune response of contamination

As mentioned in previous section, the presence of LPS contamination in NPs may generate immune response as inflammatory activities. However, this response can be due either to LPS, to NPs lonely or to their combination which existence was proven. To verify this, different concentration of *clean* AuNPs (AuNPs without incubation with LPS) and their corresponding LPS-contaminated ones (ranging from 0.25 to 2cm^2/ml by surface area) were exposed to human monocytes. LPS-conjugated AuNPs were

obtained from incubating the NPs with 200ng/ml LPS at room temperature for 1hr. Then, gene expression (by qPCR) and protein production (by ELISA) of the members of IL-1 family, which have important roles in innate immune response, were determined. In particular, the inflammatory cytokine IL-1β (and its gene IL1B), and its natural inhibitor, the IL-1 receptor antagonist (IL-1Ra, and its gene IL1RN) were studied.

Results showed that LPS-conjugated NPs were able to induce a significant expression of the inflammatory cytokine gene IL1B which is dose-dependent while *clean* NPs were found totally inactive (Figure 5.7A). On the contrary, expression of IL1RN, the gene coding for the inhibitor IL-1Ra was not significantly different between clean NPs and LPS-contaminated particles (Figure 5.7B). Moreover, this expression level of IL1RN was as high as the medium control (concentration = 0) indicating the lack of effect on IL1RN gene expression in both type of NPs. Similarly, LPS-conjugated NPs also exhibited a dose-dependent manner in the production of IL-1β protein, whereas *clean* NPs are again totally inactive (Figure 5.7C). These findings indicated that LPS attached to AuNPs can trigger similar inflammatory response as free LPS which is the activation of IL-1B gene expression and the release of mature IL-1β. Seeming independent on the dose, IL-1Ra production induced by LPS-conjugated NPs was found to be higher than both clean NPs and medium control implying their anti-inflammatory effect (Figure 5.7D).

Thus, we have known that when attaching to NPs, LPS still trigger immune response including inflammatory and anti-inflammatory activities. However, whether the adsorption of LPS onto NPs enhances or inhibits the response in comparison with the free LPS still remains unanswered since the amount of bound LPS is unknown. To determine this, quantification of LPS conjugated to NP surface is needed which can be done by indirect measurement. In details, unbound LPS can be collected first from solution of post-incubated NPs by centrifugation and then quantified with LAL assay. The amount of bound LPS is the difference between initial and unbound LPS.

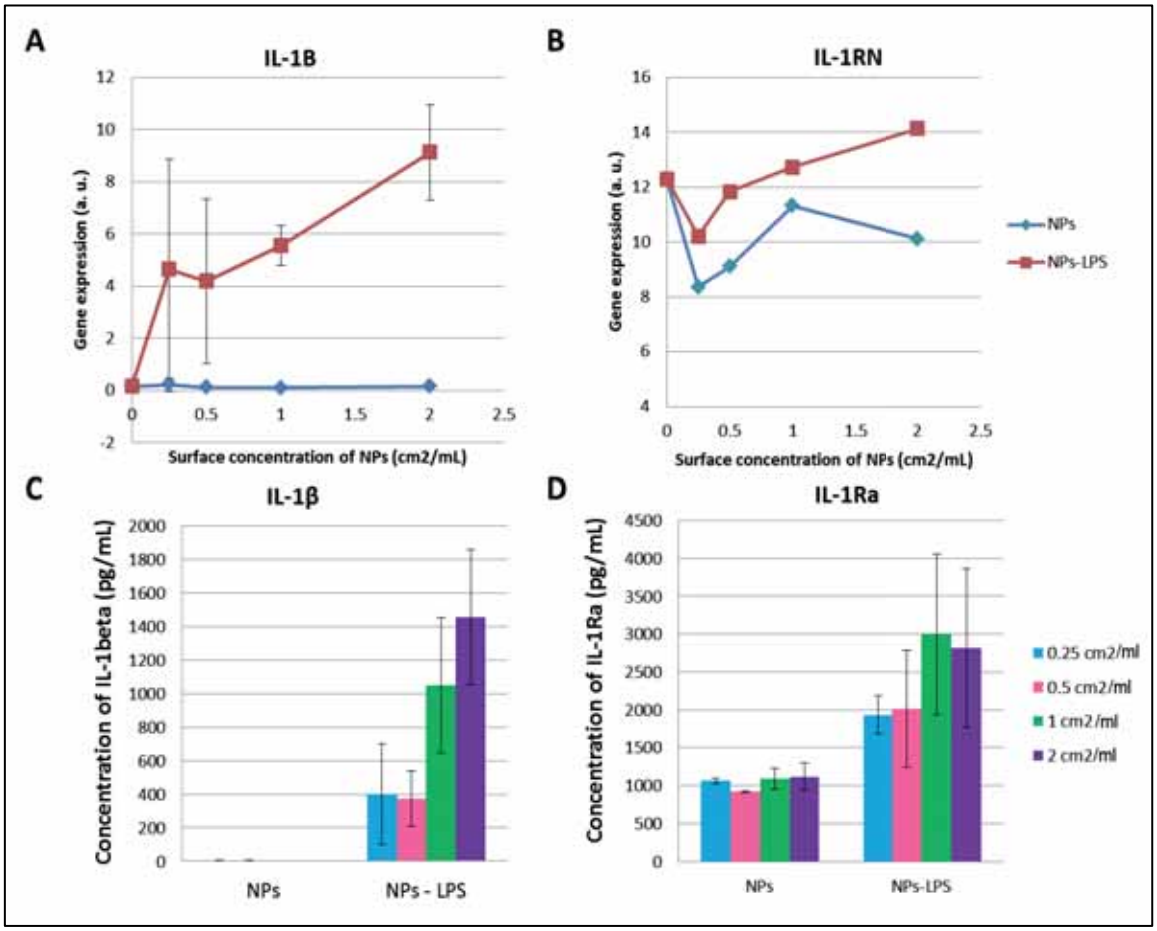

Figure 5.7. Effect of LPS-contaminated Au NPs on monocyte activation*. Gene expression (A, B) and cytokine protein production (C, D) (lower panels) of the inflammatory cytokine IL-1β (A, C) and its inhibitor IL-1Ra (B, D) in human monocytes exposed to clean Au NPs and LPS-contaminated Au NPs.*

5.3.3. Ecotoxicity of AgNPs to C-elegans

Caenorhabditis *elegans (*C-elegans), a free-living, transparent nematode in soil environments, is an emerging model species in toxicology. C-elegans own a number of characteristics that make it not only relevant but also powerful model. It is easy and inexpensive to maintain in laboratory conditions due to its short and prolific life cycle (~ 3 days with a large number of offspring). Its small body allows conducting *in vitro* assays in 96-well plate. More importantly, many basic physiological processes and stress responses, which are observed in other eukaryotes such as human, are

conserved in C-elegans. This makes C-elegans a valuable toxicity model in which prediction on toxicity in higher organisms can be referred from its results[19].

Studies with C-elegans have been performed in a range of artificial aqueous media. Among them is Synthetic Soil Pore Water (SSPW), a medium that better represents real soil solution conditions which has been recently developed by Tyne et al.[20]. This medium is a combination of relevant salts (Table 5.1) that provides major cations and anions as in natural soil solution, and possesses a lower ionic strength than conventional nematode media. For this reason, Tyne et al. showed that SSPW was able to give better stable dispersion to the NPs they used in comparison to others (M9 buffer or K-medium). The likely absence of Ag precipitation when suspending ionic Ag to SSPW (in which significant Cl^- is absent), which results in more accurate interpretation on toxicity effect, is another merit of using this medium. In this section, ecotoxicity of AgNPs of various sizes together with ionic silver was tested on C-elegans using SSPW as the testing solution.

Figure 5.8 represents toxicity test results where a significant concentration-related response was found following silver nitrate exposure. After fitting (power equation), half maximal effective concentration (EC_{50}) value was estimated to be 0.25mg/L for ionic Ag which is consistent with reported value[18]. In the silver NP test, a dose-dependent response was also observed in individual type of NPs (Figure 5.8). The same fitting was done for the data obtained from the dispersion of AgNPs. Then, EC_{50} values for 15nm, 23nm and 48nm AgNPs were estimated to be 1.95mg/L, 2.88mg/L and 13mg/L, respectively. Clearly, Ag in the ionic form induced far higher toxicity to C-elegans than the nanoparticulate form. In addition, the toxicity of NPs was correlated to their size. Indeed, smaller NPs were more toxic than the bigger ones. Since AgNP toxicity is usually attributed to the formation of Ag ions, smaller NPs are more toxic likely due to their higher ability to release ions (section 3.3.2).

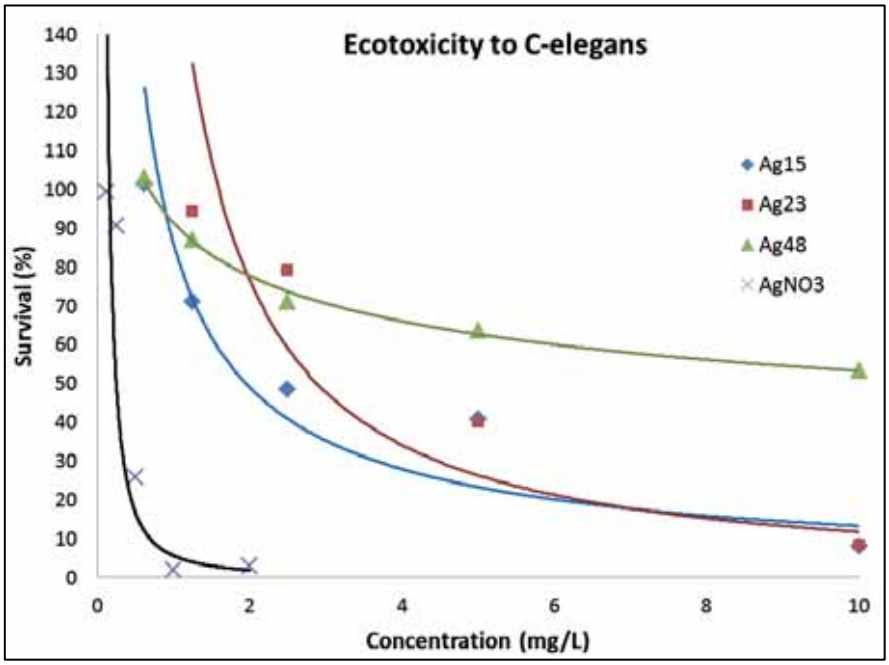

Figure 5.8. *Toxicity of silver nanoparticles with different sizes (Ag15: 15nm, Ag23: 23nm and Ag48: 48nm) and control ionic Ag ($AgNO_3$) suspension to C-elegans in synthetic soil pore water after 72hr exposure.*

5.4. Conclusions

In this chapter, different aspects of NP biological effects (cytotoxicity, immune response, ecotoxicity) were discussed. The influence of factors including chemical composition, NP size, surface charge, protein adsorption, agglomeration and presence of contaminants on NP biological response were confirmed. Therefore, as pointed out in previous chapters, to be able to accurately determine the biological effects induced by NPs, it is essential to comprehensively characterize them. Additionally, contamination with agents that can trigger biological response themselves should be examined prior to any test. Proper testing assays or cell lines should also be chosen for specific NPs.

References

1. Deng, X. Y.; Luan, Q. X.; Chen, W. T.; Wang, Y. L.; Wu, M. H.; Zhang, H. J.; Jiao, Z., Nanosized zinc oxide particles induce neural stem cell apoptosis. *Nanotechnology* **2009,** *20* (11).

2. Oberdorster, G.; Ferin, J.; Lehnert, B. E., Correlation between Particle-Size, in-Vivo Particle Persistence, and Lung Injury. *Environ Health Persp* **1994,** *102*, 173-179.

3. Gupta, A. K.; Gupta, M., Cytotoxicity suppression and cellular uptake enhancement of surface modified magnetic nanoparticles. *Biomaterials* **2005,** *26* (13), 1565-1573.

4. Weinstein, J. S.; Varallyay, C. G.; Dosa, E.; Gahramanov, S.; Hamilton, B.; Rooney, W. D.; Muldoon, L. L.; Neuwelt, E. A., Superparamagnetic iron oxide nanoparticles: diagnostic magnetic resonance imaging and potential therapeutic applications in neurooncology and central nervous system inflammatory pathologies, a review. *J Cerebr Blood F Met* **2010,** *30* (1), 15-35.

5. Li, X.; Lenhart, J. J.; Walker, H. W., Aggregation Kinetics and Dissolution of Coated Silver Nanoparticles. *Langmuir* **2012,** *28* (2), 1095-1104.

6. Salvador-Morales, C.; Flahaut, E.; Sim, E.; Sloan, J.; Green, M. L. H.; Sim, R. B., Complement activation and protein adsorption by carbon nanotubes. *Mol Immunol* **2006,** *43* (3), 193-201.

7. Mitchell, L. A.; Lauer, F. T.; Burchiel, S. W.; McDonald, J. D., Mechanisms for how inhaled multiwalled carbon nanotubes suppress systemic immune function in mice. *Nat Nanotechnol* **2009,** *4* (7), 451-456.

8. Sanchez, A.; Recillas, S.; Font, X.; Casals, E.; Gonzalez, E.; Puntes, V., Ecotoxicity of, and remediation with, engineered inorganic nanoparticles in the environment. *Trac-Trend Anal Chem* **2011,** *30* (3), 507-516.

9. Rana, S.; Kalaichelvan, P. T., Ecotoxicity of nanoparticles. *ISRN Toxicology* **2013,** *2013*, 11.

10. Wood, C. M.; Playle, R. C.; Hogstrand, C., Physiology and modeling of mechanisms of silver uptake and toxicity in fish. *Environ Toxicol Chem* **1999,** *18* (1), 71-83.

11. Barrena, R.; Casals, E.; Colon, J.; Font, X.; Sanchez, A.; Puntes, V., Evaluation of the ecotoxicity of model nanoparticles. *Chemosphere* **2009,** *75* (7), 850-857.

12. Dadosh, T., Synthesis of uniform silver nanoparticles with a controllable size. *Mater Lett* **2009,** *63* (26), 2236-2238.

13. Monopoli, M. P.; Aberg, C.; Salvati, A.; Dawson, K. A., Biomolecular coronas provide the biological identity of nanosized materials. *Nat Nanotechnol* **2012,** *7* (12), 779-786.

14. Limbach, L. K.; Wick, P.; Manser, P.; Grass, R. N.; Bruinink, A.; Stark, W. J., Exposure of engineered nanoparticles to human lung epithelial cells: Influence of chemical composition and catalytic activity on oxidative stress. *Environ Sci Technol* **2007,** *41* (11), 4158-4163.

15. Bhattacharjee, S.; de Haan, L. H. J.; Evers, N. M.; Jiang, X.; Marcelis, A. T. M.; Zuilhof, H.; Rietjens, I. M. C. M.; Alink, G. M., Role of surface charge and oxidative stress in cytotoxicity of organic monolayer-coated silicon nanoparticles towards macrophage NR8383 cells. *Part Fibre Toxicol* **2010,** *7*.

16. Hussain, S.; Boland, S.; Baeza-Squiban, A.; Hamel, R.; Thomassen, L. C. J.; Martens, J. A.; Billon-Galland, M. A.; Fleury-Feith, J.; Moisan, F.; Pairon, J. C.; Marano, F., Oxidative stress and proinflammatory effects of carbon black and titanium dioxide nanoparticles: Role of particle surface area and internalized amount. *Toxicology* **2009,** *260* (1-3), 142-149.

17. Gosens, I.; Post, J. A.; de la Fonteyne, L. J. J.; Jansen, E. H. J. M.; Geus, J. W.; Cassee, F. R.; de Jong, W. H., Impact of agglomeration state of nano- and submicron sized gold particles on pulmonary inflammation. *Part Fibre Toxicol* **2010,** *7*.

18. Oostingh, G. J.; Casals, E.; Italiani, P.; Colognato, R.; Stritzinger, R.; Ponti, J.; Pfaller, T.; Kohl, Y.; Ooms, D.; Favilli, F.; Leppens, H.; Lucchesi, D.; Rossi, F.; Nelissen, I.;

Thielecke, H.; Puntes, V. F.; Duschl, A.; Boraschi, D., Problems and challenges in the development and validation of human cell-based assays to determine nanoparticle-induced immunomodulatory effects. *Part Fibre Toxicol* **2011,** *8*.

19. Leung, M. C. K.; Williams, P. L.; Benedetto, A.; Au, C.; Helmcke, K. J.; Aschner, M.; Meyer, J. N., Caenorhabditis elegans: An emerging model in biomedical and environmental toxicology. *Toxicol Sci* **2008,** *106* (1), 5-28.

20. Tyne, W.; Lofts, S.; Spurgeon, D. J.; Jurkschat, K.; Svendsen, C., A new medium for Caenorhabditis elegans toxicology and nanotoxicology studies designed to better reflect natural soil solution conditions. *Environ Toxicol Chem* **2013,** *32* (8), 1711-1717.

Chapter 6

GENERAL CONCLUSIONS

Reactivity and persistency of NPs, especially silver, are two aspects that should be evaluated to make sure that NPs will perform the designed function with a desired safety. In some case, balancing between these two is needed though it is challenging. In that circumstance, this thesis aimed at (i) exploring the colloidal stability and chemical reactivity of the silver nanoparticles as well as (ii) controlling their persistency in biological media.

Regarding the first objective, the physical and chemical states of AgNPs in a variety of biological media were investigated.

- The thesis studied the behaviors of AgNPs in physiological conditions by incubating 12nm citrate -coated AgNPs, in simulated body fluids at different portals of entry. These fluids include saliva, intestinal fluid, gastric fluid, colonic fluid, lung fluid, synovial fluids, serum, tear and sweat. The AgNP transformations mainly aggregation (colloidal stability), protein adsorption and dissolution (chemical reactivity) in each fluids, due to their high reactivity, were identified by analyzing their UV-Vis and Z-potential temporal evolutions.
- More than one process was found to simultaneously occur in some fluids. The correlation between fluid characteristics (biomolecules content, ionic strength and pH) and the extent of the transformations was explored.
- The chemical reactivity of AgNPs in biological media was further investigated using cell culture media supplemented with serum. It was observed that citrate-coated

AgNPs of 15nm rapidly dissolved in cCCM. The NP dissolution was found to be facilitated with the presence of ion scavengers including chlorine and proteins which are abundant in physiological environments.

- The effect of factors, such as the size of NP and media composition, to the dissolution, was also studied. It was confirmed that the smaller NPs (15nm) were more reactive and dissolved faster than the larger ones (50nm). In addition, AgNPs were more stable in medium supplemented with human serum in comparison with the one supplemented with fetal bovine serum.
- The extent of the Ag dissolution in cCCM was determined and a protocol of Ag partition and speciation was developed. It was observed that around 70% of Ag was transformed from 15nm AgNPs after 8hr exposure. The species generated due to dissolution was identified as Ag_Free, Ag_proteins, AgCl and AgNPs. The distribution of these species was measured for 8hr exposure and it is possible to estimate the distribution at other time points.

Concerning the second objective, different approaches were applied to control the persistency (the chemical degradability or dissolution) of AgNPs in biological media.

- The NP surface passivation, including coating NPs with surfactants of high affinity (like MUA) and forming a thin oxide layer (by aging the NPs), was found to decrease the dissolution of AgNPs.
- Considering that the dissolution is equilibrium between the NP and its ions, and applying Le Chatelier principle, the dissolution was observed to decrease by adding Ag^{+} to the NP precursor prior to exposure.
- The persistency of AgNP was also able to be tuned by controlling the nobility of Ag using a core-shell approach. Au@Ag core-shell NPs with different core sizes and various thickness of the shell were successfully obtained by seed-mediated method. It was concluded that, with a noble Ag layer of around 2-2.3nm on top of Au core, the NPs would be chemically stable in cell culture media.

In addition, various aspects in examining biological effect of NPs (cytotoxicity and ROS production, immunotoxicity and ecotoxicity) were also investigated.

- The pre-incubation of positively charged NPs with protein was found to increase their biocompatibility. Apart from NP characteristics (composition, surface charge), the biological response was observed to vary among different cell types.
- Contaminants (like endotoxin/LPS) were detected to present in synthesized NP solution. These contaminants were found to readily attach to the NPs and give inflammatory activities.
- Ecotoxicity of AgNPs on C-elegans was observed to be dose-dependent and size-dependent. Additionally, AgNPs showed less toxic than Ag ion.

Appendix

Formulations of simulated body fluids

These formulations are described in [Marques MRC, Loebenberg R, Almukainzi M. 2011. Simulated Biological Fluids with Possible Application in Dissolution Testing. Dissolut Technol 18: 15-28]. All reagents are purchased from Sigma Aldrich.

Reagents for preparing Saliva

Reagent	Concentration
Mucin	1 g/l
Alpha amylase	2 g/l
$CaCl_2$. $2H_2O$	0.228 g/l
NaCl	1.017 g/l
Na_2HPO_4	0.108 g/l
$MgCl_2$	0.0285 g/l
K_2CO_3	0.603 g/l
NaH_2PO_4	0.237 g/l
pH	6.9

Reagents for preparing Gastric fluids

Reagent	Concentration
Lecithin	20 µM
Pepsin	0.1 mg/ml
Mucin gastric	1.4 g/l
Sodium taurocholate	80 µM
NaCl	34.2mM
$NaHCO_3$	8mM
HCl	120mM
pH	1.6

Reagents for preparing Intestinal fluids

Reagent	Concentration
Sodium taurocholate	3mM
Lecithin	0.2mM
Maleic acid	19.12mM
NaOH	34.8mM
NaCl	68.62mM
pH	6.5

Reagents for preparing Colonic fluid

Reagent	Concentration
Sodium taurocholate	0.113 g/L
Lecithin	0.222 g/L
Palmitic acid	0.026 g/L
HSA (human serum albumin)	3 g/L
pH	7.8

Reagents for preparing Lung fluids

Reagent	Concentration
$MgCl_2.6H_20$	0.095 g/l
NaCl	6.0193 g/l
KCl	0.2982 g/l
Na_2SO_4	0.063 g/l
$CaCl_2$	0.2775 g/l
Sodium acetate	0.574 g/l
$NaHCO_3$	2.6043 g/l
Sodium citrate dihydrate	0.097 g/l
DPPC	0.02% (w/v)
HSA	15 g/l
pH	7.4

Reagents for preparing Synovial fluid

Reagent	Concentration
Glucose	0.2 mg/ml
HSA	15 mg/ml
Hyaluronic acid	3 mg/ml
NaCl	8 g/l
KCl	0.2 g/l
Na_2HPO_4	1.44 g/l
KH_2PO_4	0.24 g/l
pH	7.4

Reagents for preparing Tear

Reagent	Concentration
Lysozyme	2.68 g/l
D-glucose	6.5 g/l
Gamma globulin	1.34 g/l
Lactoferrin	1.4 g/l
HSA	2.68 g/l
NaCl	6.5 g/l
$CaCl_2$	0.06 g/l
pH	7.4

Reagents for preparing Sweat

Reagent	Concentration
Lactic acid	0.1 % in mass
Urea	0.1 % in mass
NaCl	0.9 g/L
KH_2PO_4	0.2 g/L
$CaCl_2$	0.015 g/L
$MgSO_4$	0.0013 g/L
pH	4.9

List of Abbreviations

λ_{max}: Maximal Absorption Wavelength

A549: Human Lung Adenocarcinoma Epithelial Cells

AgNPs: Silver Nanoparticles

BBB: Blood Brain Barrier

cCCM: complete Cell Culture Media

C-elegans: Caenorhabditis *elegans*

CNTs: Carbon Nanotubes

CTB: CellTiter Blue

DCFH-DA: Dichloro-Dihydro-Fluorescein Diacetate Assay

DLS: Dynamic Light Scattering

DLVO: Derjaguin and Landau, Verwey and Overbeek

DMEM: Dulbecco´s Modified Eagle Medium

DNA: Deoxyribonucleic Acid

DWCNTs: Double-Walled Carbon Nanotubes

EC_{50}: Half Maximal Effective Concentration

EDX: Energy-Dispersive X-ray Spectroscopy

ELISA: Enzyme-Linked Immunosorbent Assay

FBS: Fetal Bovine Serum

fcc: face-centered cubic

FWHM: Full Width at Haft Maximum

HAADF: High Angle Annular Dark Field

HeLa: Henrietta Lacks immortal cells

HuS: Human Serum

ICP-MS: Inductively Coupled Plasma-Mass Spectroscopy

IL-1β: Interleukin-1 Beta Protein

IL-1B: Interleukin-1 Beta Gene

IL-1Ra: Interleukin-1 Receptor Antagonist Protein

IL-1RN: Interleukin-1 Receptor Antagonist Gene

LAL: Limulus Amoebocyte Lysate assay

LDH: Lactose Dehydrogenase

LPS: Lipopolysaccharides

MRI: Magnetic Resonance Imaging

MUA: 11-Mercaptoundecanoic Acid

NPs: Nanoparticles

PBMC: Peripheral Blood Mononuclear Cells

PC: Protein Corona

PEG: Polyethylene Glycol

QDs: Quantum Dots

pNA: 4-Nitroaniline

qPCR: real time polymerase chain reaction

ROS: Reactive Oxygen Species

RPMI: Roswell Park Memorial Institute

SAMs: Self-Assembled Monolayers

SERS: Surface-Enhanced Raman Spectroscopy

SPIONs: Superparamagnetic Iron Oxide Nanoparticles

SPR: Surface Plasmon Resonance

SSPW: Synthetic Soil Pore Water

STEM: Scanning Transmission Electron Microscope

SWCNTs: Single-Walled Carbon Nanotubes

TEM: Transmission Electron Microscopy

U937: Human Leukemic Monocyte Lymphoma

UV-VIS: Ultra-Violet Visible Spectroscopy

XRD: X-Ray Diffraction

Z-potential: Zeta-potential

List of Publications

1. N. T. T. Tran, N. Bastus, C. Schulzt, C. Svendsen, D. Spurgeon, V. Puntes, *Engineering Au@Ag nanoparticles optical properties and their chemical stability in biological environments*. In preparation.

2. N. T. T. Tran, J. Piella, E. Casals, N. Bastus, V. F. Puntes, *Dissolution, its prevention and speciation of silver nanoparticles in biological media.* In preparation.

3. N. T. T. Tran, E. Casals, V. F. Puntes, *Silver nanoparticles transformations in different simulated body fluids: sweat, tear, saliva, gastric fluid, intestinal fluid, colonic fluid, lung fluid, synovial fluid and serum*. **Nanotoxicology**. Under review.

4. P. Schlinkert, M. Boyles, U. Tischler, E. Hornig, E. Casals, N. Tran, J. Zhao, G. J. Oostingh, M. Himly, M. Riediker, V. Puntes, A. Duschl, Comparing the effects of charged nanoparticles on three different lung epithelial cells. **Particle and Fibre Toxicology**. Under review.

5. Y. Li, P. Italiani, E. Casals, N. Tran, V. F. Puntes, D. Boraschi, *Optimising the use of commercial LAL assays for the analysis of endotoxin contamination in metal colloids and metal oxide nanoparticles*. **Nanotoxicology**. Accepted.